

POLITECNICO DI TORINO

Department of Structural, Geotechnical and Building Engineering

Master's degree
in Civil Engineering

Thesis of Master of Science



Influence of the existing stress state on the pull-out test for concrete structures

Tutors

Mauro Corrado
Giulio Ventura

Candidate

Daniela Maya Vélez

Turin, Italy. December, 2019

Abstract

In the last years, prestressed concrete structures, particularly bridges, have been increasing in popularity in consequence of its versatility and the multiple advantages that they have in terms of durability, resistance and design. Inducing a state of tension and deformation, the prestressing technique improves the structural behavior, and with a low amount of steel cables allows obtaining a higher load carrying capacity. The advantages of dealing with prestressed elements extend to the possibility of reducing the dimensions of the transversal section and increasing the length of the spans between pillars.

Nevertheless, the performance of prestressed structures depends on the prestressing level, related to the real state of its components, and this could be considered as a drawback which can lead into a brittle and catastrophic failure. Due to the nature of the technique, there are present some losses of prestress from the construction phases and during its serviceability life. The reductions due to friction, anchorage slip, creep, shrinkage and relaxation of the steel are mathematically predicted at the design stage through multiple theories that describe their development. The reliability on the calculations is high enough not to be worried in the future. On the other hand, there are other causes of loss such as the corrosion of the steel cables, that is not considered during the design because it is not expected to happen. This type of deterioration is strictly related to the aggressive environmental conditions. Therefore, it demands the entire attention through a constant monitoring, since steel cables are potentially well protected because of the construction methodology and the issues are not clearly visibly.

The aim of the thesis lies into the assessment of the prestressing level in prestressed structures, using the pull-out test, which is a non-destructive technique commonly used for the in-situ determination of concrete strength. The test gives the tensile force allowing the extraction of a screw ion the structural element surface and can be correlated to the concrete strength. The idea behind this work is that the result of the pull-out test is influenced by the surrounding stress state, so that the extraction force will depend on the prestressing state.

This conjecture is herein investigated through numerical analyses by means of the Finite Element Method (FEM). The modelling procedure is achieved by exploiting the software LUSAS. Different geometries are considered in order to maximize

the effect of prestressing on the pull-out test, thus identifying the most suitable setup to carry out the test. Furthermore, the numerical model is complemented by several experimental tests, performed at the laboratory of the Department of Structural, Geotechnical and Building Engineering of Politecnico di Torino, by means of several load combinations.

A ti, que no necesitaste muchos años en esta tierra para enseñarme el significado del amor y estuviste el tiempo suficiente para convertirte en mi mayor ejemplo a seguir. Esto es para ti, porque sé que donde estás, lo estamos celebrando juntos. Lo logramos Papá !

Gracias mamá por darme la fuerza y enseñarme que las dificultades solo son un motivo más para luchar más fuerte por lo y los que queremos. Gracias Sebas por ser mi apoyo incondicional.

Gracias a mi familia, mis tíos y primos, ustedes han sido un gran soporte en mi vida y me llenan el alma de alegría y amor. No podría desear otra familia diferente a ustedes.

Gracias a mis amigos, personas maravillosas que quedarán por siempre en mi memoria, por apoyarme cuando más sola me encontré y por formar conmigo una pequeña familia.

Index

1	Introduction	1
2	Pull-out test	5
2.1	Description of the method	5
2.2	Concrete strength vs Pull-out force	11
3	Experimental test	12
3.1	Uniaxial compression test	12
3.2	Pull-out test performance	15
4	Numerical modeling	20
4.1	LUSAS finite element analysis software	22
4.2	Modeling procedure	24
4.3	Geometries	38
4.4	Numerical procedure	41
4.4.1	Tensile analysis	46
4.4.2	Prestressing contribution	47
5	Results and Discussion	56
5.1	Uniaxial compression test	56
5.2	Pull-out test	57
5.3	Modeling procedure	59
5.4	Numerical procedure	62
5.4.1	Tensile analysis	63
5.4.2	Prestressing contribution	74
5.5	Geometry influence	93
6	Conclusions	99
7	Bibliography	101

Table Index

1	Geometry of the bolts	18
2	Arrangement of geometries	39
3	Uniaxial compression test results	56
4	Elastic modulus of Mortar and Concrete	56
5	Pull-out test results using the second geometry	57
6	Pull-out test results using the first geometry	58
7	Average value of the compressive strength for Concrete and Mortar	59
8	Compression force results related to the prestressing contribution	93
9	Same α_1 results	94
10	Same failure cone height results	95
11	Same bearing ring diameter results	96
12	Same bearing ring diameter results for Model 2	97

Figure Index

1	Bridge collapses caused by loss of prestress. From [13],[14],[16],[8]	3
2	Schematic procedure for post installed pull-out test [4]	7
3	Scheme of the mechanism of failure on the concrete	8
4	Mechanism of failure of the concrete due to the variation of the angle of the conic surface.	9
5	Prestressing stress induced by the compression testing machine . .	10
6	Uniaxial compression test performance	13
7	Satisfactory failure of concrete specimens [4]	13
8	Unsatisfactory failure of concrete specimens [4]	14
9	Uniaxial compression test samples at rupture level	14
10	Pull-out test development	16
11	Cubic specimen under 10 MPa of uniaxial compression	17
12	Bolts for the pull-out test	17
13	Bearing ring geometry	18
14	Failure cone for geometry 1	19
15	Failure cone for geometry 2	19
16	LUSAS Interface	23
17	LUSAS features	23
18	Model 1	24
19	Model 2	25
20	LUSAS model 1	26
21	LUSAS model 2	26
22	Models line mesh	28
23	Structural elements type on a line - Lusas	28
24	Structural elements type on a line	29
25	Volume mesh assignments	30
26	Final models	31
27	Material properties of the models	32
28	Support configuration of the models	33
29	LUSAS Loadcases	34
30	Truncated cone geometry	35
31	Area of the second screw	36
32	Loading cases for model 1	37
33	Loading cases for model 2	38
34	Arrangements of geometry	40

35	Flowchart of the numerical procedure	41
36	Nodes along the line	42
37	Local reference system	43
38	Line selected for the mathematical procedure	45
39	Direct cosines definition	45
40	Maximum shear development	48
41	Coulomb Envelope of failure	49
42	Mohr circles due to several load combinations	49
43	Pure tension and Pure compression Mohr circumferences	50
44	State according to the envelope of failure	51
45	Envelope of Mohr simplification	51
46	Prestressing contribution convention	52
47	Discretization for the influence area of the stresses	54
48	Area frames for the prestressing load estimation	54
49	Modeling results for 3-4-5	59
50	Modeling results for 6-7-8	60
51	Modeling results for 9-10-11	61
52	LUSAS results layout	62
53	Model 1 stress distribution in Local coordinates due to extraction.	63
54	Model 2 stress distribution in Local coordinates due to the extrac- tion force	64
55	Model 3 stress distribution in Local coordinates due to the extrac- tion force	65
56	Model 4 stress distribution in Local coordinates due to the extrac- tion force	66
57	Model 5 stress distribution in Local coordinates due to the extrac- tion force	67
58	Model 6 stress distribution in Local coordinates due to the extrac- tion force	68
59	Model 7 stress distribution in Local coordinates due to the extrac- tion force	69
60	Model 8 stress distribution in Local coordinates due to the extrac- tion force	70
61	Model 9 stress distribution in Local coordinates due to the extrac- tion force	71

62	Model 10 stress distribution in Local coordinates due to the extraction force	72
63	Model 11 stress distribution in Local coordinates due to the extraction force	73
64	Model 1 - stresses distribution due to prestressing in Y direction .	75
65	Model 1 deformed mesh	77
66	Mesh deformation implications on the stress distribution	78
67	Model 2 - stresses distribution due to prestressing in Y direction .	79
68	Model 3 - stresses distribution due to prestressing in Y direction .	80
69	Model 4 - stresses distribution due to prestressing in Y direction .	81
70	Model 5 - stresses distribution due to prestressing in Y direction .	82
71	Model 6 - stresses distribution due to prestressing in Y direction .	83
72	Model 7 - stresses distribution due to prestressing in Y direction .	84
73	Model 8 - stresses distribution due to prestressing in Y direction .	85
74	Model 9 - stresses distribution due to prestressing in Y direction .	86
75	Model 10 - stresses distribution due to prestressing in Y direction	87
76	Model 11 - stresses distribution due to prestressing in Y direction	88
77	Model 1 - stresses distribution due to prestressing in X and Y directions	89
78	Model 1 deformed mesh after X and Y prestressing	90
79	Model 2 - stresses distribution due to prestressing in X and Y directions	91
80	Model 2 deformed mesh after X and Y prestressing	92
81	Values of prestressing contribution with alpha constant	94
82	Values of prestressing contribution with height of failure cone constant	95
83	Values of prestressing contribution with bearing ring diameter constant	97
84	α versus the Compression force	98

1 Introduction

Bridges have been considered through history as the quintessential construction to guarantee the effective integration between surrounding towns. The versatility on their design is considered one of the main drawbacks because it allows the connection besides the difficulty on the topography. To construct them there is an evolution of the different techniques. Starting with the prehistoric era surpassing environmental obstacles such as body waters and valley with the stone designs. Crossing through the ancient Romans their arc bridges made with masonry and concrete that are still on feet and finally, arriving to the 20th century where the technological development of the materials brings unexpected possibilities, even a sea can be crossed.

This options are related to the improvement of the mechanical properties and the design of them. Nowadays one of the most popular materials to develop this type of structures is the prestressed concrete. Due to the nature of its construction and the presence of both materials the steel cables and the concrete, one of this enhancement is the possibility to combine the high tensile strength of one with the high compressive strength of the other one. The benefits of this coalition are greater compared with respect to the traditional construction.

The increment of the mechanical properties allow the designer to conceive extraordinary designs breaking the schemes and developing larger projects. With this type of materials the flexural cracks at the mid span and the supports are avoided, the length of the span can cover greater distances, the cross section of the bridge can be reduced and all of this guaranteeing the support of equivalent loads. The aforesaid advantages have positive repercussions on the cost of the project.

Nevertheless, around the world there are so many cases of bridges collapse, but the causes are still an investigation subject. The methodology employed to construct a prestressed section determine few drawbacks that can be prevented or not. If they are not considered then the consequences are catastrophic. The disadvantages are related to the possible losses that the prestressing techniques generates on the section.

The aforesaid reduction on the properties is estimated by mathematical proce-

dures at the design stage, this diminutions are due to friction, anchorage slip, creep, shrinkage and relaxation of the steel. There are multiple theories that describe their development and the reliability on the calculations is high enough not to be worried in the future.

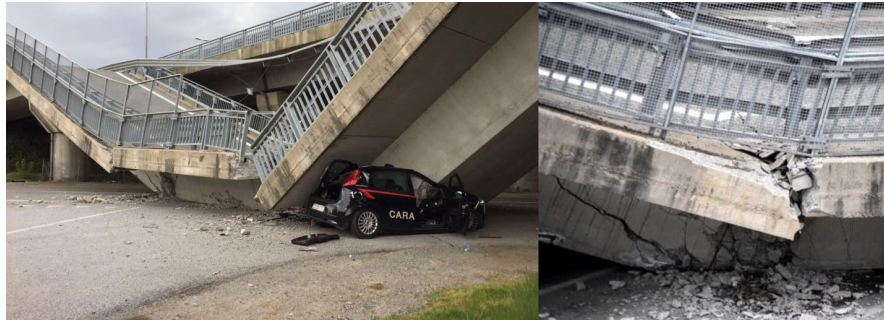
On the other hand, there are other causes of loss that are not considered during the blueprint stage because they are not expected to happen. One of them is the degradation of the involved materials. Making emphasis on the corrosion of the steel cables, this type of deterioration is strictly related to the aggressive environmental conditions. Therefore, it demands the entire attention through a constant monitoring, since steel cables are potentially well protected because of the construction methodology and the issues are not clearly visibly.

The corrosion on the steel cables is not a novelty and there are cases dating from 1985 where this was the main cause of the collapse. In the Figure 1 are shown different cases of prestressed structures collapse where the principal reason of subsidence is the steel corrosion.

According to different investigations there is a common discussion between the engineers in all the cases. The prestressing tendons were severely corroded where they crossed the longitudinal and transverse joints. The structure collapsed when the sectional area of the tendons had been reduced to the point where they could no longer carry the imposed load. [16]

Currently there are available diverse techniques that allow the in situ determination of the concrete strength. These techniques are destructive or not destructive and they are defined according to the requirements. The aim of the thesis lies into the assessment of the prestressing level in prestressed structures owing to the pull-out test.

Considering the problematic determination of the state of the steel cables, this thesis is developed hypothesizing that the extraction force resulting from the the pull-out test is influenced by the surrounding stress state due to the nature of the structure. In other words, the obtained tensile force will depend on the prestressing state. To analyze the behavior alternative geometries are considered with the purpose of optimize the effect of prestressing on the pull-out test. The final results



(a) Fossano bridge - Italy



(b) M -527 road bridge - Spain



(c) Ynys-y-Gwas bridge - South Wales



(d) Speedway bridge - United States of America

Figure 1: Bridge collapses caused by loss of prestress. From [13],[14],[16],[8]

will be conducted into a recognition of the the most appropriate setup to carry out the test.

Additionally, the conjecture of the contribution of the prestressing state is herein analyzed through a finite element analysis and the theoretical approach is based on the Mohr Coulomb criterion. This principle relates the maximum shear stress supported by an element with the induced compression state. The thesis is conducted under the linear analysis considering the linear elastic material behavior.

The thesis is devised in five sections. The first chapter is dedicated to the theoretical framework required to explain the pull-out test and the normative involved to process the information obtained. On the second chapter is explained the experimental test performed. This section is divided into the characterization test of the employed samples and the development of the before mentioned technique.

The third chapter consists on the numerical modeling of the problem by means of the finite element analysis (FEM). Eleven different geometries of the problem are assessed and the mathematical calculations are formulated with the help of Matlab. The problem is divided into several load cases and they are treated separately.

The fourth chapter describes the results and discuss the analysis behind them. There are shown not only the numerical modeling results but also the experimental test characterization outcomes. Finally the conclusions chapter is developed suggesting the most suitable set up to carry out the pull-out test in order to determine the real strength of the concrete.

2 Pull-out test

The mechanical properties of a material in a structure presents few variations on time. As an overall behavior the trend relates the properties with a decremental performance due to influence of external and inherent factors. Since those fluctuations on the quality could affect the stability of the structure, specific test must be conducted. Additionally a constant monitoring on time should be considered compulsory.

Non-destructive tests (NDT) have been increasingly used in the last few decades for the assessment of in situ quality and integrity of concrete elements. Especially for estimation of in situ concrete compressive strength this test presents some significant advantages such as speediness of operation, immediate availability of results, less costs and, above all, less damage for concrete elements under tests. The before-mentioned techniques are specially designed for estimation of the in situ concrete compressive strength and do not allow a direct quantitative measurement of such property. Therefore, it would be necessary to develop and use empirical correlations. [10]

Moreover, it is important to consider that if practical relationships are used, there is an uncertainty present. The ambiguity can be considered as a drawback of the methods, but if the correlations are firm, the accuracy improves. Each technique involves a different concept in terms of reliability, degree of destruction caused, speed of tests, immediacy of results and cost involved, for that reason must be selected the most appropriated considering the requirements of the monitoring procedure.

The pull-out test is recognized as the most accurate test within the ND tests [10] and this is the experimental technique applied on the thesis.

2.1 Description of the method

The methodology of the pull-out test consists on the determination of the pull-out strength in hardened concrete. This is achieved measuring the force required to pull an embedded metal screw inserted on a concrete test specimen or even on a real structure.

The experimental procedure is developed employing a jack reacting against a bearing ring. The annulus acts as a constraint, and, integrated with the bolt dimensions, determine the failure geometry. The tension force at the moment of the extraction is taken. The bolt could be either cast into fresh concrete or installed in hardened concrete, it will depend on the aim of the study case.

The described tensile force can be correlated through equations to the compressive strength of the concrete. The magnitude is affected by parameters such as the bolt properties and dimensions, depth of embedment, bearing ring dimensions, type of aggregate. Hence the conditions must be established before the test. The type of aggregate is an important consideration since could generate local effects during the test and cause alterations of the result.

The installation process on the concrete will depend on the nature of the test. Dealing with existing structures, the post installed method is employed. The hole is performed after the hardening process. The necessary equipment to develop the test is

- Core drill

- Steel bolt

- Bearing ring

- Extraction pump

The Figure **2** explain the schematic procedure for post installed pull-out test. Initially is drilled a perpendicular hole with specific dimensions in a concrete specimen. The sample must contain flat surfaces to ensure a suitable working avoiding the inaccuracies. Secondly there is disposed the steel bolt inside the hole guaranteeing the perfect embedment and the bearing ring is placed around the inserted bolt. Finally the system is loaded by a uniform rate until reach the maximum tensile force at concrete failure.

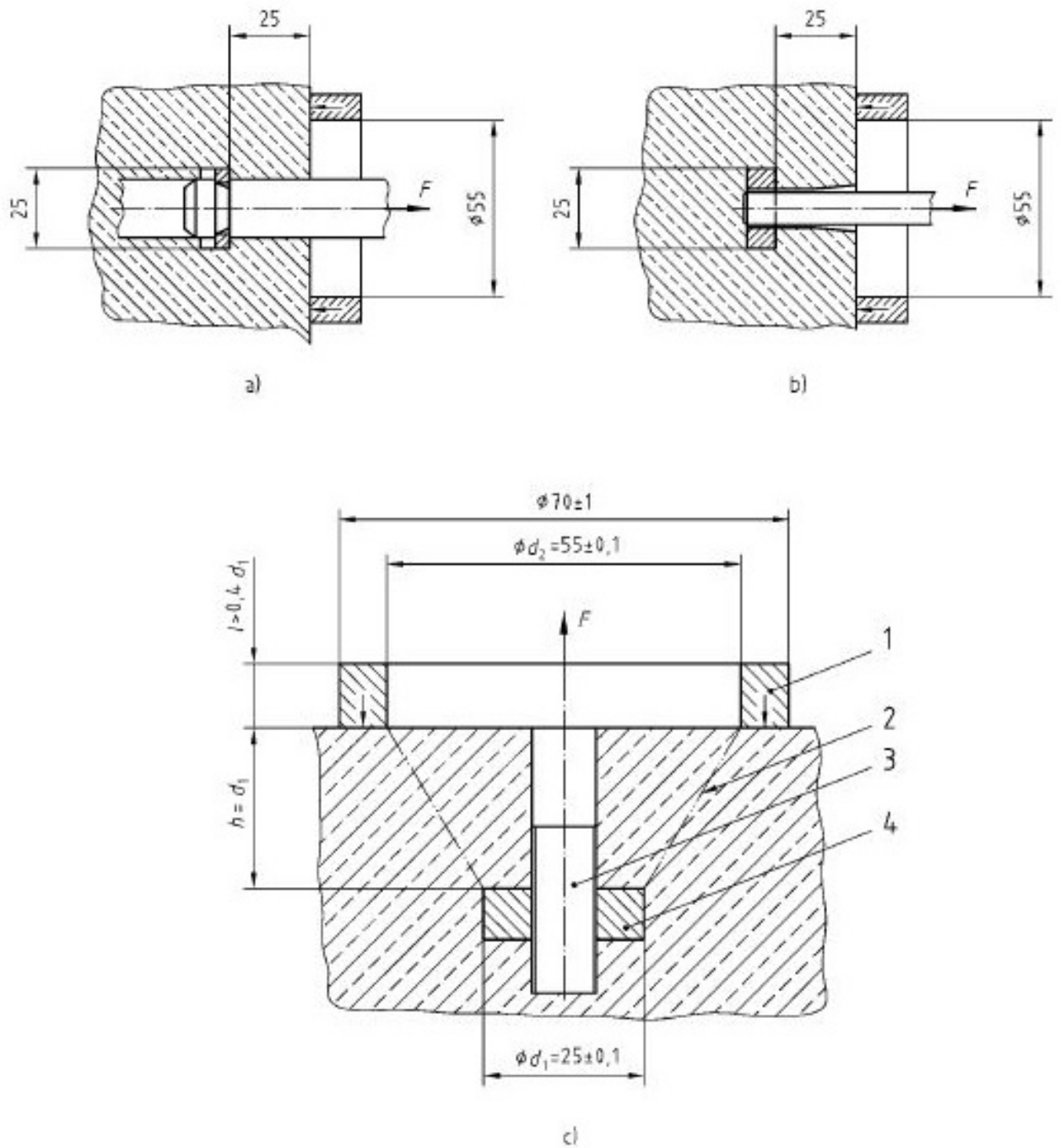


Figure 2: Schematic procedure for post installed pull-out test [4]

The typical shape failure is a truncated cone determined by the diameter of the bolt at the base and the bearing ring at the top, as is shown in c). Making reference to the P. Bocca (1979) article [12], there is a simple representation of the stresses

along the conic failure surface during the extraction phase on the specimen. To explain that the Figure 3 is employed.

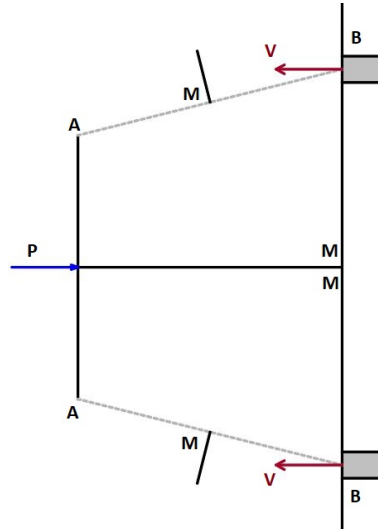


Figure 3: Scheme of the mechanism of failure on the concrete

The AB zone of the concrete , due to the applied load P and the reactions V from the bearing ring, are schematized as a rolling constraint with the axis on the opposite direction of the extraction. The tensile zones, perpendicular to the compression one are represented by the M-M straps.

A symbolic representation of the previous scheme is done by the Figure 4 Clarifying, with AB are represented the compressive zones while MM are the tensile zones.

There are four particular cases that allow the comprehension of the obtained results with the pull of test. Those cases associate the friction angle of the material φ with the α angle defined geometrically.

- $\alpha < \varphi$ the movement of the mechanism is withstand by the friction angle, then, the force P is absorbed entirely for the AB zones while the traction stress on the straps are zero. The rupture is reached by the deformation of the compressed concrete.

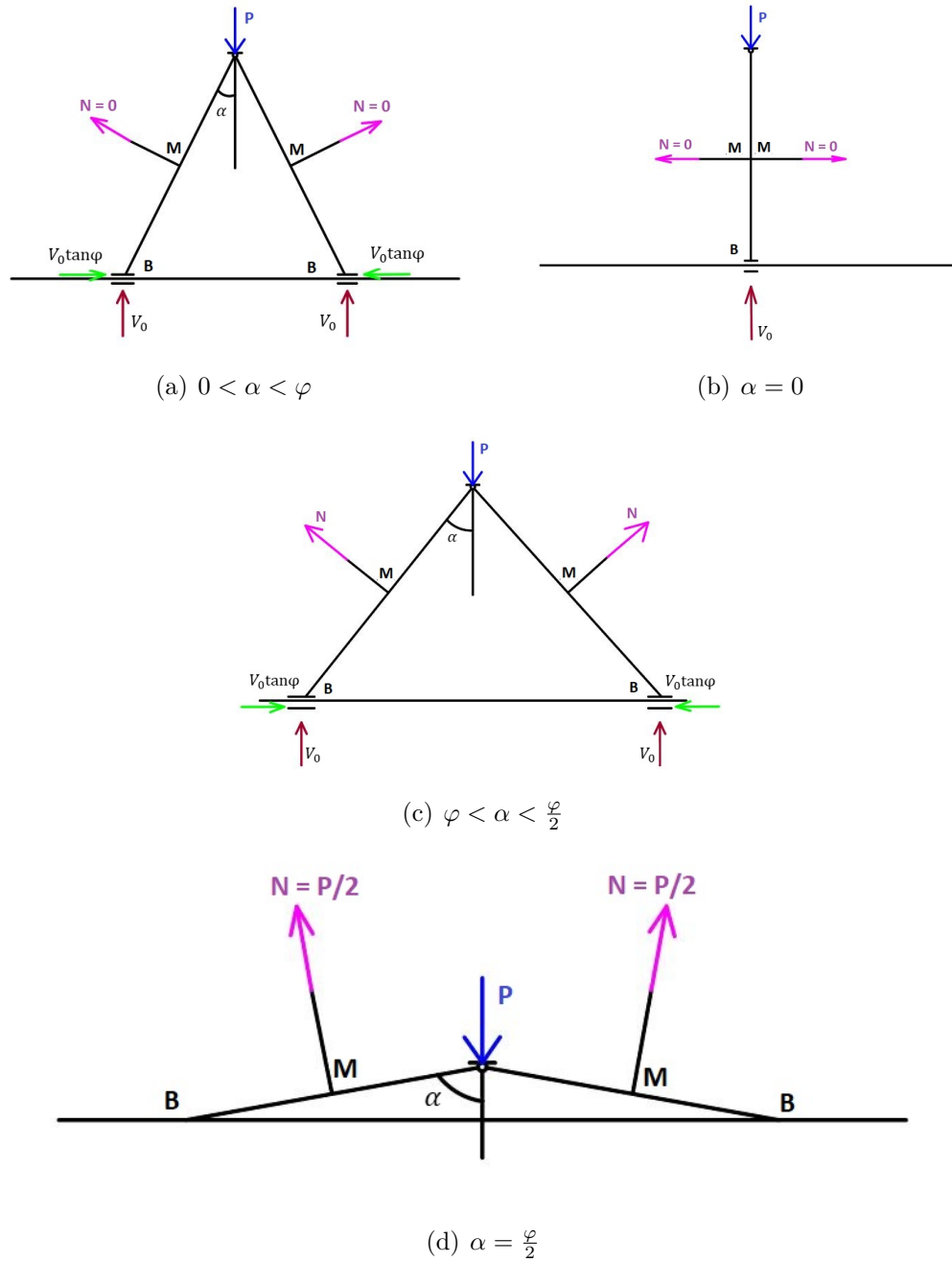


Figure 4: Mechanism of failure of the concrete due to the variation of the angle of the conic surface.

- $\alpha = 0$ Consider the same analyses before mentioned and the failure occurs due to the compressed concrete.
- $\alpha > \varphi$ there is a displacement on the supports B. The friction reaction V_o is defined as the Eq. 1

$$V_o \times \tan \varphi \quad (1)$$

Furthermore there are present either stresses on AB or on the straps MM. The rupture is reached by tension or compression.

- $\alpha = \frac{\varphi}{2}$ the failure is reached by only tension because the force P is supported completely by the straps.

For the purpose of the tesis, the procedure of the pull-out test is complemented by the application of an additional compression stress. This load simulates the prestressing effect in the concrete. The application is carried out by the compression testing machine as is shown in the following figure 5.

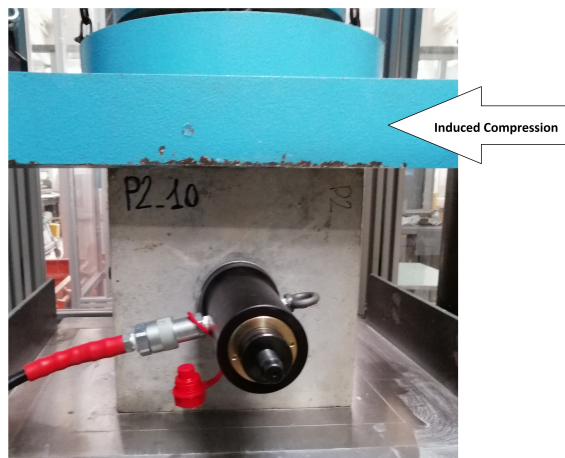


Figure 5: Prestressing stress induced by the compression testing machine

2.2 Concrete strength vs Pull-out force

The pull-out test is ruled under the ASTM C900 -15 international standard. When a stress calculation is desired it is possible to compute a nominal normal stressed on the assumed conical fracture surface. The performance is explained by the ASTM C900 -15 normative by means of the division between the pull-out force and the area of the truncated cone. Subsequently the result is multiplied by the sine apex angle.

The aforesaid procedure is illustrated by means of the Eq. **2,3, 4** and **5**.

$$f_n = \frac{P}{A} \times \text{sine}\alpha \quad (2)$$

$$\text{sine}\alpha = \frac{d_3 - d_2}{2S} \quad (3)$$

$$A = \pi S \frac{d_3 + d_2}{2} \quad (4)$$

$$S = \sqrt{h^2 + \frac{d_3 - d_2}{2}^2} \quad (5)$$

where:

f_n = Nominal stress in MPa

P = Pull-out force in N

α = Truncated cone apex angle

A = Failure surface area mm^2 d_2 = Diameter of the pull-out insert head in mm

d_3 = Diameter of the bearing ring or large base diameter of assumed conic surface in mm

h = Height of the truncated cone from the insert head to the surface in mm

S = Slant length of the cone in mm

The calculation performed by means of these equations gives an average value of the normal stress on the assumed fracture surface. Nevertheless, because the state of stress on the truncated cone is not uniform, the it is considered as fictitious value. The magnitude is useful when comparing pull-out strengths obtained with different test geometries that fall within the limits of this test method. [4]

3 Experimental test

The experimental test chapter corresponds to the performance of several pull-out test carried out on two types of material with two different feature geometries. The arrangement of characteristics is referred to the geometry of the bolt employed on the test. There are other tools that affect the test behavior as the bearing ring diameter, this is considered too. The samples were tested in the laboratory of DISEG (Department of Structural, Geotechnical and Building Engineering) in Politecnico di torino.

The initial step consist on the characterization of the specimens and this is explained in the following subsection.

3.1 Uniaxial compression test

As was said before, previously to the realization of the pull-out test the determination of the mechanical properties of the samples was required. This is performed with the aim of determine the compression strength of the material employed and the elastic modulus associated. For that, the uniaxial compression test was developed.

As the British standards BS EN 12390 - 3: 2009 demands, to determine the maximum axial compression strength that a specific sample of concrete can withstand before failing, its required to employ a specific sample with predefined dimensions. The size of the specimen will depend on the particular shape selected shape. The test can be performed through cylinders or cubes. For the aim of the thesis the cubical geometry is employed with 30 x 30 x 30 centimeters of length.

The first step consist into register the weight of the tested cubes, then the sample is disposed inside the compression test machine and assuring the cleanliness of machine surfaces and removing any kind of material on them, the test is performed by selecting a rate of loading and applying it perpendicularly to the upper and lower faces of the sample. The procedure continue until the sample reach the failure state.

The procedure described above is shown on the Figure 6

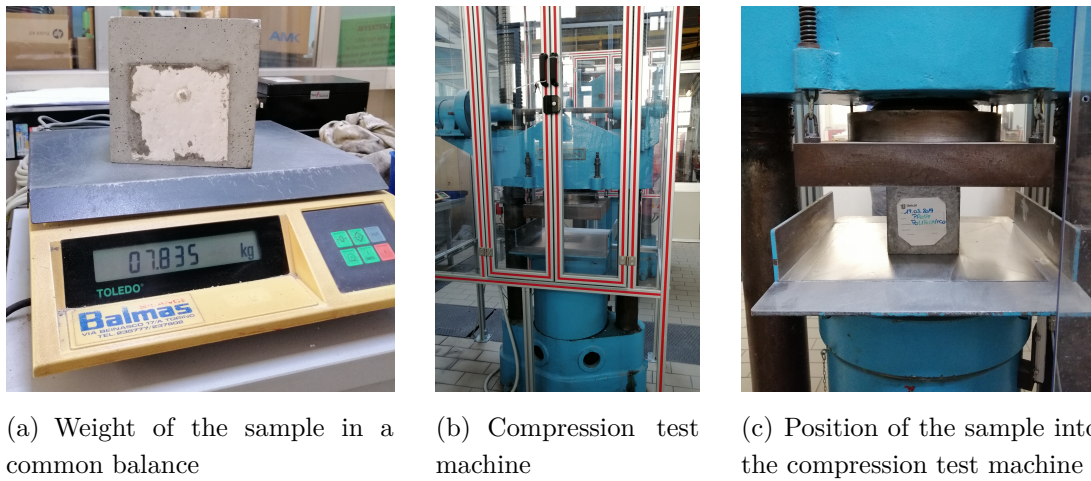


Figure 6: Uniaxial compression test performance

According to the standard there are some failures that are acceptable or refutable according to the shape or the features developed on them. To exemplify the afore-said cases the Figure 7 is employed. On the illustration are present three types of satisfactory failure on the concrete specimens. Satisfactory means acceptable.

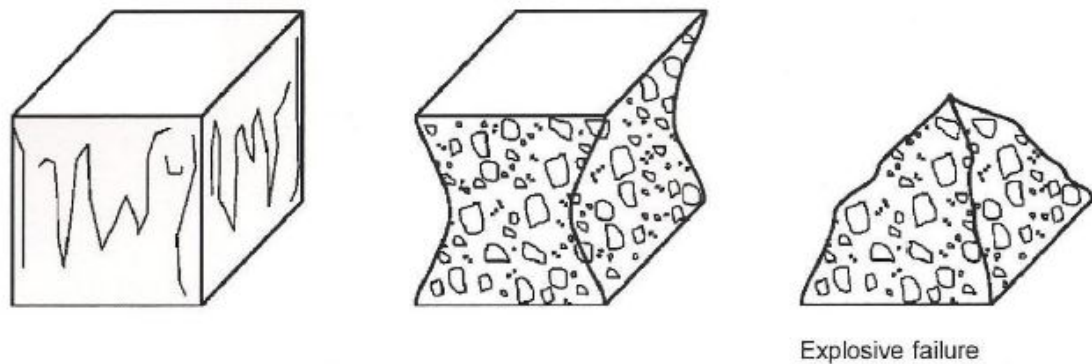


Figure 7: Satisfactory failure of concrete specimens [4]

And also in Figure 8 are present the cases when the failures are considered by the code as unsatisfactory. This means that the test must be repeated because the result is refutable.

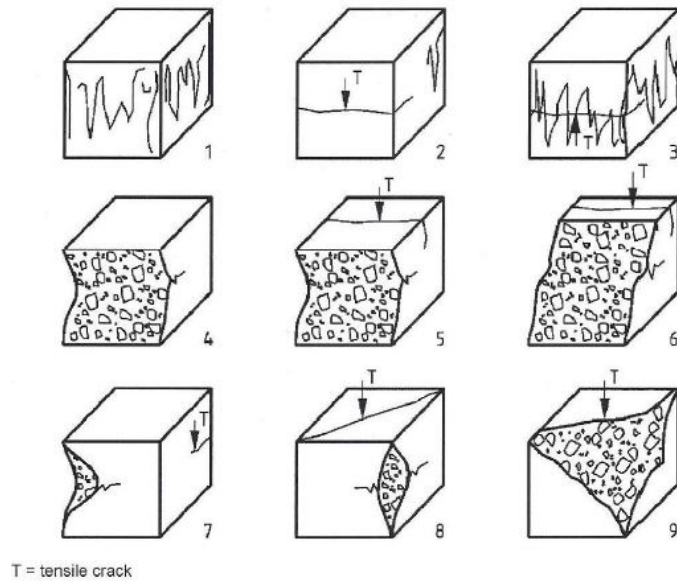


Figure 8: Unsatisfactory failure of concrete specimens [4]

Figure 9 shows the results for the three specimen employed.



(a) Sample 1



(b) Sample 2



(c) Sample 3

Figure 9: Uniaxial compression test samples at rupture level

On the other hand, as was before mentioned the failure is reached and the correspondent value is taken to determine the resistance. The Eq. 6 express the relationship between the area and the pressure induced by the compression machine.

$$f_c = \frac{F}{A_c} \quad (6)$$

Where:

f_c = compression strength of concrete in MPa N/mm²

F =maximum load at failure in N

A_c = cross-sectional area of the specimen on which the compression force acts in mm²

In addition, once the strength of the concrete is determined, other properties can be derived by employing few correlative equations that are also considered in codes. One feature of interest for analysis like the numerical modeling explained in the previous chapter is the elasticity modulus or young modulus, and can be obtained through the Eq. 7 and 8

- MC 2010 [6]

$$E_c = 22000 \left(\frac{f'_c}{10} \right)^{\frac{1}{3}} \quad (7)$$

- ACI 318 [1]

$$E_c = 4700 \sqrt{f'_c} \quad (8)$$

3.2 Pull-out test performance

Once the characterization procedure is finished, the pull-out test is performed. For that, several specimens are disposed and few load cases are defined. The procedure consist on the installation of a metallic bolt with an enlarged end into one face of the cubical specimen, this bolt is defined according to the requirements of the project and also considering the material characteristics, in that way the correct development of the test is ensured.

When the screw is properly disposed, the bearing ring and the extraction pump are located and the extraction procedure starts. The test is finished when the failure occurs and the value of the pressure at rupture is registered. The before mentioned resultant value is changed into a extraction force through different

equations, generally specified by the manufacturer of the extraction pump. For this case the Eq. 9 was employed:

$$F_r = -1.1434x10^{-7}(P^2) + 1.7503x10^{-1}(P) + 2.4062x10^{-3} \quad (9)$$

Where:

F_r = Extraction force in kN

P = Pressure at failure in bar

Figure 10 shown the experimental procedure performed for one sample.



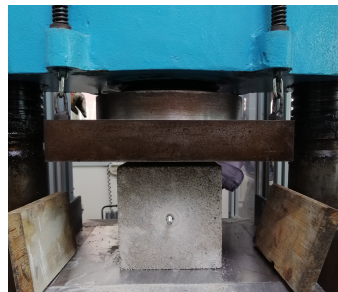
(a) Boring



(b) Installation



(c) Installed bolt



(d) Sample positioning



(e) Extraction pump



(f) Extraction procedure

Figure 10: Pull-out test development

The above mentioned procedure was described without considering an induced external force. For the aim of the thesis and in order to simulate the prestressing stress state on a prestressed concrete section, a compression force is added varying from 0 MPa until 30 MPa. In addition, the test is replicated for five of the six faces of the cube taking into account the aforesaid loading cases.

The compression testing machine used for the Uniaxial compression test is used to recreate the loading cases. In the Figure 11 is shown the disposition of the sample inside the compression testing machine.

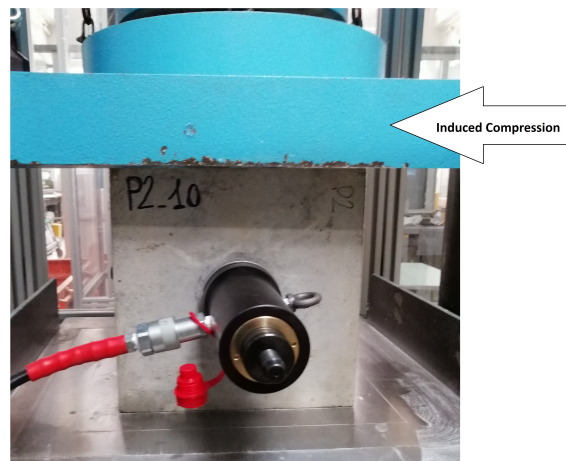


Figure 11: Cubic specimen under 10 MPa of uniaxial compression

The test is developed considering two type of screws, there are shown in the Figure 12

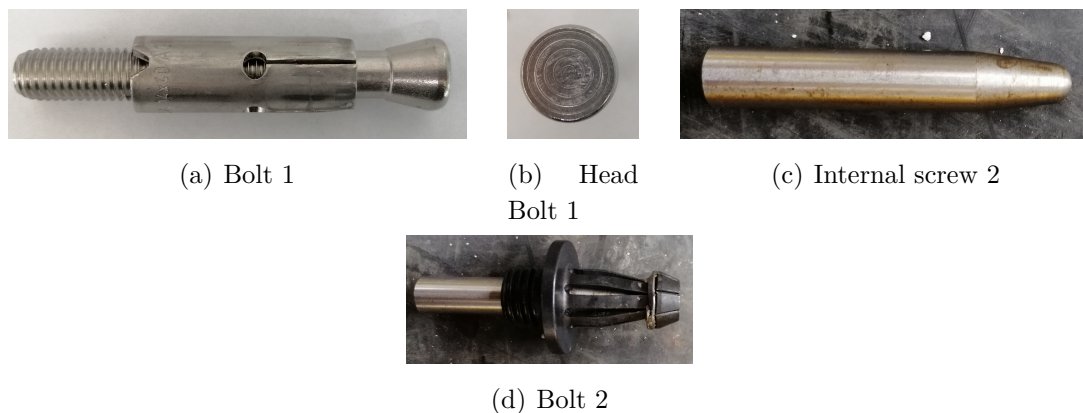


Figure 12: Bolts for the pull-out test

And the bearing ring employed for the test is shown in the Figure 13



(a) Bearing ring 110 mm diameter

(b) Bearing ring 55 mm diameter

Figure 13: Bearing ring geometry

The geometry description of each of them is shown in the Table 1

Geometry Bolt 1		
Diameter [mm]	Height [mm]	Bearing ring diameter [mm]
14	35	110
Geometry Bolt 2		
Diameter [mm]	Height [mm]	Bearing ring diameter [mm]
18	25	55

Table 1: Geometry of the bolts

According to the information gave before, the pull-out test will conducted into two different results, because the geometry is considered the fundamental parameter to determine the shape of the failure cone. In the fist case the cone is higher than the second one either by the height of the screw or by the diameter of the bearing ring. In the Figure 14 is shown the failure cone obtained for the geometry one.

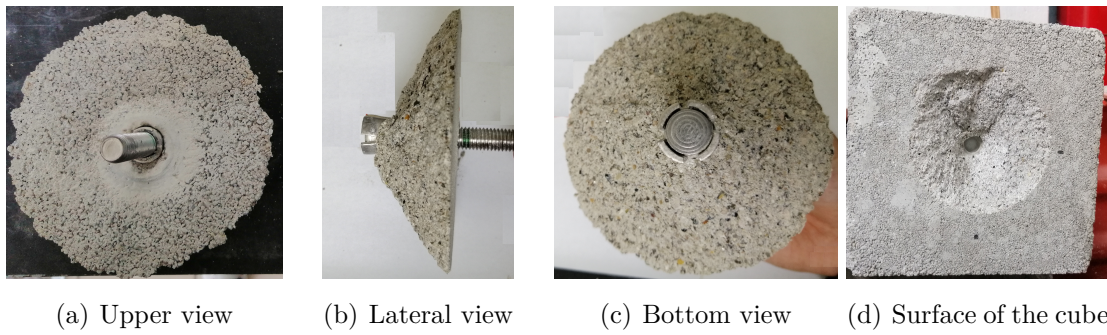


Figure 14: Failure cone for geometry 1

Now the failure due to the second geometry configuration is shown in the Figure 15

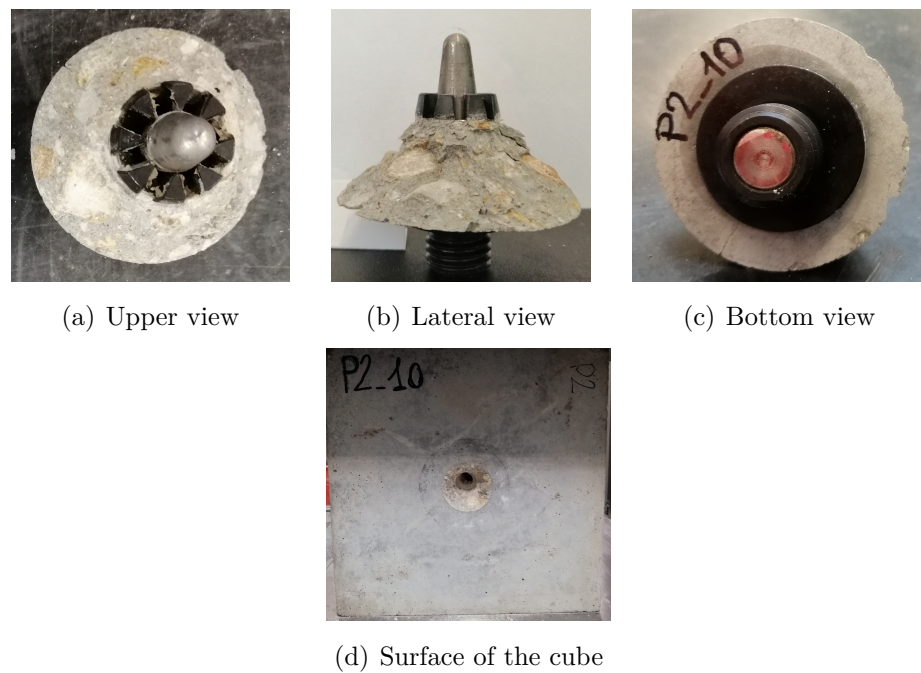


Figure 15: Failure cone for geometry 2

4 Numerical modeling

The main goal of the thesis lies on the employment of a numerical modeling to identify the most suitable setup to carry out the pull-out test. In that way can be determined if the result of the test is influenced by a surrounding stress state due to a prestressing state. To develop this procedure a Finite element analysis (FEA) is used.

An engineer designing any kind of structure will need to know how the proposed structure will behave under a determinate load, to understand it the equation describing the distribution of structural stresses must be known, but due to the complexity of the analysis they cannot be directly solved because the complicated shapes and properties that are being studied. However, the equations can be solved if the problem is subdivided replacing the single complex shape into an approximately equivalent network of simple elements, and this method is called Finite Element Method (FEM).

FEM is a numerical method to solve engineering problem using a subdivision of the solution domain into elements of simple geometrical shape, called discretization, and a set of basic functions written as a linear combination creating a finite space, applied to each element and then rearranged to compute the entire problem. [15]

The overall pattern of elements above mentioned is referred to as the finite element mesh, a predefined property of the model with an unique template to each new problem. The initial step is to design it, and for this it is necessary to decide primary what kind of elements will be used, such as triangles, squares, tetrahedra, hexahedra, in one, two or three dimensions, because the accuracy of the calculation is going to depend on the number of elements chosen to have in the mesh, the more elements we have the smaller each one will be and the more accurate the results.

Nevertheless, more elements necessarily implicate more calculations, then just enough elements to give adequate accuracy are designed to develop the calculation within a reasonable computing time. The essentials selected to represent the model are composed by a quantity of nodes according to its physical nature and are associated by a finite number of degrees of freedom. In general, the nodes

inside the mesh are free to move both horizontally and vertically, the exception will be those points around the outside edge that are established related to the description of the physical problem and the boundary conditions determine its behavior.

Finally, we must specify the elastic properties of the material, for concrete the young modulus and the poisons ratio are fundamental parameters, and the loading regarding the problem like concentrated, distributed – by area or length – loads. The finite element analysis as is explained by [15] derives the final solution by starting from relationships expressing the displacement of the nodes as function of the coordinates, this represents the starting point to solve a matrix configuration with n number of equations with the fundamental laws of mechanics. The first step consists to relate the above mentioned displacements to stresses, then the stresses to strain energy, this to potential energy and finally obtain a system of equation for the complete element.

The mathematical basis of the analysis is the analogy with the equation of a spring and represents the mode to obtain the stiffness matrix of the element instead of the displacement matrix. The last procedure is carried out for every element in the mesh and the main goal is to combine all these individual matrixes into a single large one representing the stiffness of the whole system. The matrixes could be combined by a simple merging technique done concurrently with the process known as reduction but also the substitution concept can be employed, it will depend on the particularities of the method.

The results can be shown in different manners, one of them is a contour diagram with the areas of greatest compression and tension or any kind of action in any direction with a specific band color. This process requires vast numbers of individual calculations to be done and for this reason can only be done on the computer. Few finite element software allows the reproduction of the results by a continuous animated sequence showing the behavior of the elements while the load moves across it or is changed.

The main advantage of finite element method is the ability to work with arbitrary shapes, this overcomes many of the limitations of older numerical techniques and gives the method of flexibility comparable to the use of physical models but with-

out their limitations. For example, different materials can be studied easily by specifying different material properties as programmed data properties that are difficult to vary in physical models. The finite element method can be applied to the widest possible engineering problems, and undoubtedly it can be said to lead the field in modern engineering computing methods.

For the reasons gave above the finite element analysis is adopted to describe the behavior and the contribution of the prestressing stress in the concrete specimens, with the aim to represent the real behavior of a prestressing structure such a bridge during the pull-out test. The finite element software used is called *LUSAS*

4.1 LUSAS finite element analysis software

LUSAS is a finite element analysis software application developed by LUSAS ltd company for the analysis, design and assessment of all type of structures. Through its functions can be carried out linear static analysis of a simple structural frame, a dynamic analysis of a masonry or concrete building, soil-structure interaction or even a nonlinear analysis which includes geometry, material and contact modeling.

The above mentioned software is available in a different range of levels according to the requirements of the project, such as Analyst plus, Composite plus, Civil and structural plus and Bridge Plus, using the same interface, shown in the Figure **16**, but with specific facilities, load application and combination of load case results. The services will depend on the type of analysis performed, like 2D/3D frame elements with linear static analysis, 2D/3D surface, volume and other elements with linear static and linear modal dynamic analysis or advanced high-performance elements analysis using the appropriate configurations.

The models elaborated through this software, are formed of layers where the visibility and properties of each layer can be controlled and accessed, assigning by the drag and drop technique and removing the attributes easily. In the Figure **17** is shown an example of the tree view list, where the created and assigned features like layers **a)**, attributes **b)** and loading cases **c)** are exhibited.

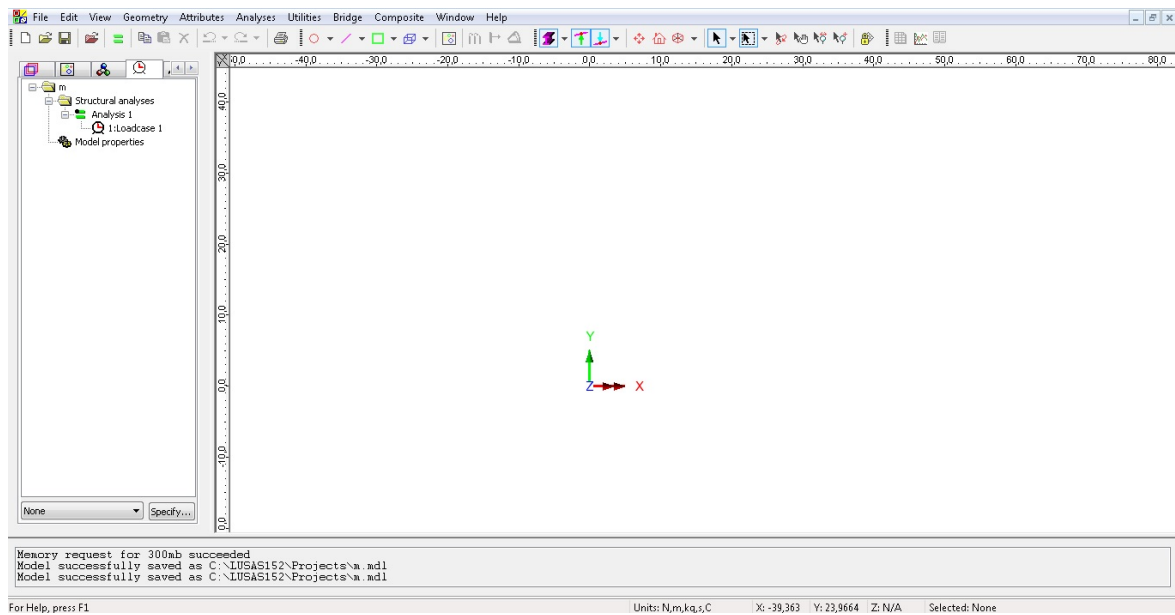
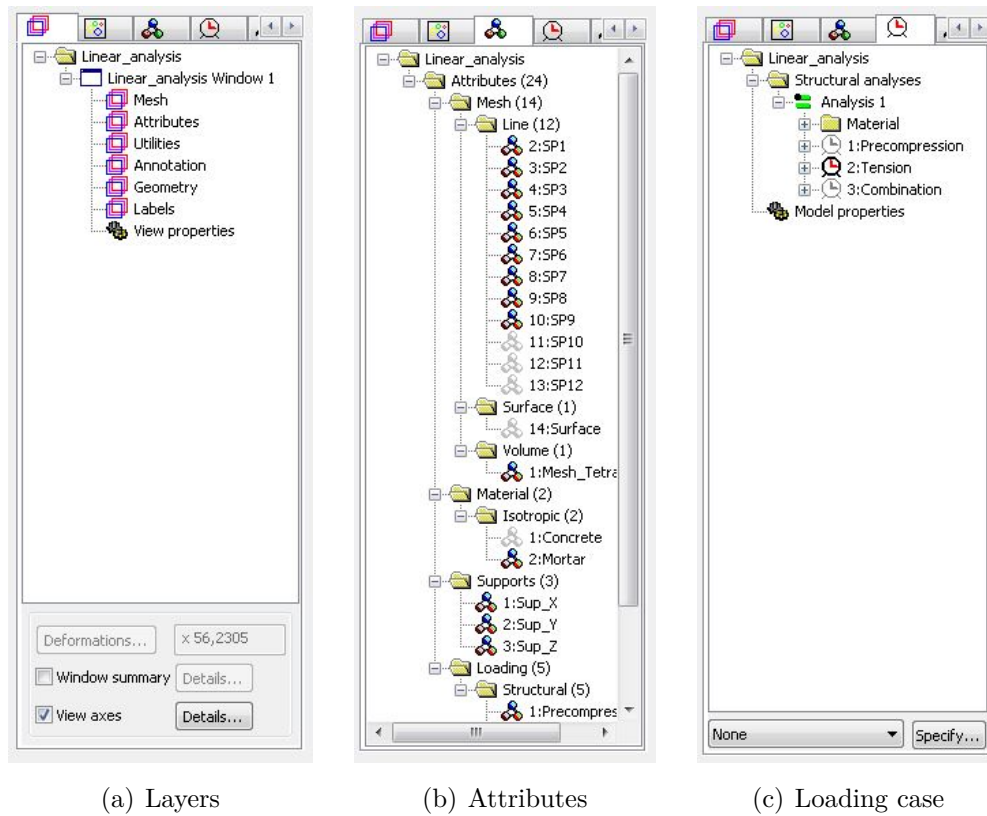


Figure 16: LUSAS Interface



(a) Layers

(b) Attributes

(c) Loading case

Figure 17: LUSAS features

One possibility that LUSAS offers to the registered users is the capability of the software to import/export CAD files, a good tool to design points, lines, surfaces and volumes using a feature-based geometry method and allowing the workers the implementation of a very well known program in the civil engineering field. Once the CAD model is inserted, the properties such as thickness, material, loading and mesh/element type are defined and assigned.

Finally, the program employed before is considered as a good option to develop the numerical analysis of the thesis, due to the easy handling of the platform and the advantages in terms of the mesh definition that it gives even if its been employed the academic licensed version.

4.2 Modeling procedure

The numerical modeling is developed by the use of different geometries of the features involved on the pull-out test such as the diameter of the bearing ring and the height and diameter of the bolt. Considering two types of them as reference and exploring multiple combinations, the idea behind this work is to maximize the effect of the prestressing by means of the pull-out test identifying the most suitable setup to carry out the test.

The first step consist on the identification of the geometries that are going to be pointed out as the reference shape. In the Figure 18 can be appreciated the first arrangement.

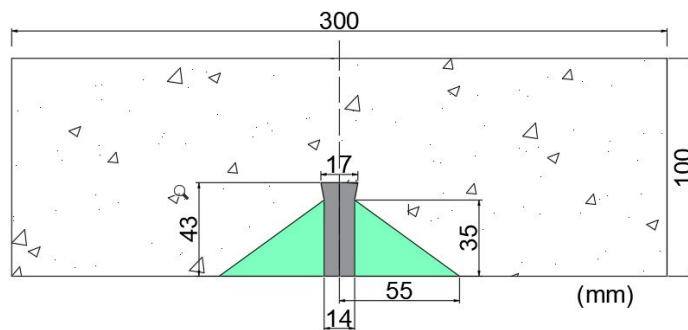


Figure 18: Model 1

In the same way, the Figure 19 show the second model, considered as the second base configuration.

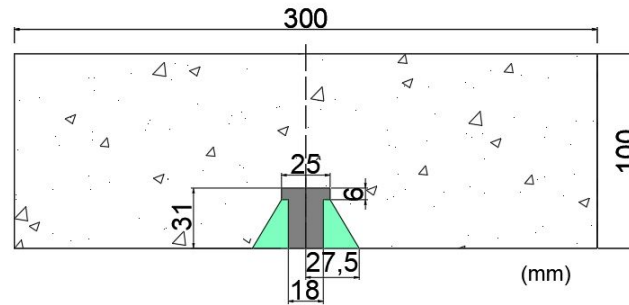


Figure 19: Model 2

The following step consists in the definition of the final scheme that is going to be inserted on LUSAS to exemplify the real problem. For instance several assumptions can be considered and a simplification of the problem can be performed. Dealing with a linear elastic problem with isotropic and homogeneous material properties, and also with a symmetric shape, the specimen can be divided and analyzed in a quarter of the original condition.

As well as the entire cube is treated as a portion of it, the height of the sample is reduced into 100 mm x 100 mm x 100 mm, since there is a premise explaining that the behavior of the stresses, once a depth of 4 times the height of the bolt $4h$ is passed, is almost negligible. Therefore a third is sufficient to represent the performance of the material due to the extracting and compression force.

According to the mechanism of failure described on the pull-out section of the thesis, the expected cone of failure represents the fundamental point on the analysis. Subsequently, there is a particular attention on its design and the obtention of the information on the volume. To guarantee the competent coverage of the volume it is subdivided into 4 portions delimited by 5 lines that bring all the information required.

In addition, all the models were designed by dividing the whole geometry in several parts, thus ensuring the description of a better performance by means of the assigned mesh. The refinement in the mesh is proportional to the level of detail that is demanded by the problem, in this case, the closer to the hole the more detailed the mesh should be.

In the Figure 20 is shown the resultant model 1 considering all the postulations above.

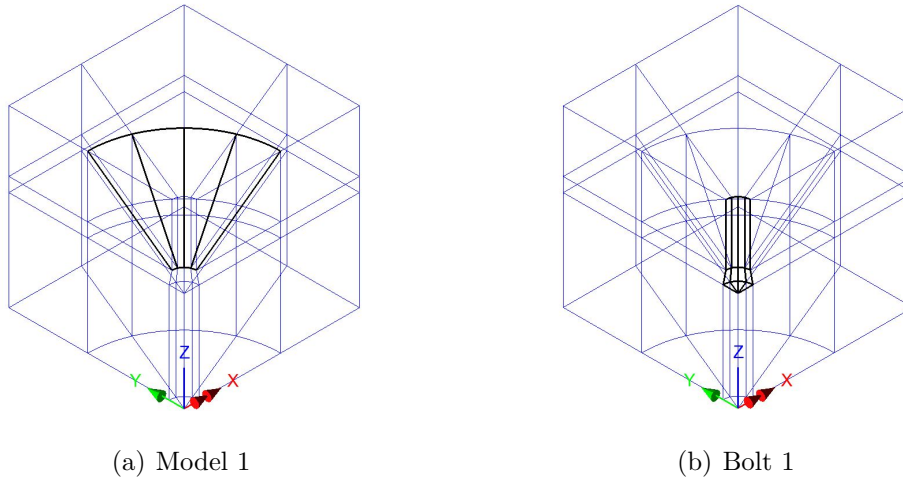


Figure 20: LUSAS model 1

In the same way than the previous exemplification, the Figure 21 shown the result model for the second reference geometry.

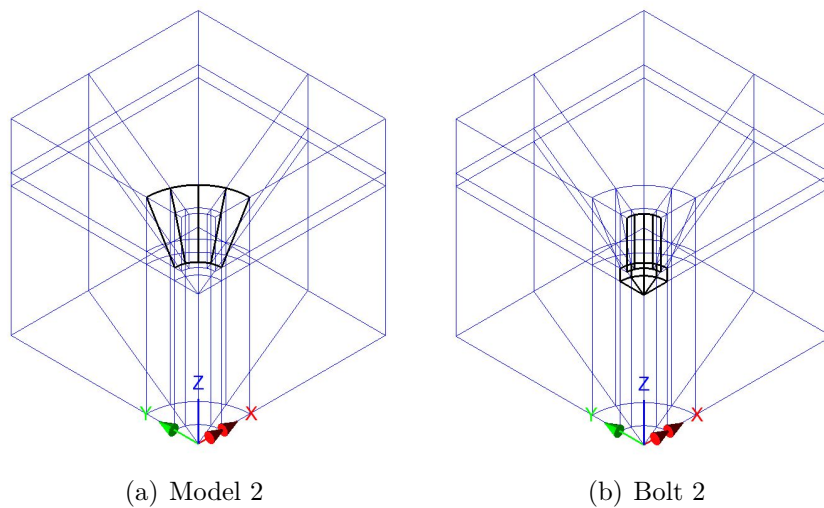


Figure 21: LUSAS model 2

To reach the final result of the of each of the models, it was necessary to defined the following features.

- **Geometry**

The geometry item consist on the employment of points, lines, surfaces and volumes to define the whole volume. As the problem deals with symmetric geometry even if it is being developed a quarter of the system, it is enough to define 45° degrees of solid and then apply the mirror command around the z axis.

For the creation of the failure cone demarcated by the diameter of the bearing ring and the diameter of the bolt, the lines are disposed any 22.5° to ensure the symmetry even on that.

The program includes few options that facilitate the elaboration of the solid, such as the volume by extrusion, an advantageous tool that allows the construction of the volume starting with a particular surface previously created.

- **Attributes**

Define the attributes corresponds to the designation of all the properties that the cubic has either intrinsically or determined by the evaluating situation.

- *Mesh*

The discretization process is carried out on the relevant features that make up the model such as lines, surfaces and volumes. Talking about the lines, the Figure **22** show an example of the configuration assigned, because, as the length changes depending on the shape of the volume and the position on the block, the spacing and distribution is transformed too. Nevertheless all the models have the same structural element type: None.

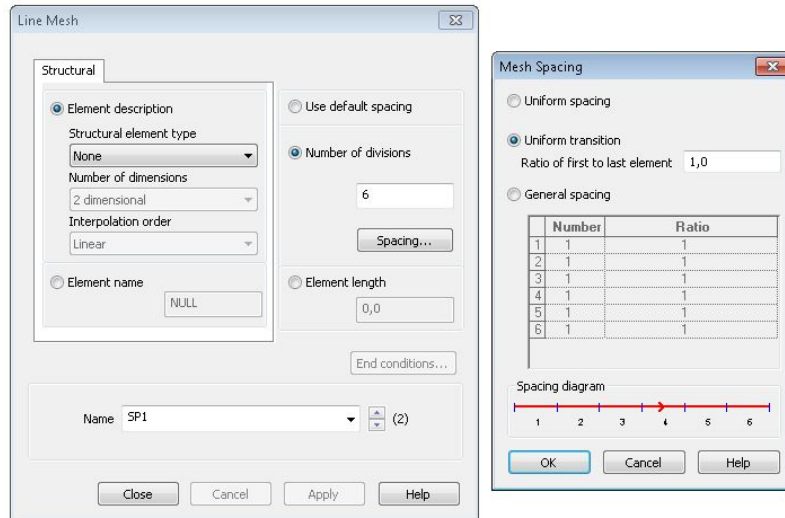


Figure 22: Models line mesh

In conformity with the LUSAS manual, the none element type generates no structural elements on the line. The mesh attribute is used purely to control the line discretization. However there are many different options as can be seen in the Figure 23

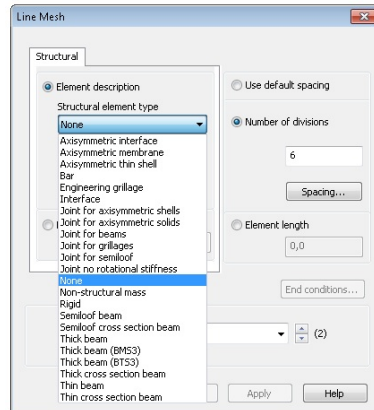


Figure 23: Structural elements type on a line - Lusas

Once the meshing of all the lines includes on the block is finished, the volume mesh can be defined. There is necessary to create just one mesh for all the subdivisions. Since the volume is formed by 3D continuum elements, These type of elements are tetrahedral, pentahedral

and hexaedral solid elements available to model stress - fields. In the Figure 24 are shown the elements described above.

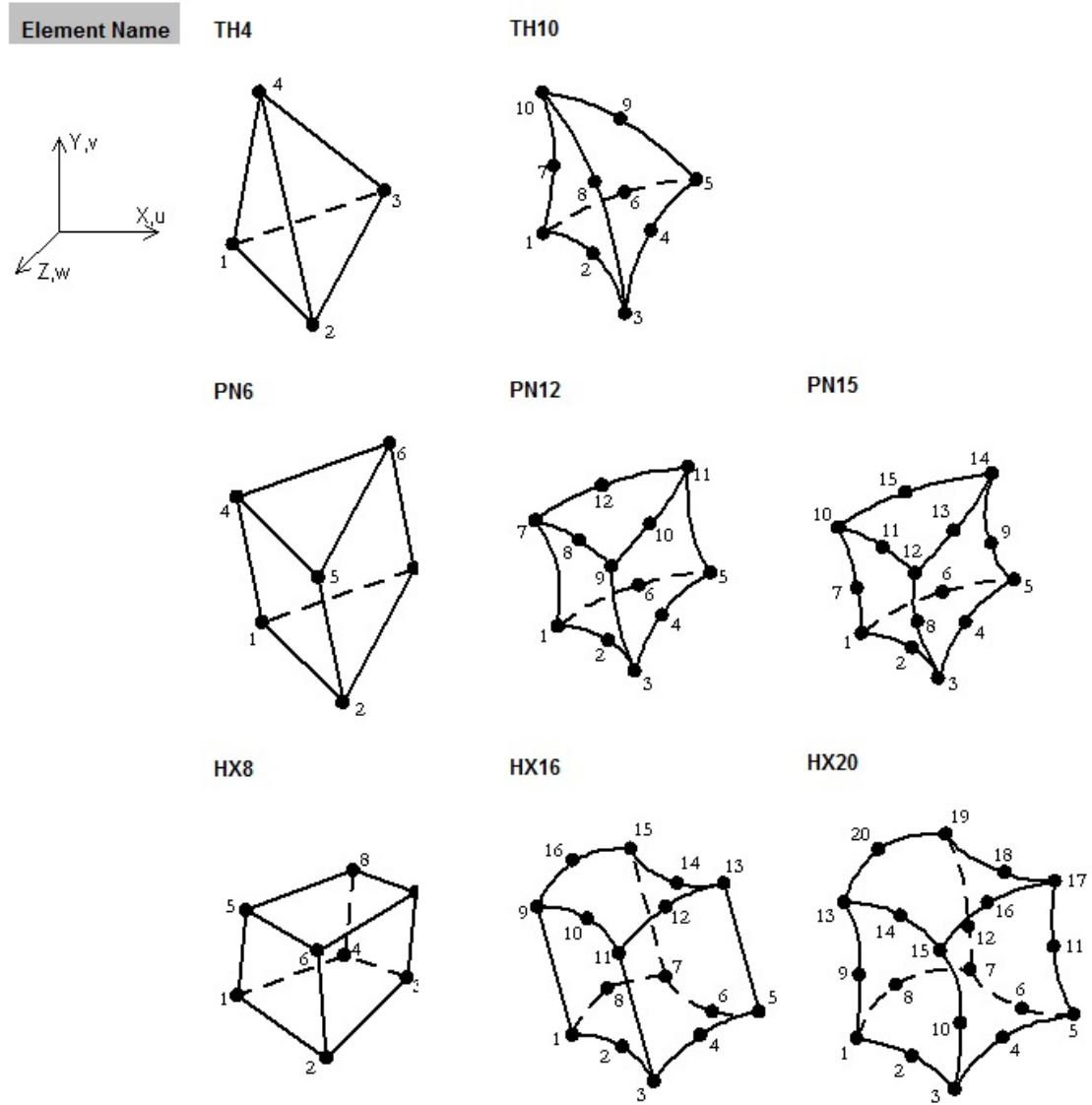
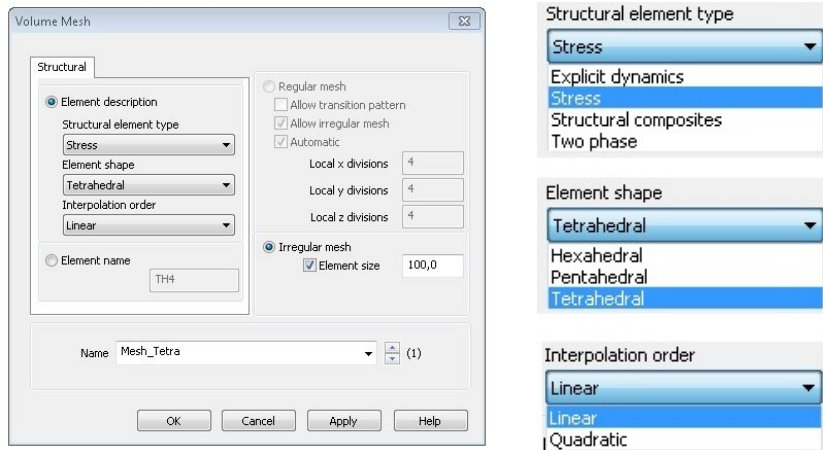


Figure 24: Structural elements type on a line

According to the problem requirements, the tetrahedral element shape TH4 is enough to cover the curved boundaries. This feature is conformed by four nodes and all of them are numerically integrated either by quadratic or by lineal integration. For this case is selected the linear integration. This information is shown in the Figure 25

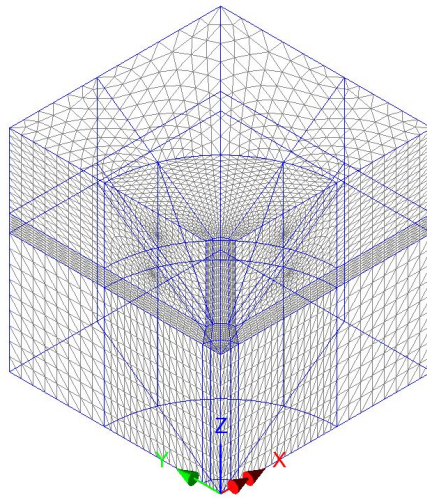


(a) Volume mesh

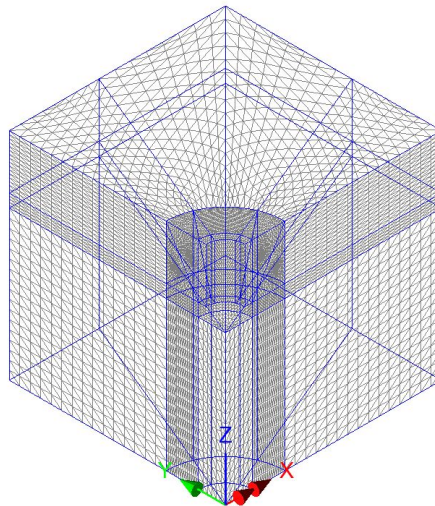
(b) Element description options

Figure 25: Volume mesh assignments

The final arrangement of the mesh depends on the degree of detailed wanted for the project, then the element size will increase or decrease as the guidelines. In the Figure 26 is shown the resultant mesh for the reference models.



(a) Mesh model 1



(b) Mesh model 2

Figure 26: Final models

Additionally, the geometry subdivision generates an influence on the mesh too. This is because LUSAS estimates the Jacobian when the assignment of the mesh is performed. Furthermore, it must be guaranteed.

– *Material*

Dealing with concrete, the material can be considered as an isotropic

an homogeneous for the purposes of structural calculations and design. However, in a micro structural scale there are features than produce an alteration of this behavior but its not the case. Furthermore, in the Figure 27 are shown the parameters assigned to the models.

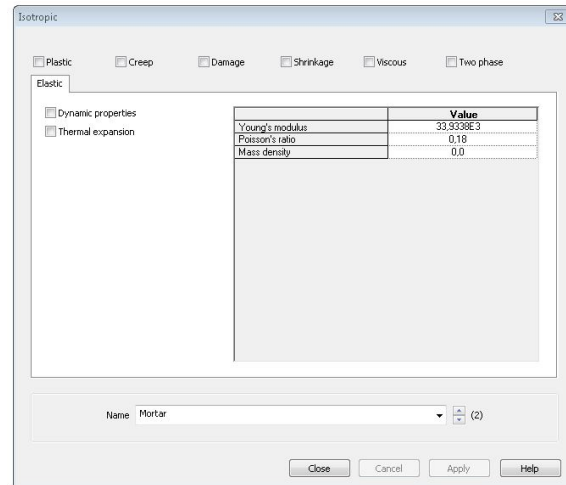


Figure 27: Material properties of the models

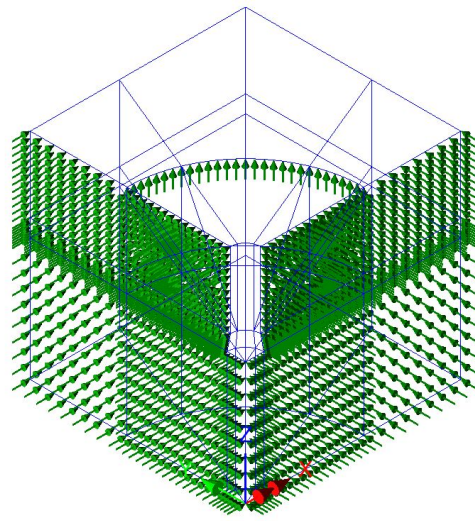
The parameters above are based on the experimental test performed at the laboratory and explained on the previous section. The results are given by the Eq. 7 and 8 and the minimum value between them is selected, in that way is guaranteed that the worst condition is taken into account and the results are not overestimating.

– Support

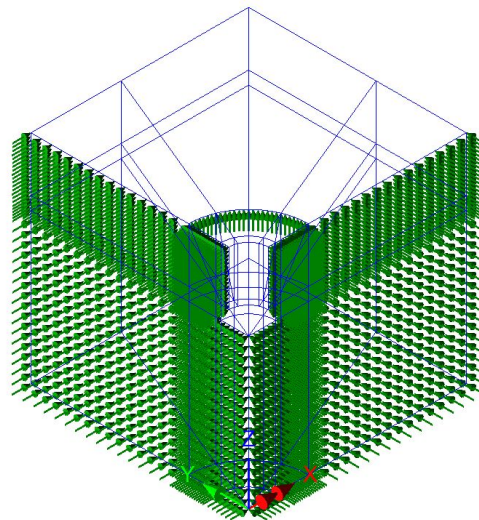
Due to the fact that the block is divided in four and just one quarter of it is designed, there are some constraints that must be considered. To guarantee the exact configuration of the whole concrete cube, the following restrictions are induced:

- * In y direction
- * In x direction
- * In z direction along the bearing ring

These restraints that act as a support for the structure are shown in the Figure 28 for both models.



(a) Supports model 1



(b) Support model 2

Figure 28: Support configuration of the models

– Loading

LUSAS brings the possibility to define different load cases according to the load attributes created as the Figure 29 show. In this case on the block are considered two type of forces:

* Tension force = corresponds to the extraction force obtained at failure during the performance of the pull-out test.

* Compression force = corresponds to the compression induced through the compression testing machine to simulate the prestressing state on a prestressing concrete structure.

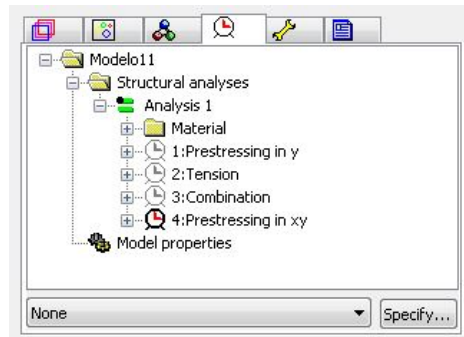


Figure 29: LUSAS Loadcases

The loadcases defined for the analysis are:

*Prestressing Y = this case corresponds to the application of a compression force equal to 20 MPa in y direction according to the global coordinates of the system.

*Prestressing XY = this case takes into account the contribution of a compression force arriving from x and y direction following the global coordinates of the system.

*Tension/Extraction force = this loadcase simulates the obtained extraction force applied on the bottom of the bolt.

There is a particular analysis that must be carried out to apply the extraction force to the model. Considering the section of the bolt either for the model one or two, the force is applied an uniform distributed load, which means that the load is divided by the area. As there are different types of screw involved on the thesis, the example of calculation will be conducted for the reference models.

The first area in study is the area correspondent to the bolt 1 which

is defined as a truncated cone. Its geometrical features are exemplified on the Figure 30

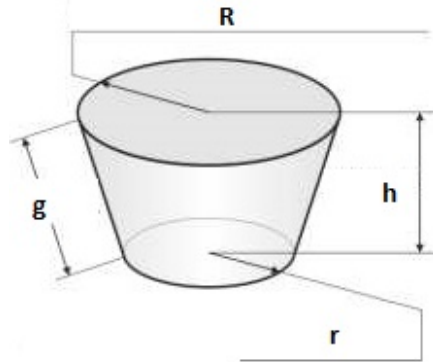


Figure 30: Truncated cone geometry

The radius R is defined by the bottom of the bolt, the small radius r by the constant section of the screw, the height h is the distance between the radii and the generatrix g by the tilt length between them. Numerically, the geometry is:

$$* R = 8.5\text{mm}$$

$$* r = 7\text{mm}$$

$$* h = 8\text{mm}$$

$$* g = 8.14\text{mm}$$

The Eq. 11 denotes the area as:

$$A = A_{base} + A_{top} + A_{lateral} \quad (10)$$

$$A = \pi \times R^2 + \pi \times r^2 + \pi \times g \times (R + r)$$

But for our purpose the lateral area is enough, then the equation is reduced into

$$A = \pi \times g \times (R + r) \quad (11)$$

Finally the uniform distributed load applied is

$$Load = \frac{Extraction\,force}{Area} \quad (12)$$

For the model 2 the procedure carried out is almost the same, despite the difference on the geometry. Here the section corresponds to a circle frame and is shown in the Figure **31**.

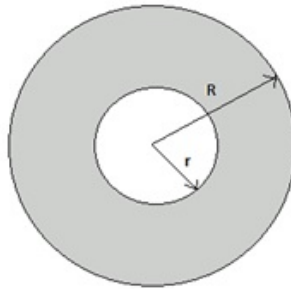


Figure 31: Area of the second screw

The main features are the external R and the internal r radii. The area is estimated through the equation

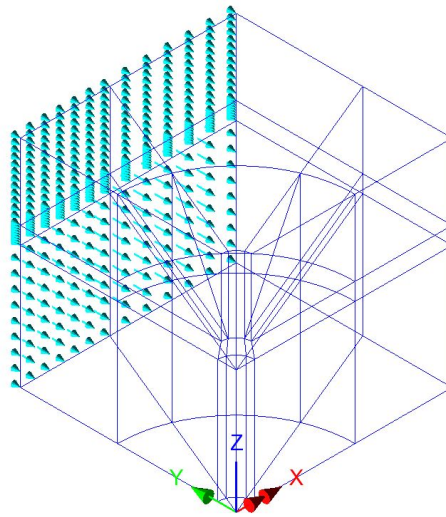
$$A = \pi \times (R^2 - r^2) \quad (13)$$

For this model the radii are:

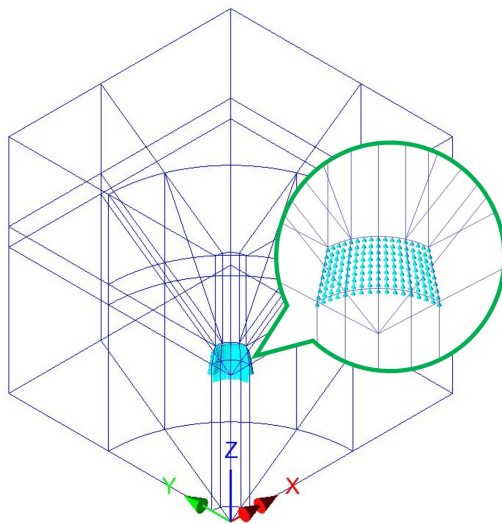
- * $R = 12.5\text{mm}$

- * $r = 9\text{mm}$

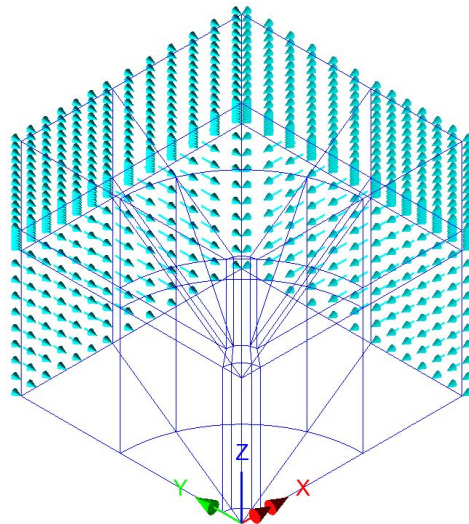
Lastly, the information about the loads applied on the model is represented through the Figure **32** for the model 1.



(a) Prestressing Y direction



(b) Tension/Extraction force



(c) Prestressing XY direction

Figure 32: Loading cases for model 1

The Figure 33 illustrates the composition of the model 2 loading.

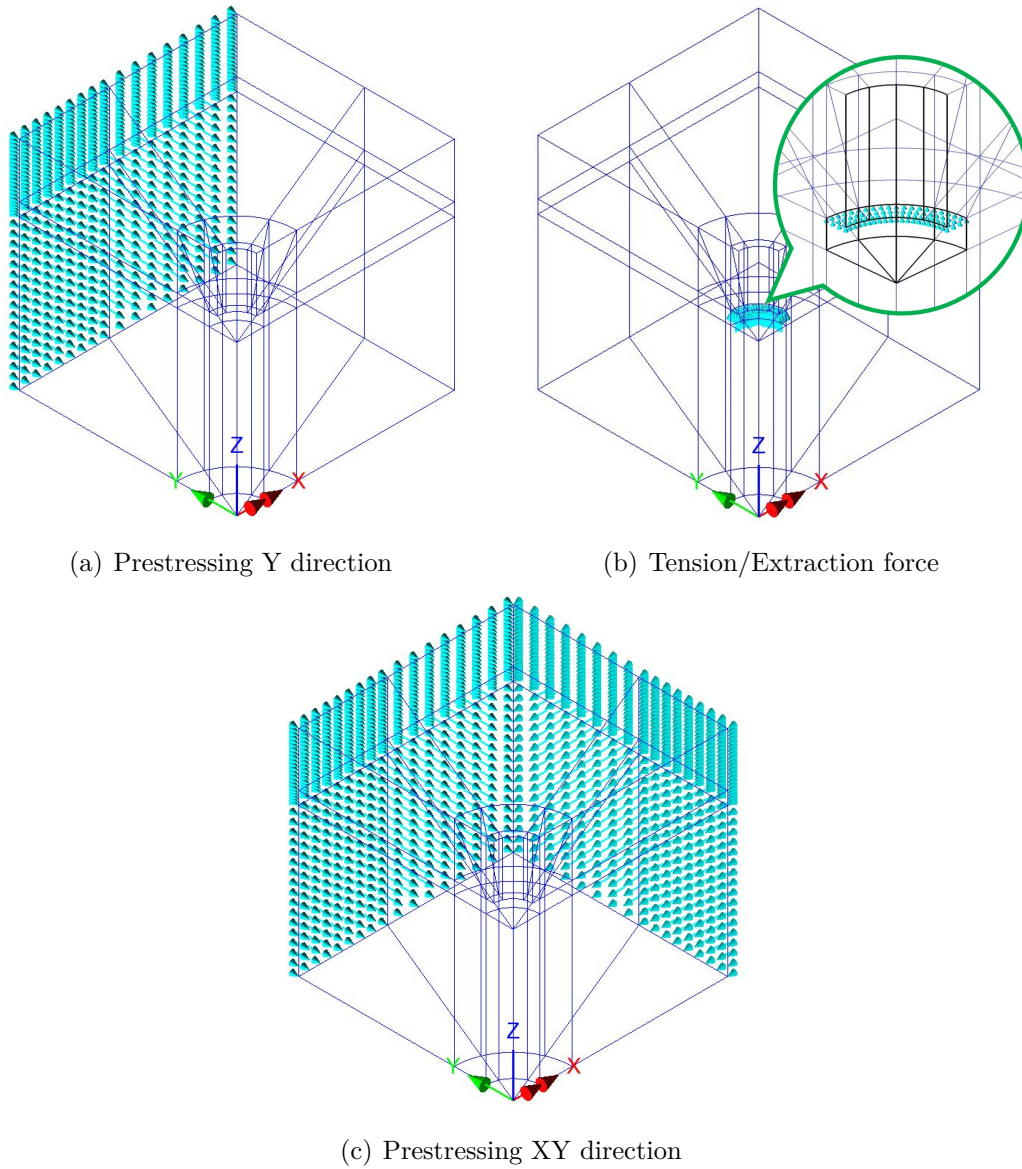


Figure 33: Loading cases for model 2

4.3 Geometries

Following the same procedure described above and including the same characteristics on the models, to develop the main goal of the thesis and determine the

most suitable setup to carry out the pull-out test, the following geometries were tested. The arrangement of shapes are illustrated on the Table 2

Model number	h [mm]	d [mm]	D [mm]	α [°]
1	35	14	110	54
2	25	18	55	31
3	45	14	110	47
4	20	14	110	67
5	35	18	55	23
6	35	14	55	30
7	35	14	140	61
8	35	14	69	38
9	50	14	150	54
10	25	14	82	54
11	40	14	124	54

Table 2: Arrangement of geometries

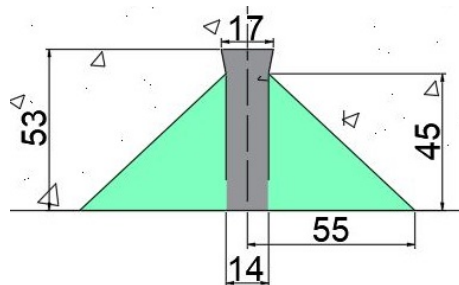
where:

h = Height of the failure cone.

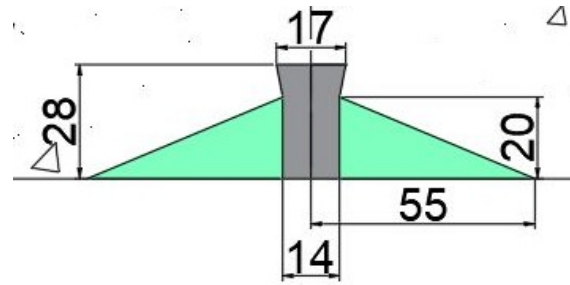
d = Diameter of the bottom of the cone equal to the diameter of the bolt.

D = Diameter of the bearing ring.

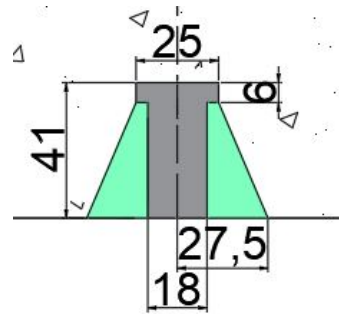
In addition, the Figure 34 illustrate graphically the all the shape combinations.



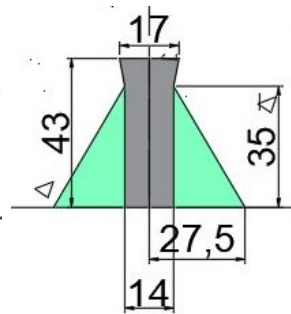
(a) Model 3



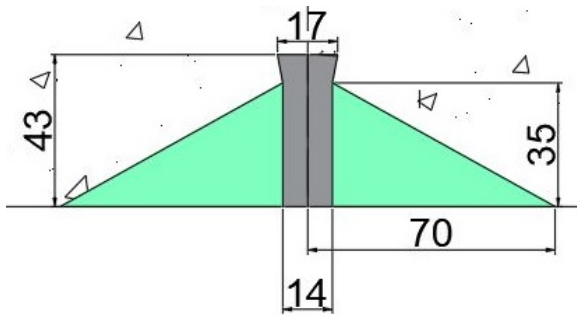
(b) Model 4



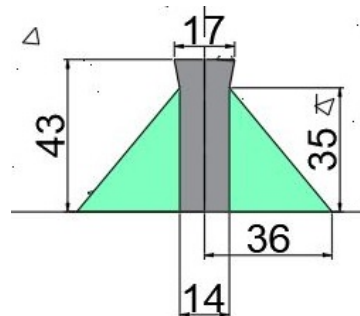
(c) Model 5



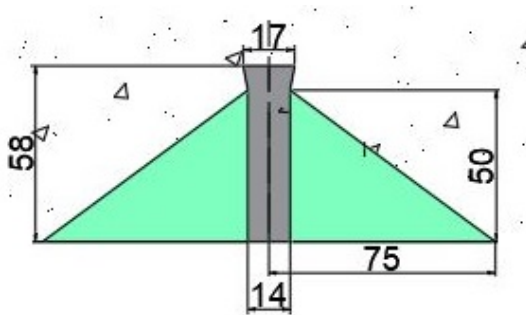
(d) Model 6



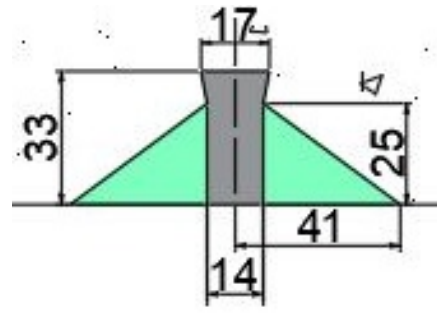
(e) Model 7



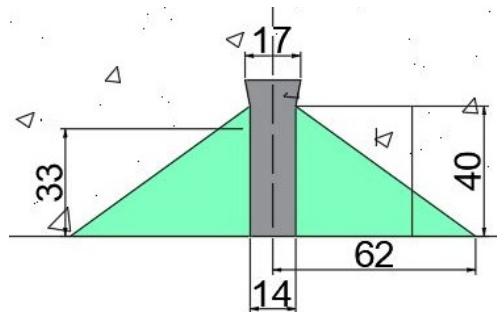
(f) Model 8



(g) Model 9



(h) Model 10



(i) Model 11

Figure 34: Arrangements of geometry

4.4 Numerical procedure

The numerical procedure section is developed to explain the mathematical approach performed to summarize the information thrown by LUSAS and estimate the stress level. The calculations were performed by means of Matlab software due to the amount of information available related to the level of detail of the analysis. The procedure is described by a flowchart shown on the Figure 35.

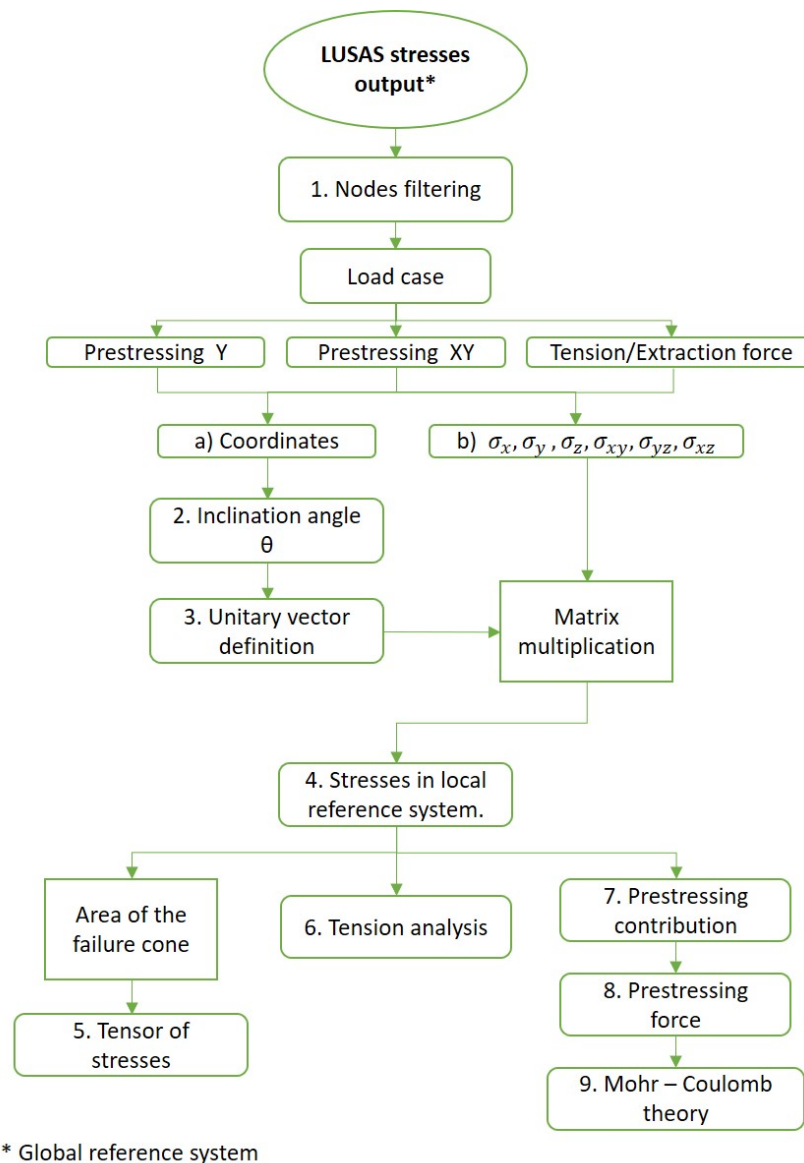


Figure 35: Flowchart of the numerical procedure

The first step consist on the extraction of the data corresponding to the nodes that are included on the failure cone. These nodes enclose the whole surface and are disposed on the 5 lines previously mentioned. One example of the nodes distribution is shown in the Figure 36

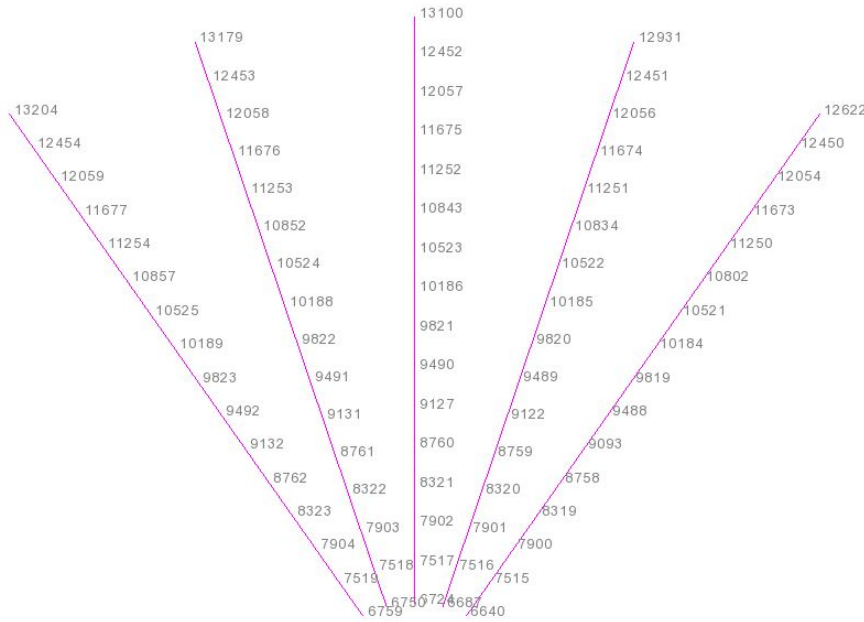


Figure 36: Nodes along the line

The location of the lines is predefined on the Modeling procedure section, where the mesh is assigned. With an uniform spacing division, 16 points are considered appropriate to describe reasonably the behavior. Each of them are designated by a specific number and this is the way to find them inside the whole output.

The second step consist into the determination of the inclination angle of the lines. This is the input value of the forward analysis. Theta, as is called, is obtained by the coordinates filtrated on the first step, applying trigonometry with the (x,y,z) components and the length of the line.

The target is to reach the transformation of the Global coordinates stresses into the local coordinates ones. The local reference system is defined for each line

inside the failure cube. This network is defined as:

\vec{n} = Perpendicular axis to the line.

\vec{t} = Tangent axis to the line

\vec{k} = Perpendicular axis to the line parallel to the XY plane.

The new triad is illustrated with the Figure **37**

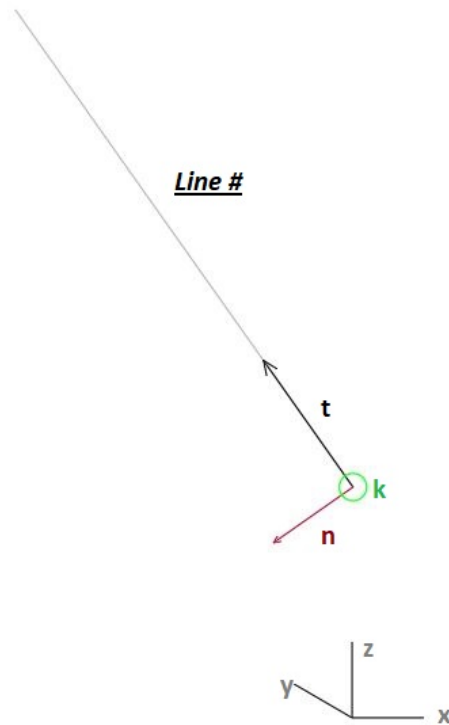


Figure 37: Local reference system

The direction cosines concept or the definition of the new vectors: \vec{n} , \vec{t} and \vec{k} can be described by the angles that the segment makes with X,Y and Z axis. The initial transition is realized by means of the Eq. **14** and represent the global stresses along the tilt plane associated to the line.

$$transition = T \times \vec{n} \tag{14}$$

where:

T = Tensor of stresses for each node $[\text{N}/\text{mm}^2]$ and is defined as:

$$T = \begin{bmatrix} \sigma_x & \sigma_{xy} & \sigma_{xz} \\ \sigma_{yx} & \sigma_y & \sigma_{yz} \\ \sigma_{zx} & \sigma_{zy} & \sigma_z \end{bmatrix} \quad (15)$$

To get the values of the stresses in the local reference system for each node along the lines, the Eq. **16**, **17** and **18** are performed.

$$\text{transition.} \vec{n} = n \quad (16)$$

$$\text{transition.} \vec{t} = t \quad (17)$$

$$\text{transition.} \vec{k} = k \quad (18)$$

It is convenient to remark that \times = matrix multiplication and \cdot = scalar product. Finally, the stresses can be summarized by means of the vector \vec{LS} and they are expressed as Eq.**19**:

$$\vec{LS} = \begin{bmatrix} n \\ t \\ k \end{bmatrix} \quad (19)$$

If the final estimations are verified, the following property is used:

- The scalar product between the components of the vector are equal to zero.

Let us develop the procedure to get a triad of vectors for a line in the model 1 **38** as an example. This is enough to describe the methodology because the principle applies for all the models.

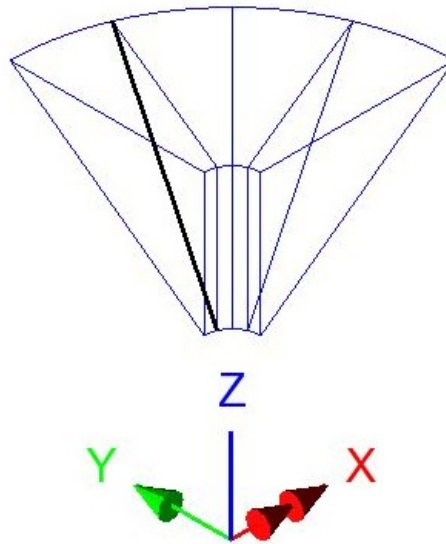


Figure 38: Line selected for the mathematical procedure

To clarify the concept of the characterization of a vector the Figure **39** is used.

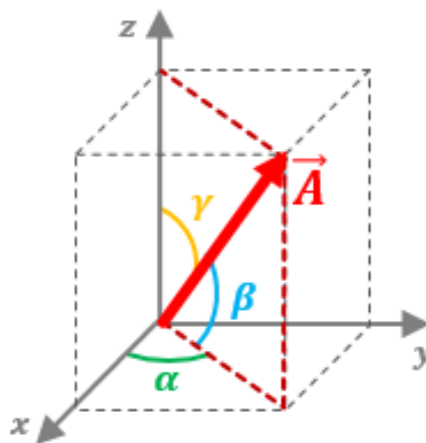


Figure 39: Direct cosines definition

Contextualizing the problem with the thesis case, the main angles in the line 2 (moving from left to right) are:

$$\begin{aligned}\alpha &= 22.5^\circ \\ \beta &= \theta\end{aligned}$$

Subsequently the vectors are:

$$\vec{t} = \begin{bmatrix} \cos\beta * \sin\alpha \\ \cos\beta * \cos\alpha \\ \sin\beta \end{bmatrix} = \begin{bmatrix} \cos\theta * \sin\alpha \\ \cos\theta * \cos\alpha \\ \sin\beta \end{bmatrix} \quad (20)$$

$$\vec{k} = \begin{bmatrix} \cos\alpha \\ -\sin\alpha \\ 0 \end{bmatrix} \quad (21)$$

Only those are necessary since making use of the mathematical properties of this kind of vectors the third component can be obtained by the Eq. **22**

$$\vec{n} = \vec{t} \times \vec{k} \quad (22)$$

The above mentioned procedure is developed for all the load cases described on the modeling procedure subsection. Once the procedure is finished, two types of valuations are conducted: the tensile and the prestressing effect.

4.4.1 Tensile analysis

The tensile analysis is the assessment of the tensile stresses along the failure surface. Knowing the symmetry involved on the problem, there is an almost uniform distribution expected on the five lines.

To develop the evaluation the stresses are considered in the local coordinates system. Estimating the relative position of the nodes Eq.**23**

$$d(i, 1) = \sqrt{\text{coordinates}(i, x - y - z) - \text{coordinates}(1, x - y - z)} \quad (23)$$

$$d = \sqrt{(x_i - x_1)^2 + (y_i - y_1)^2 + (z_i - z_1)^2}$$

This is useful for the graphical representation. From the extraction force are analyzed either the σ or τ stresses. The distribution of the stresses give an idea about the distribution of the extraction force with respect to the geometry.

It is important to remark that the same extraction force was adopted for all the geometries. The average value was taken remembering the explanation given on the experimental test section. The pull-out test performed was replicated 5 times, one for each available face of the cube.

Moreover, for the first set up is know the average extraction force but changing the geometry there is a different distribution of stresses. Can be concluded qualitatively that the real extraction force will be lower or higher to remain on the same range of stresses than in the reference tested model.

4.4.2 Prestressing contribution

The prestressing contribution is estimated either for the loading acting on Y or the loading acting on X and Y directions contemporary. The hypothesis of the contribution of the prestressing state on the tensile force obtained through the pull-out test, is evaluated by means of the correlation of the Mohr - Coulomb criterion.

Mohr - Coulomb analysis

Before the development of the procedure, the principle is explained. The Mohr Coulomb failure criterion is based on the fact that the permanent deformation around a point in a structure, due to the application of a compression force, is reduced almost to the sliding between several parallel plane elements. The position of these planes determines the tangent plane to the fracture surface on the analyzed point. The rupture occurs depending on the values that the normal and tangential stresses assumes on it.

In other words, the Mohr Coulomb theory express that the limits of plasticity and rupture of a material are defined by the stresses that it develops in the planes of

sliding and fracture. The tangential tension in the failure plane reach for the limit state a maximum value, and it is function of the correspondent normal force and the material features.[3]

The material characteristics is represented either by the typology at failure or by the internal shear coefficient. The typology considers the brittle or ductile behavior at failure. The friction coefficient is defined as a measure of the ability of a material to withstand a shear stress. It and is attained when failure just occurs and the value is determined experimentally.[3] The conventional expression used to describe the shear strength at failure is the Eq. **24**.

$$\tau = c + \sigma_n \tan \varphi \tag{24}$$

$$\tau = f(\sigma)$$

where:

τ = Shear strength [Pa]

c = cohesion [Pa]

σ_n = normal stress [Pa]

$\tan \varphi$ = coefficient of internal friction of the material [°]

The premise of the theory is that the maximum shear stress supported by an element is greater under an induced compression state, as the Figure **40** shown. The failure criterion is linear and the cohesion is a constant that can be supported without any normal stress applied.

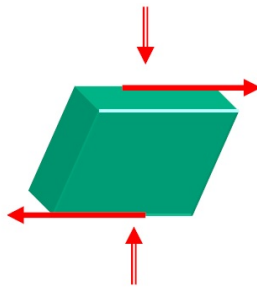


Figure 40: Maximum shear development

The Mohr Coulomb criterion is also graphically represented by the Intrinsic curve or also named Envelope of Mohr shown in the Figure 41. This is a useful tool to understand the concept behind the linear equation. The intrinsic curve is an envelope line determined by the Mohr circles that come from increasing the principal stresses σ_1 and σ_2 until the development of the rupture or the plastic state.

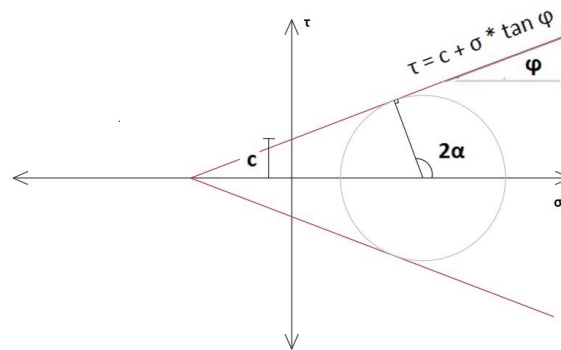


Figure 41: Coulomb Envelope of failure

The increment of the stresses is performed by means of the triaxial shear test, where several combination of actions are performed. These arrangements bring different stress states through circles as can be seen in the Figure 42.

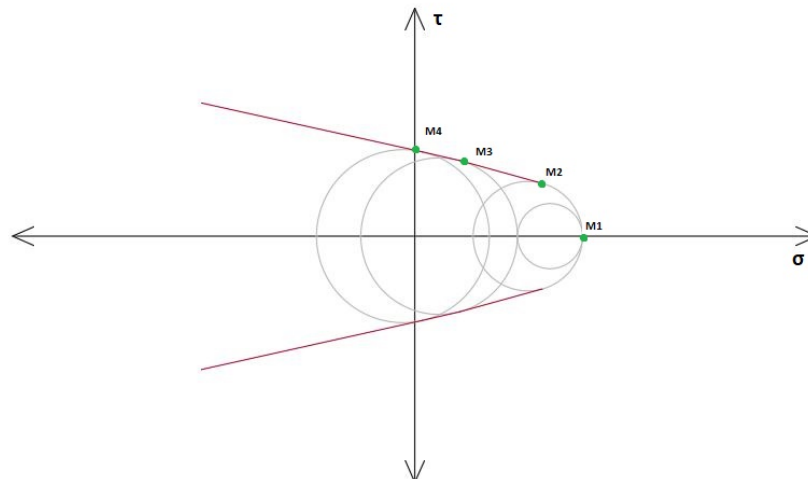


Figure 42: Mohr circles due to several load combinations

The envelope can be also constructed by means of two main load cases, the pure

compression and pure tension. Reducing the load into this pair of test a single contribution is obtained at any sides of the axis. The aforesaid situation means that the tension state is associated with a positive contribution and the compression state is developed due to the opposite case. The Figure 43 illustrates the convention.

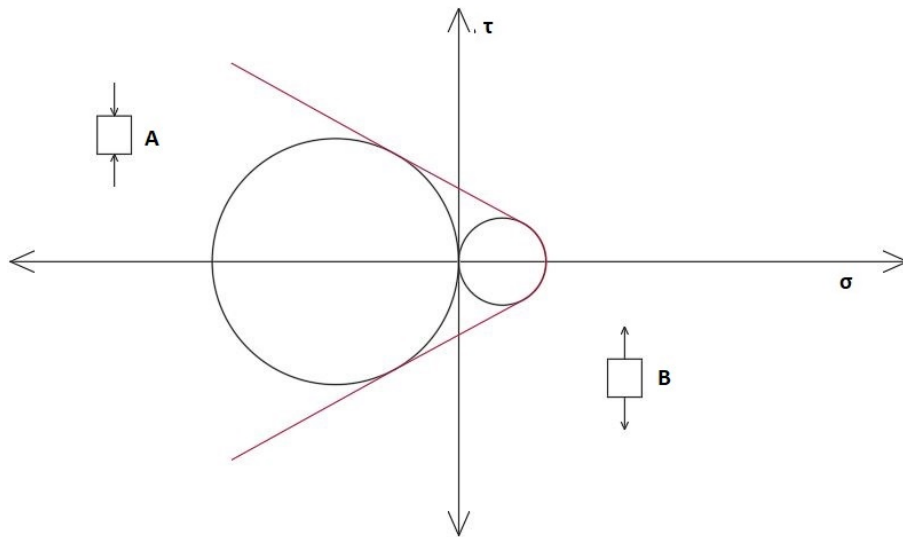


Figure 43: Pure tension and Pure compression Mohr circumferences

As can be seen, the envelope is defined by the tangential line than intersects both circles. The failure is indicated always by the biggest circle. By definition, the envelope can be constructed by drawing circles as much as tests conduced. Furthermore, the elastic range can be easily represented.

Following the definition above mentioned and making reference to the Figure 44, if the circle of the specimen under analysis lies on A, the structure is on the elastic range. Otherwise reaching the position B intersecting the line, the rupture is reached or the structure is in dangerous.

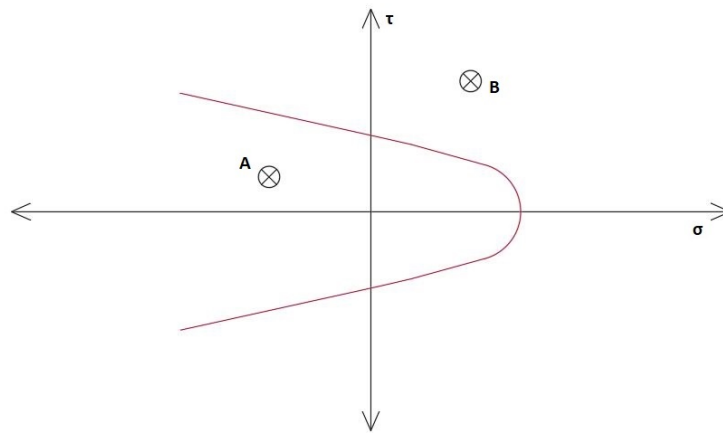


Figure 44: State according to the envelope of failure

Dealing particularly with concrete specimens, it is a material whose tensile resistance represents the 8 to 14 percent of the compression strength approximately [9]. Hence the curve can be simplified and the trend follows the circle instead of intersect the σ axis. This streamlining is shown in the Figure 45. Moreover for the specimens subjected to a tension stresses, the failure happens due to the separation of the faces more than the sliding of them.[12]

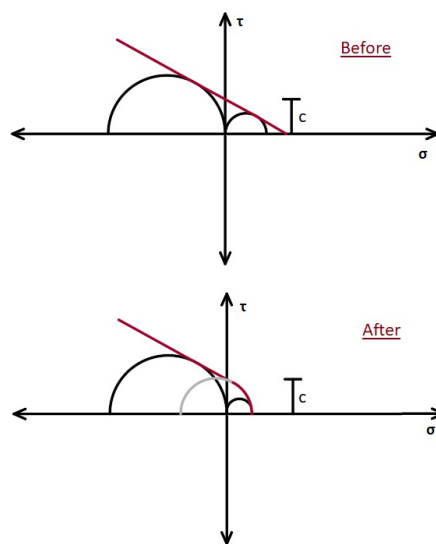


Figure 45: Envelope of Mohr simplification

Finally, the isotropic property of the material affirms that the friction does not depend on the position of the force N (the perpendicular force) neither on τ on the perpendicular plane. Furthermore it can be defined as an absolute value.

At this point the development of the procedure is explained. Working with the local stresses obtained on the numerical procedure section, the first step consist in the establishing of the actions that will contribute on the precompression state. For that the following convention is adopted (Figure 46)

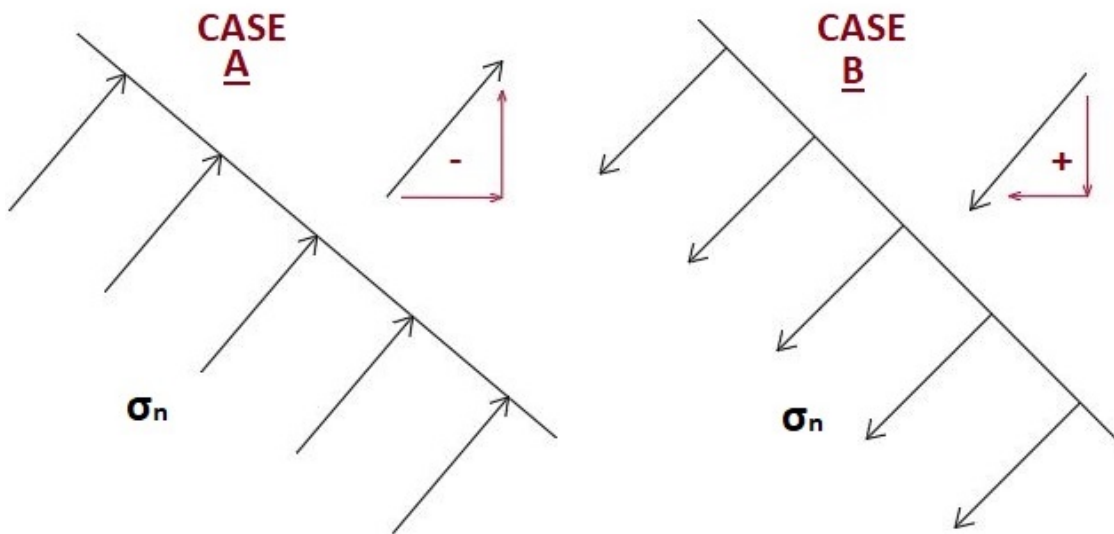


Figure 46: Prestressing contribution convention

In the CASE A, can be seen that the compression stress σ_n is negative with respect to the sign assumption expressed in the Figure 37. Decomposing the force the vertical component will be disposed in the same direction than the extraction force. On the other hand, the CASE B will bring the opposite behavior and the force will be withstanding.

As the premise says that the prestressing state contributes on the tensile force, the CASE A is the starting point for the subsequent analysis. The filter of the negative σ_n is the input data. Once the values are obtained, a new vector is called. At this moment, two situations can appear: or the whole arrangement of nodes contributes or only part of them do. Now the application of the Eq. 24 is carried out.

The friction angle of the material - concrete - is a function of the quality of the aggregates and the water/cement ratio. It could vary between 34° and 43° . [12] Considering the mean value of this range, the friction angle is

$$\varphi = 35^\circ$$

Then, according to the previous explanation of the theory, the absolute value of the shear is considered. Finally the summarizing procedure is carried out and the final prestressing stress is found. Nevertheless, the operation can continue if a load analysis wants to be effected. For that the influence area of the stresses on the nodes must be calculated.

The estimation of the area is carried out following the definition of a truncated cone. The concept is illustrated by the Figure **30** and the Eq. **11**.

The radio R is defined by the bearing ring, the small radio r by the screw, the height h by the distance between the bottom of the constant section of the screw and the surface of the concrete cone, and the slant length g by the tilt length between them. According to that, all the cone areas are going to be different for each model. Making the example for the model 1, the geometry involved on the calculation is:

- $R = 55\text{mm}$

- $r = 7\text{mm}$

- $h = 35\text{mm}$

However, there is a variation on the area for the failure cone, because the analysis lies on the nodes not on the whole surface. Moreover a discretization process is required. For that, the following scheme **47** is assumed:

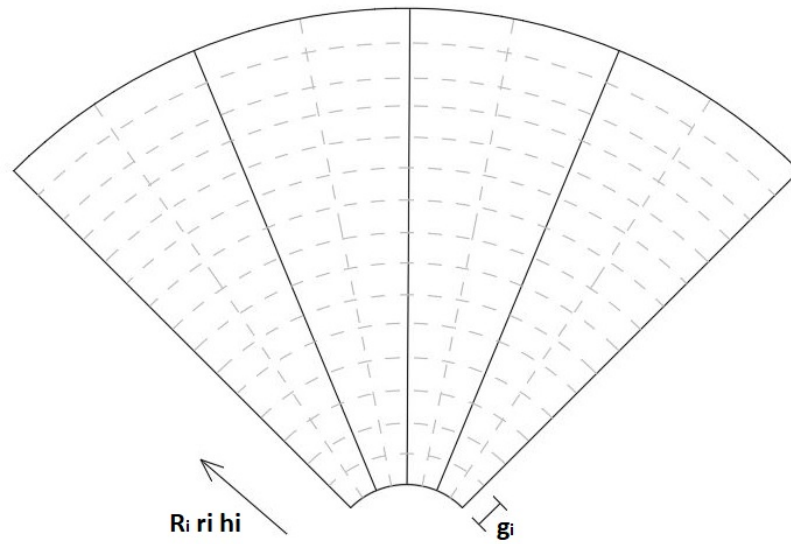


Figure 47: Discretization for the influence area of the stresses

The diagram shows the increment on the dimensions as there is an advancement on height. The division of the area by frames allows the estimation of the forces for the whole surface applying a final sum. The frame is also divided into portions in conformity with the location on the surface. The Figure 48 illustrates the concept aforesaid.

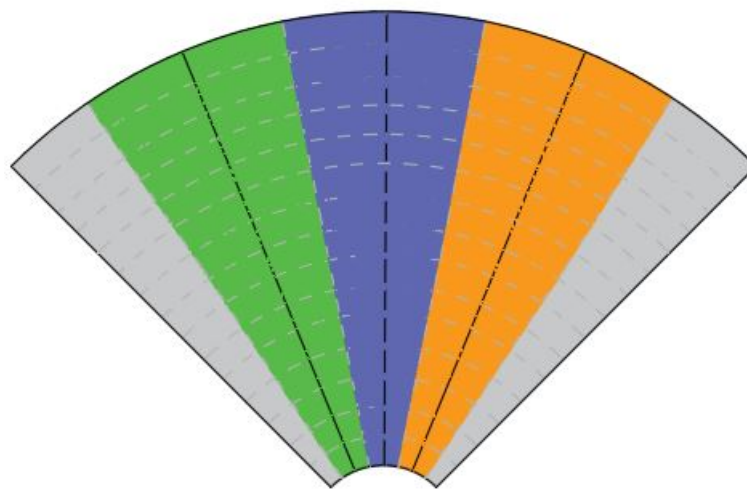


Figure 48: Area frames for the prestressing load estimation

The distribution follows the subsequent condition:

- Boundary stresses with $\frac{1}{8} \times A_i$
- Internal stresses with $\frac{1}{4} \times A_i$

In summary the Prestressing force contribution is defined with the help of the Eq. **25**

$$CP = \sum_{i=1}^n \sigma_n \times A_i \quad (25)$$

5 Results and Discussion

5.1 Uniaxial compression test

The uniaxial compression performance throws two type of results. The first one is related to the average compressive strength of the concrete samples. In the table 3 are shown the results.

The outcome is divided in recognition of the material employed. For the concrete case three samples were tested and the average compressive resistance obtained is 62.67 MPa. The mortar analysis was carried out by means of two cube samples and the average compressive resistance achieved is 42.40 MPa.

Concrete cube compression									
Cube N [°]	Cube mark	Manufacturing date	Dimensions [mm]			Weight [Kg]	Maximum force[kN]	Resistance [MPa]	Average Resistance [MPa]
			L1	L2	H				
1	C1	19-03-2019	150	150	150	7.835	1433.3	63.7	62.67
2	C2	19-03-2019	150	150	150	7.885	1404.71	62.43	
3	C3	19-03-2019	150	150	150	7.903	1392.22	61.88	
Mortar cube compression									
1	C1	04-07-2019	150	150	150	-	-	43.3	42.40
2	C2	04-07-2019	150	150	150	-	-	41.5	

Table 3: Uniaxial compression test results

Once the strength is estimated the forward calculations are developed. Subsequently through the use of the equations defined on the ACI 318 7 code and the EUROCODE 8 the elastic modulus of the materials is calculated. The equations are outlined in the Experimental test section. The results are shown in the table 4

Elastic modulus [MPa]	
Concrete	
ACI 318	MC 2010
37207	38154
Mortar	
30604	33934

Table 4: Elastic modulus of Mortar and Concrete

The last computation conform the input data of the linear analysis formulated on the modeling section.

5.2 Pull-out test

The pull-out test results are made up of the the extraction forces obtained through the execution of the method. The valuation of the aforesaid forces is carried out for several faces of the different samples. In addition, a different load combination was induced.

In the table 5 are shown the results obtained for the second geometry of the screw. That means the named bolt 2. In this table is also shown the pressure read on the extraction pump and the force calculated with the Eq. 9 as an example of the procedure.

Pull-out test results Bolt 2				
Sample N [°]	Date of the test	Load [kN]	Pressure [bar]	Fr [kN]
1	11-06-2019	0	203	35.53
		900	255	44.63
		1800	215	37.63
		1800	245	42.88
		2700	264	46.20
2	13-06-2019	0	256	44.80
		900	251	43.93
		1800	256	44.80
3	13-06-2019	0	244	42.70
		900	248	43.40
		1800	256	44.80
		2700	215	37.63

Table 5: Pull-out test results using the second geometry

The additional compression induced is implemented by multiples of 9, which means 0 - 900 - 1800 - 2700 kN. The load combinations are not always executed by the same loads. In some cases priority is given to the lower compression cases or the test is stopped in a certain value.

Similarly the results for the first geometry- bolt 1- are shown on the table 6.

Pull-out test results Bolt 1			
Sample N [°]	Date of the test	Load [kN]	Fr [kN]
1	09-09-2019	0	85
2			95
3			100
4			102
5			78
1	09-09-2019	1800	123
2			87
3			85
4			103
5			107
6			137

Table 6: Pull-out test results using the first geometry

Following the before mentioned premise, for the geometry one was decided to consider two load cases instead of four. The analysis of the two screw geometries together is done under the same load configuration. The magnitude of 1800 kN is selected.

Contrasting the results for the first and second geometry under the same load configuration the extraction force obtained are different between them. Using the geometry one the amount can reach values of almost twice the force of the acquired by means of the geometry two. As a first approximation to the final result, the experimental outcomes give us an idea of the behavior of the geometry under the induced prestressing state. The geometry number one throwing a greater result allows to infer a greater interaction of the screw inside the concrete cube with the induced compression state.

Summarizing the results for any load case carried out before, the average extraction force is computed and shown in the table 7.

Average value of the extraction force			
Concrete-Loadcase [kN]			
0	900	1800	2700
41.43	43.67	42.14	41.01
Mortar-Loadcase [kN]			
0		1800	
92		107	

Table 7: Average value of the compressive strength for Concrete and Mortar

5.3 Modeling procedure

The eleven configurations considering the different bolt geometries are shown in the Figures 49, 50 and 51 There are the final quarter cubes with the respective assigned mesh.

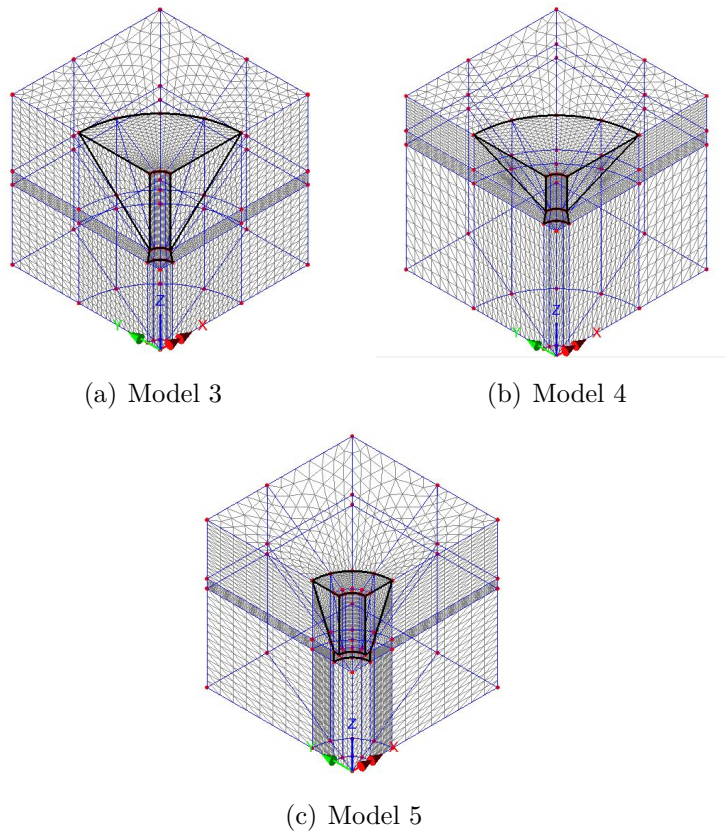
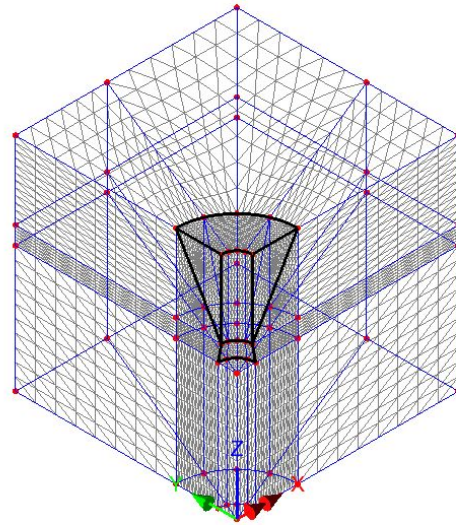
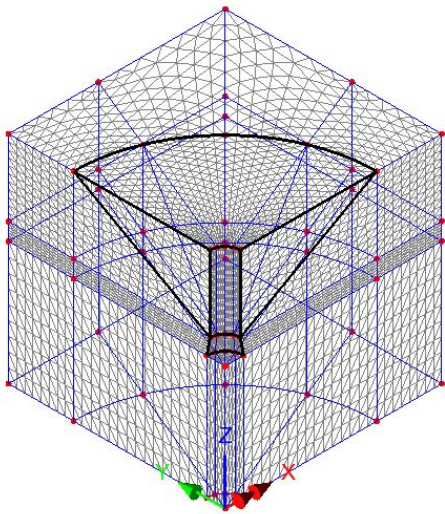


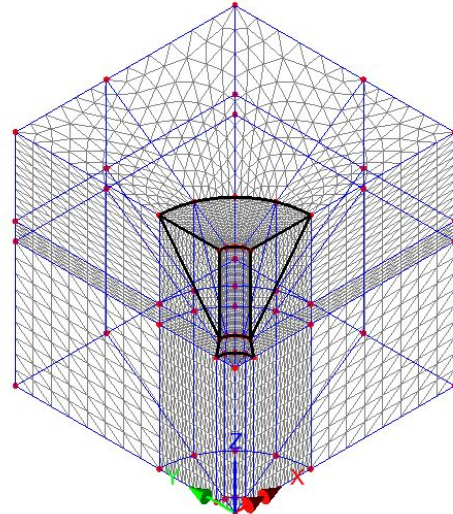
Figure 49: Modeling results for 3-4-5



(a) Model 6



(b) Model 7



(c) Model 8

Figure 50: Modeling results for 6-7-8

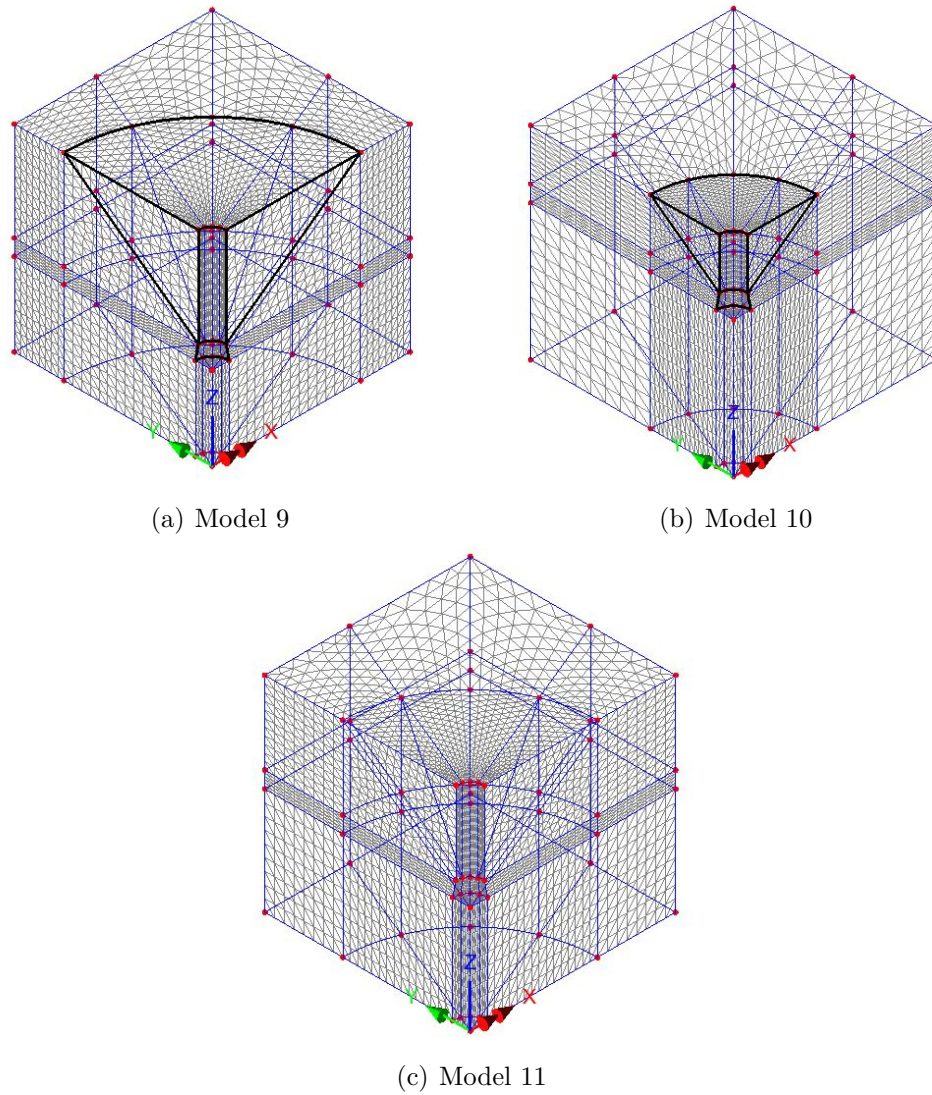


Figure 51: Modeling results for 9-10-11

For each of the models the following results are printed:

- Global stresses due to Prestressing in Y direction
- Global stresses due to Prestressing in X and Y directions
- Global stresses due to the Extraction force
- Global reactions.

These results are printed as a .text file. Nevertheless this is not show because the problem deals with thousand of nodes. For that reason Matlab is employed as a solver. The Figure 52 is an example of the output that LUSAS brings.

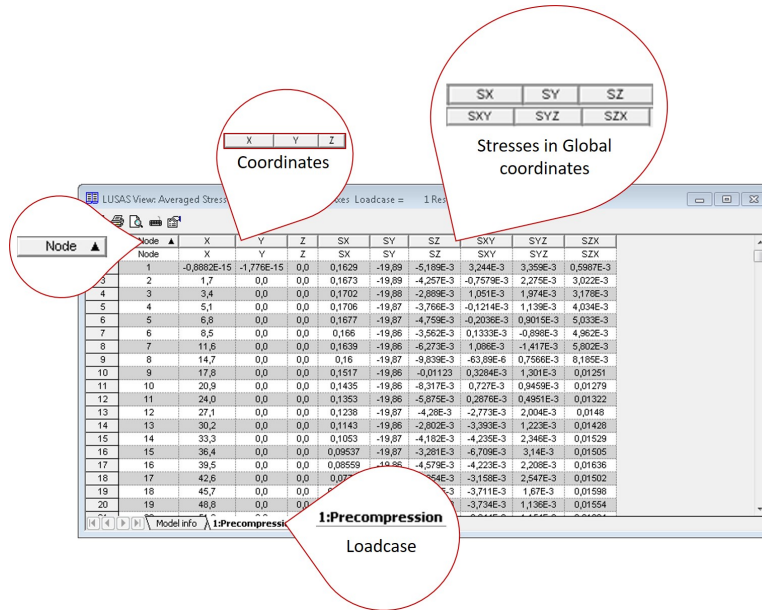


Figure 52: LUSAS results layout

5.4 Numerical procedure

Before presenting the obtained results in numerical modeling the following proposition must be stipulated. The successive results are derived by one quarter of the cube sample. To find the whole contribution the symmetry allows the multiplication by four to complete the section.

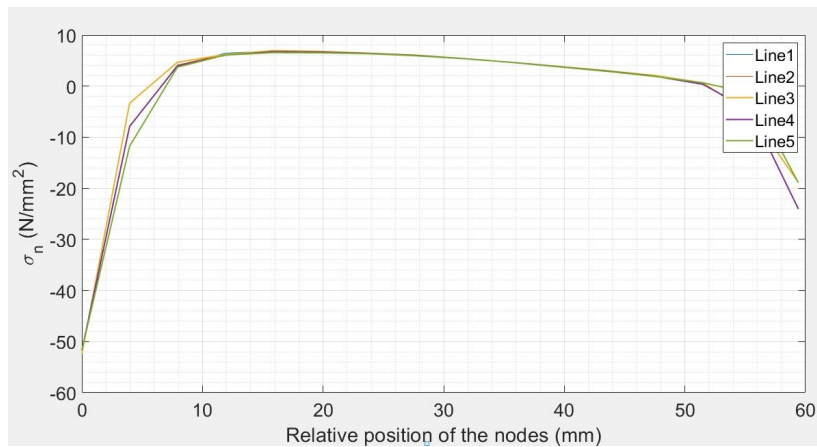
In addition, the outcome is divided into three components:

- The tensile analysis
- The prestressing contribution obtained by means of the compression induced and also employing the Mohr Coulomb hypothesized contribution.
- The geometry assessment.

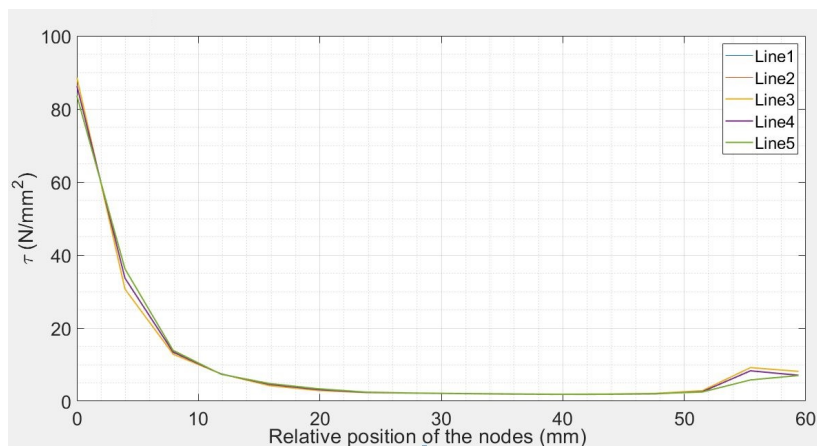
5.4.1 Tensile analysis

The tensile analysis brings the distribution of the stresses along the five lines due to the application of an extraction force at the bottom of the enlarged screw. According to the real conditions and the symmetry involved on the design, the expected behavior for the normal and shear stresses in local coordinates is almost uniform. Several variation on section are predicted because the failure shape corresponds to a truncated cone and not a perfect cylinder. Nevertheless, the regular distribution must be guaranteed for the lines 1-5 and 2-4. The order of the lines is specified in the previous section.

The results for the thesis analysis are shown in the following figures.

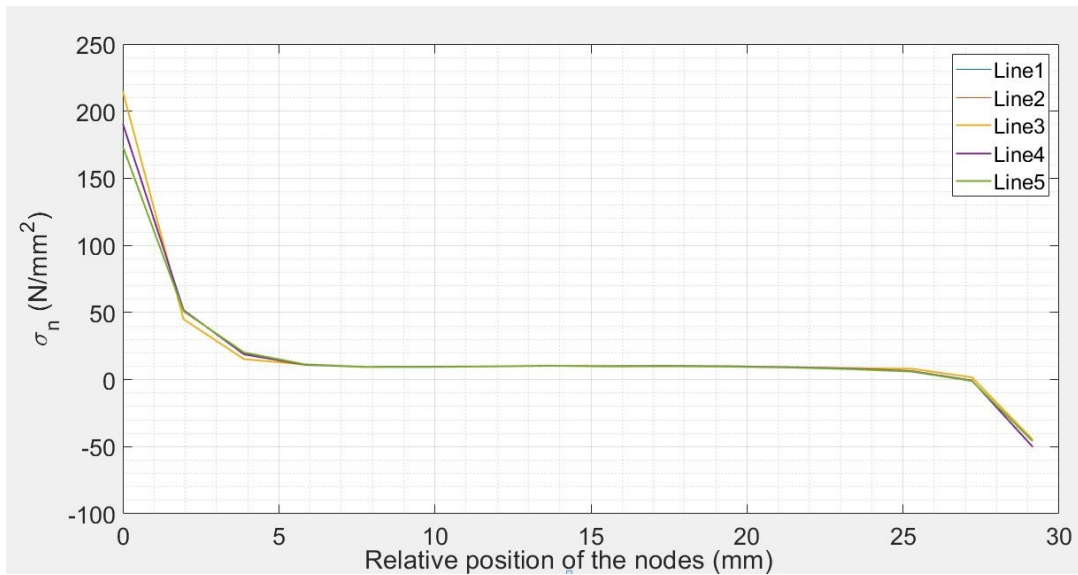


(a) Normal stress

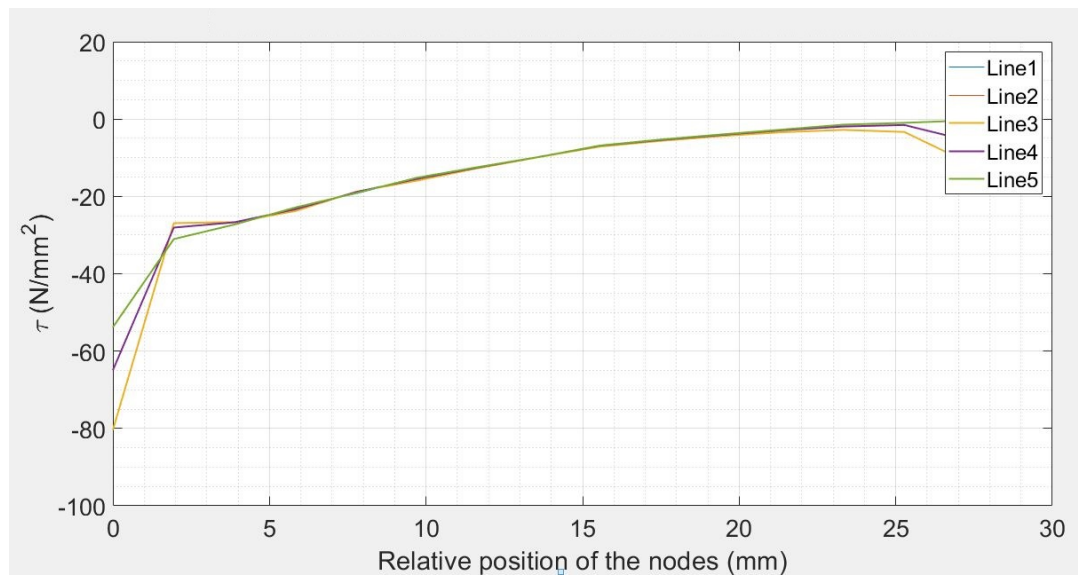


(b) Shear stress

Figure 53: Model 1 stress distribution in Local coordinates due to extraction.

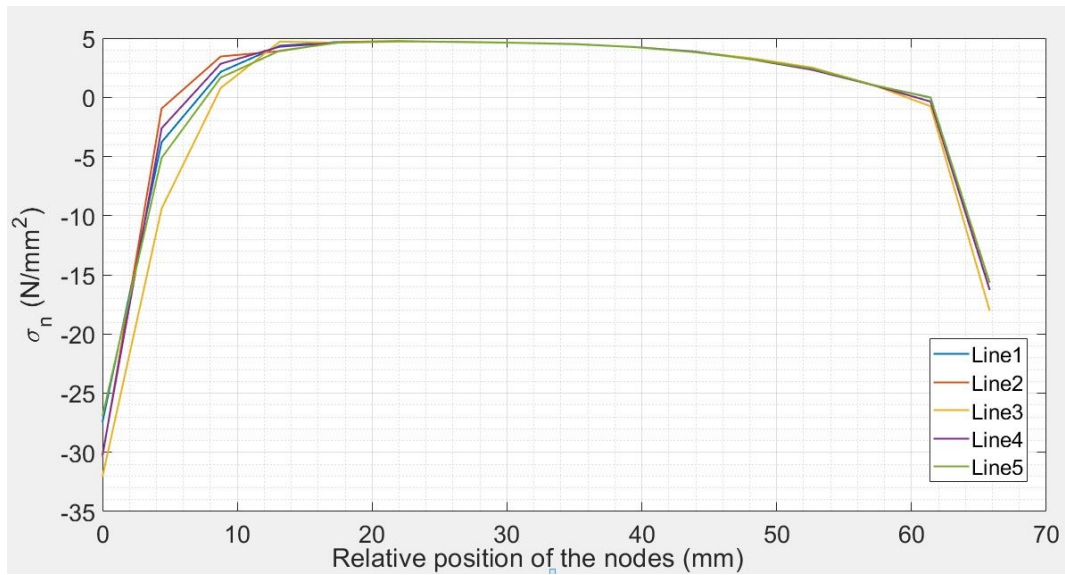


(a) Normal stress

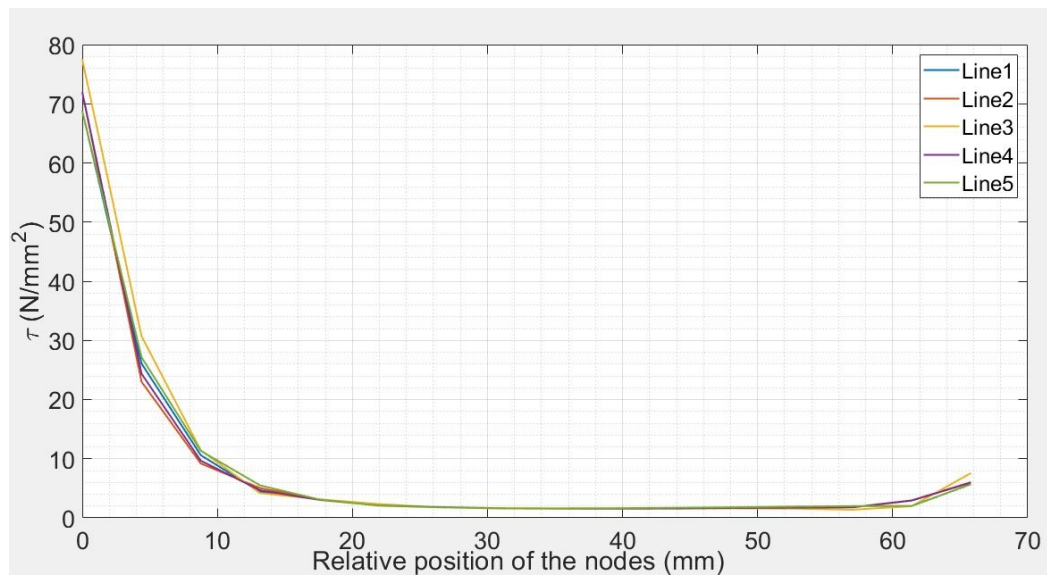


(b) Shear stress

Figure 54: Model 2 stress distribution in Local coordinates due to the extraction force

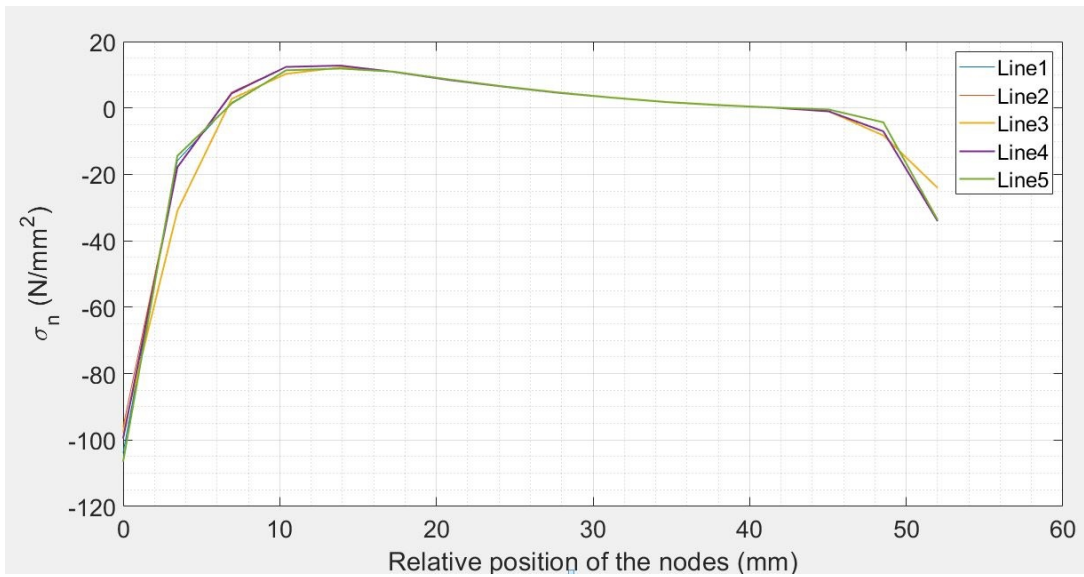


(a) Normal stress

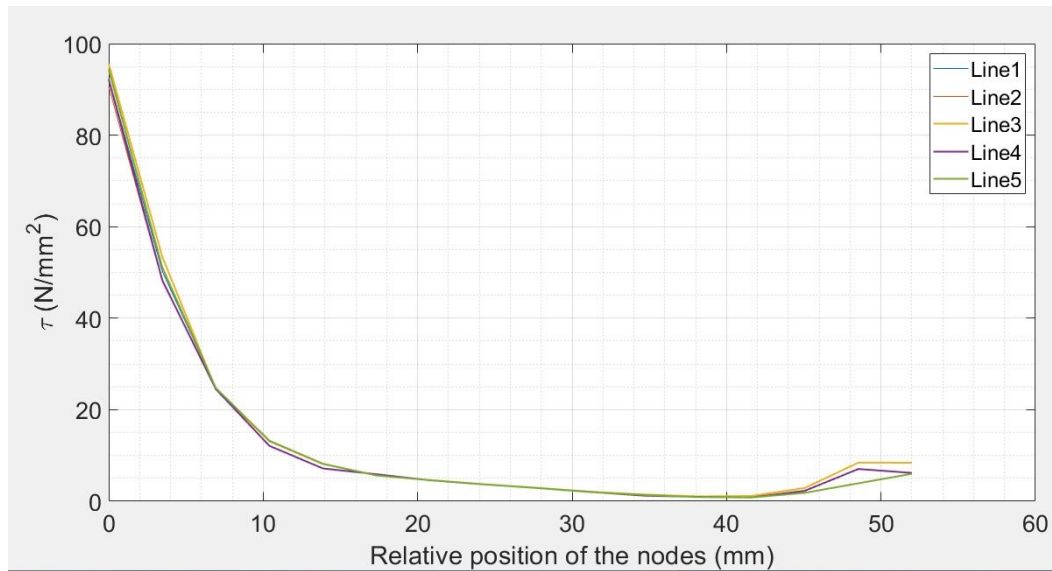


(b) Shear stress

Figure 55: Model 3 stress distribution in Local coordinates due to the extraction force

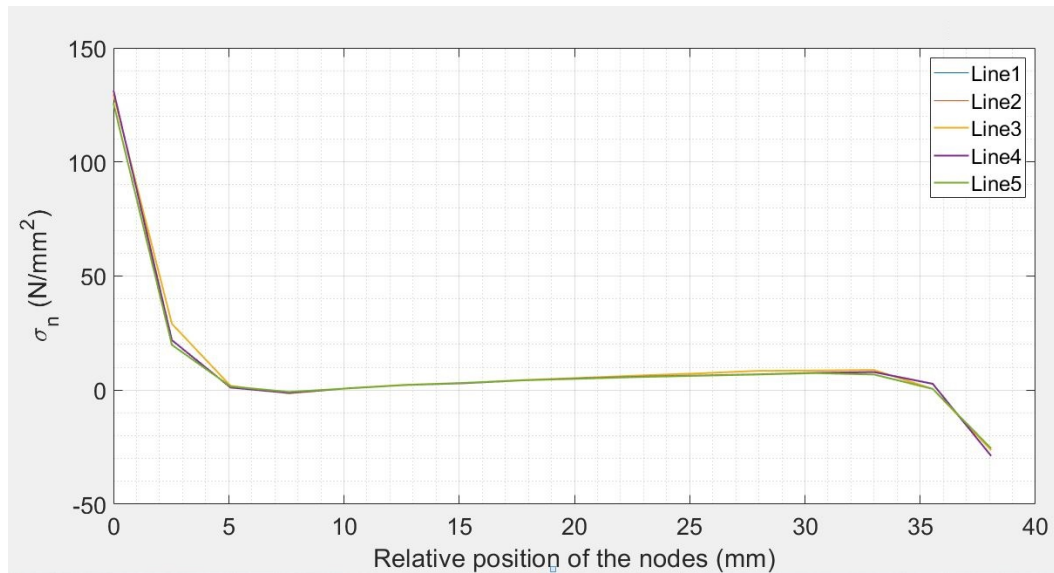


(a) Normal stress

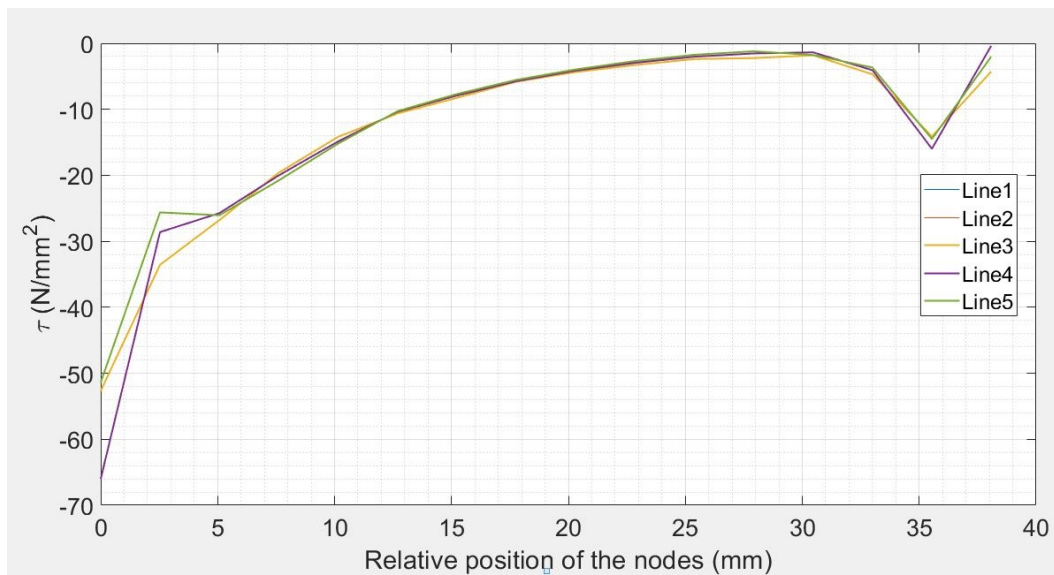


(b) Shear stress

Figure 56: Model 4 stress distribution in Local coordinates due to the extraction force

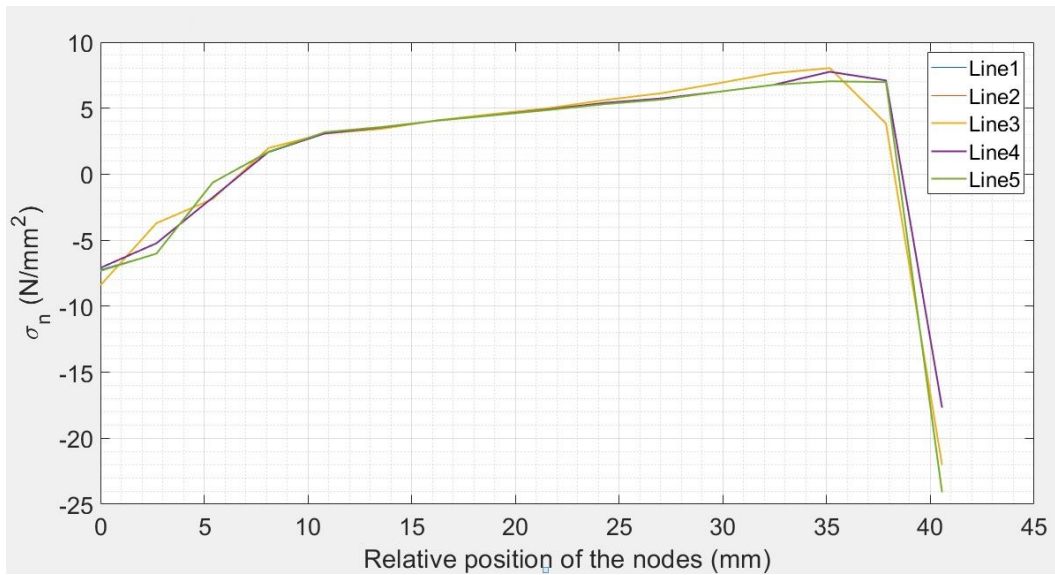


(a) Normal stress

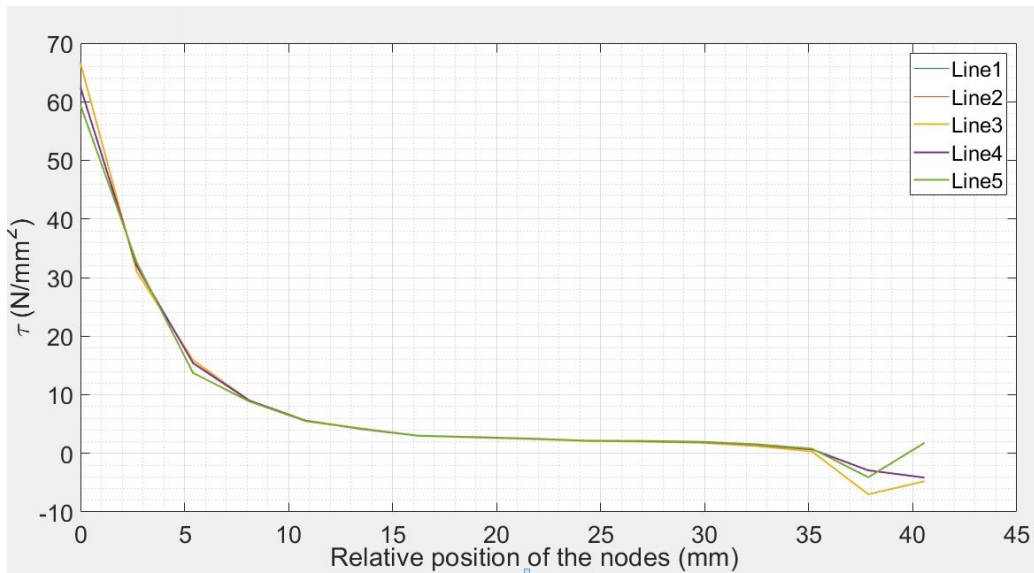


(b) Shear stress

Figure 57: Model 5 stress distribution in Local coordinates due to the extraction force

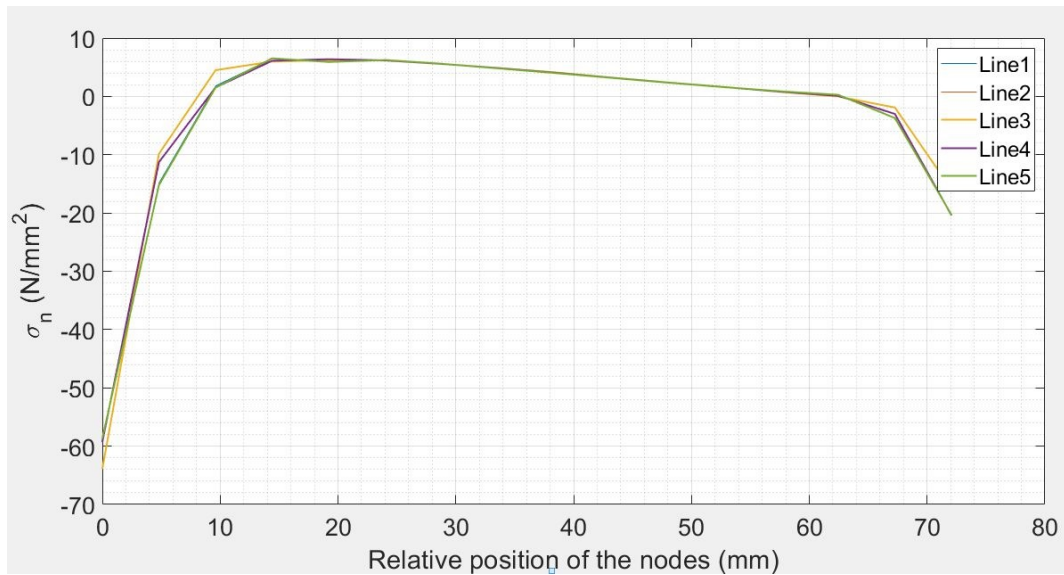


(a) Normal stress

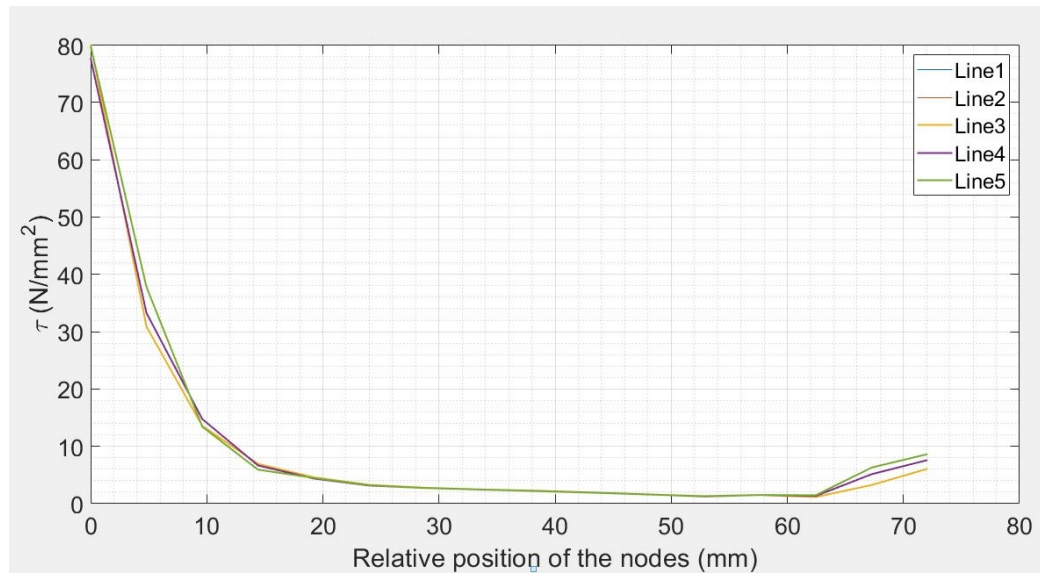


(b) Shear stress

Figure 58: Model 6 stress distribution in Local coordinates due to the extraction force

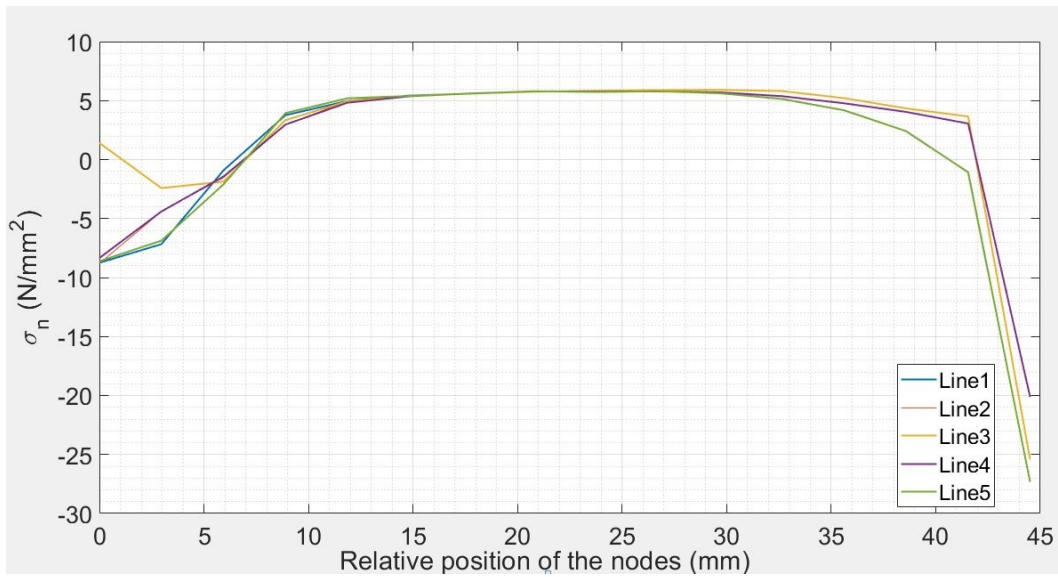


(a) Normal stress

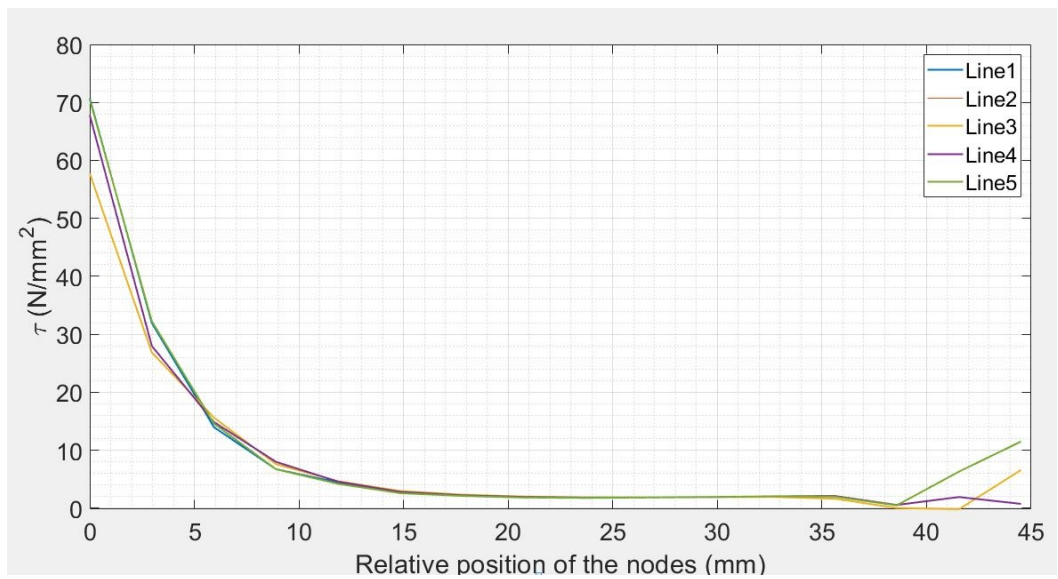


(b) Shear stress

Figure 59: Model 7 stress distribution in Local coordinates due to the extraction force

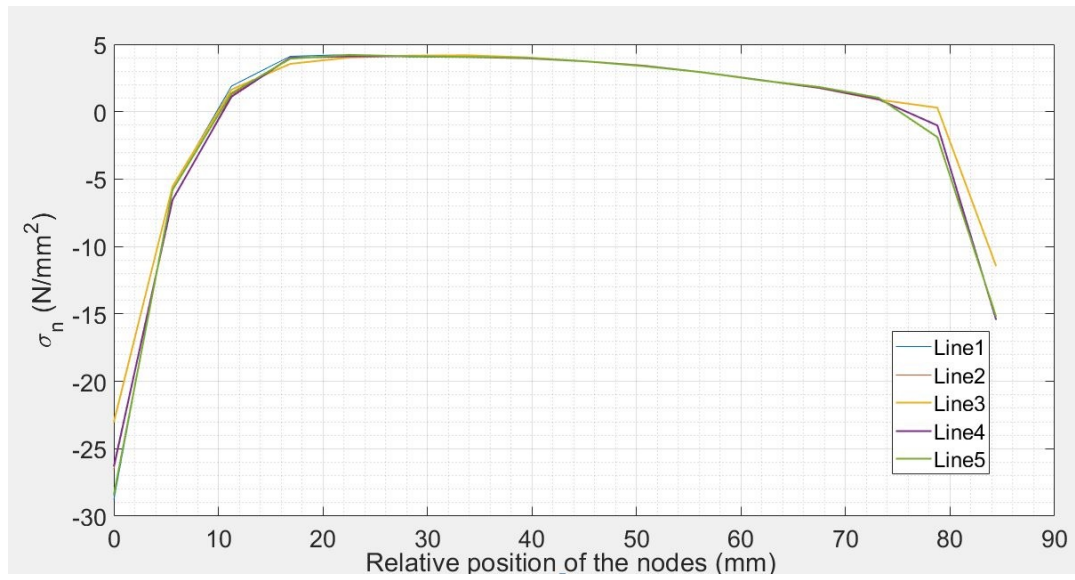


(a) Normal stress

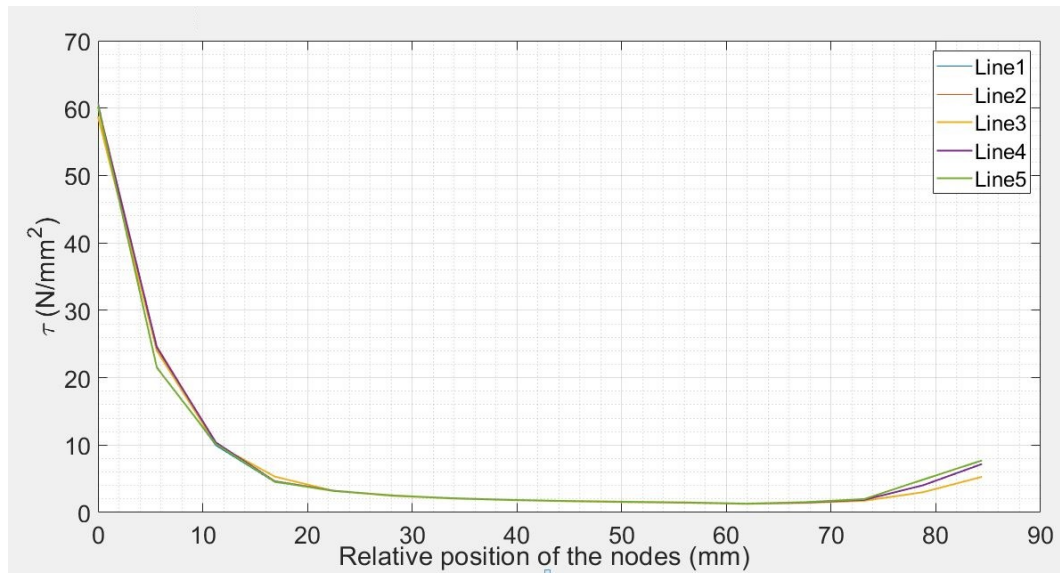


(b) Shear stress

Figure 60: Model 8 stress distribution in Local coordinates due to the extraction force

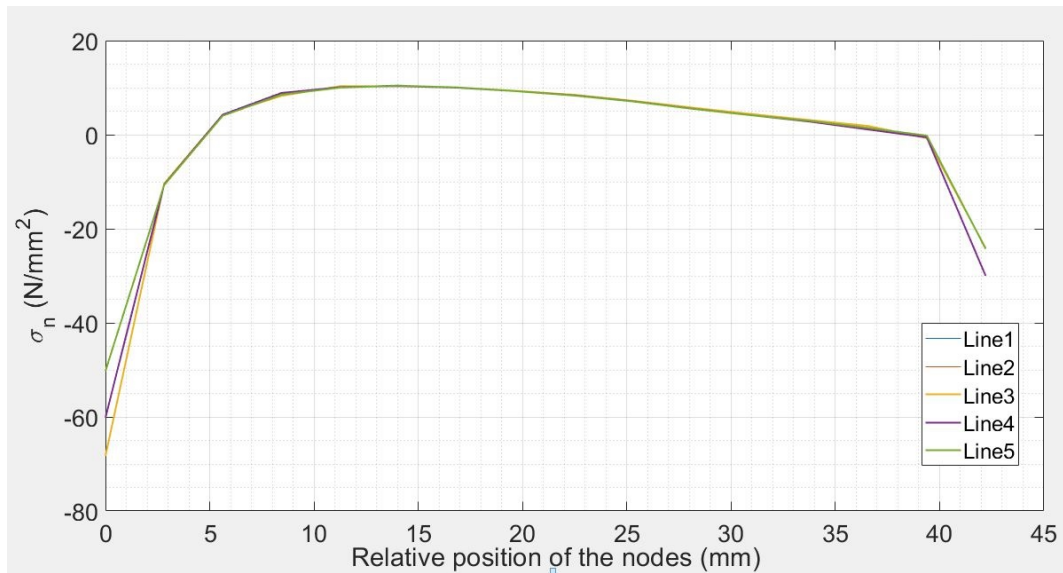


(a) Normal stress

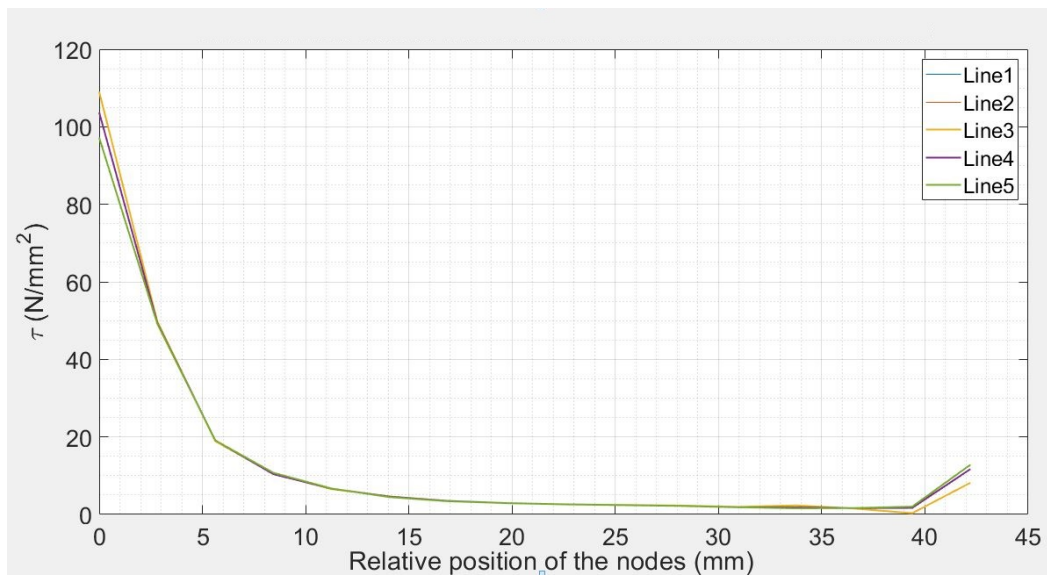


(b) Shear stress

Figure 61: Model 9 stress distribution in Local coordinates due to the extraction force

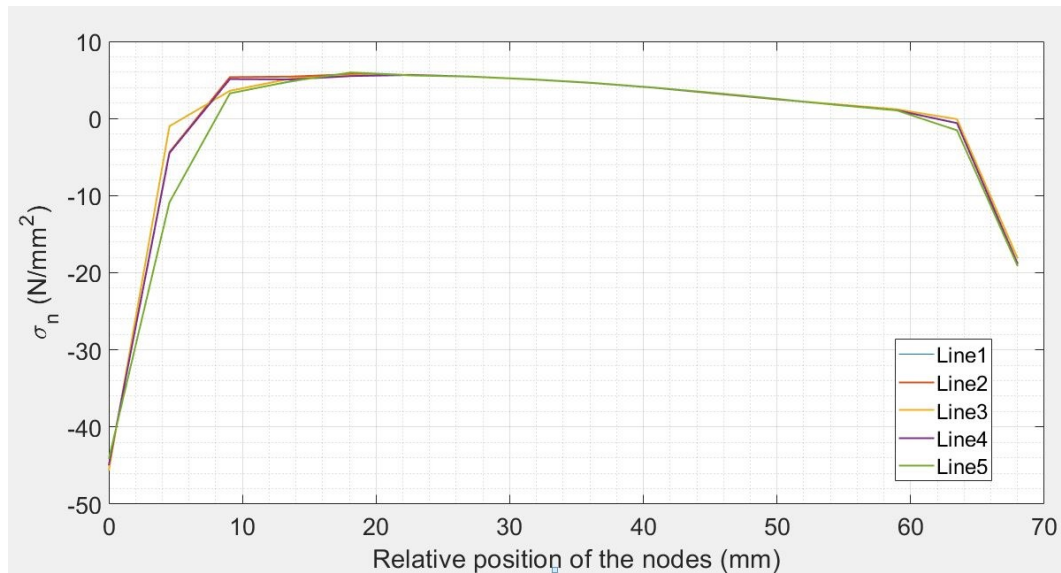


(a) Normal stress

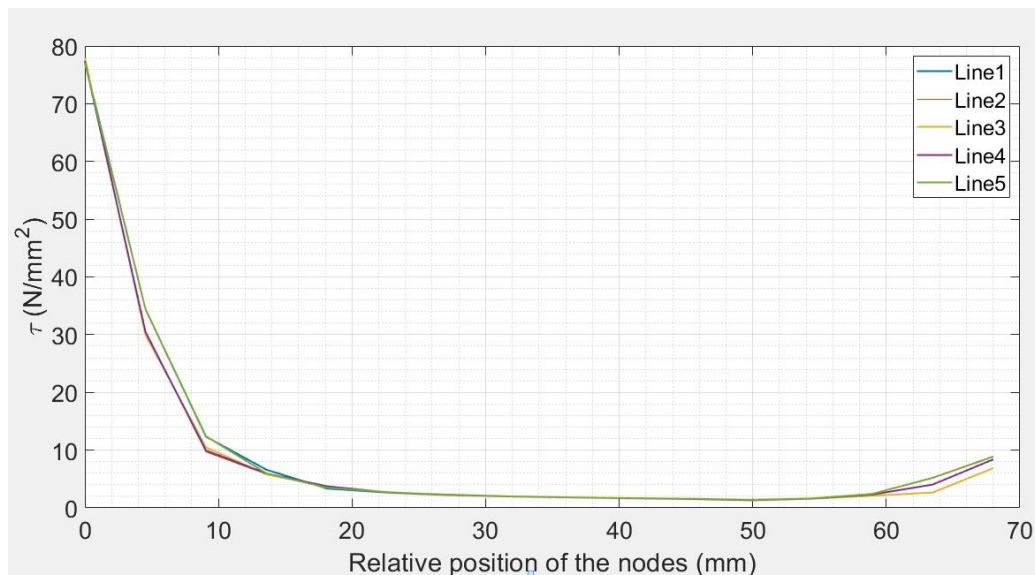


(b) Shear stress

Figure 62: Model 10 stress distribution in Local coordinates due to the extraction force



(a) Normal stress



(b) Shear stress

Figure 63: Model 11 stress distribution in Local coordinates due to the extraction force

As can be noticed, there is a discrepancy between the trend lines related to the geometry one and two, either for the normal or the shear stress. The model 2 and 5 which corresponding to the second bolt present a contrary behavior of the regular stresses. The normal stress starts with positive values on the first nodes of

the line. However there is a decrement developed along them and the line behaves under negative stresses at the end. For the shear stresses instead, at the beginning of the line there are the highest negative values and a gradually increment is developed until achieved almost a null distribution.

At the same time, for the geometry one the normal stresses increase from a negative value and the shear stresses decrease. Considering the stress distribution for both geometries, there is a concentration of stresses at the extremes of the line. The magnitude of them varies while the relative position of the nodes increase.

The before mentioned result is expected and explained by theoretical approaches. When a force is applied and distributed over an area and this geometry presents a reduction, it will result into a localized increase in stress considerably higher than average.[11]

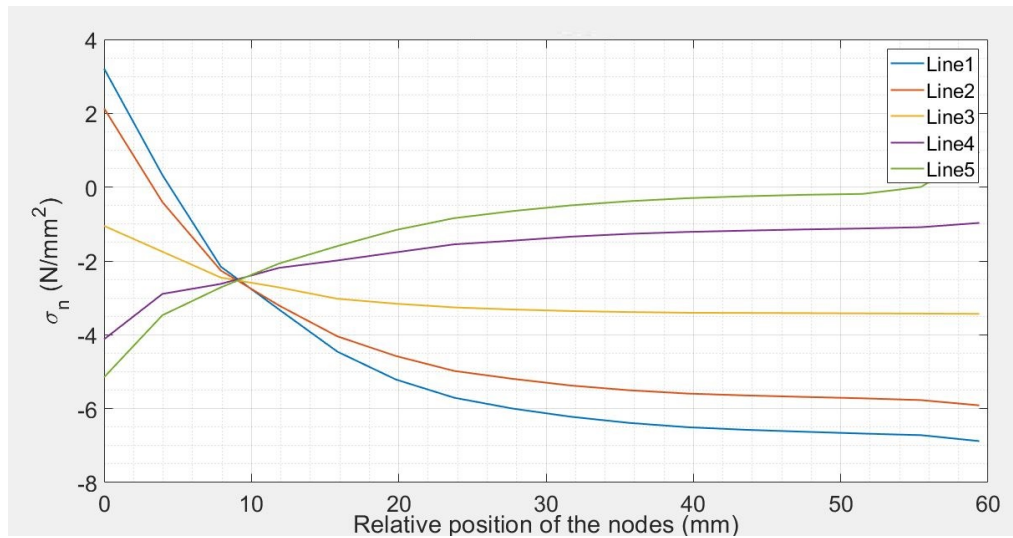
In this case, the geometric discontinuity is related to the hole caused by the inserted screw geometry. In addition, at the surface of the cone is disposed the bearing ring that acts as a constraint in Z direction and this will generate a localized effect too.

5.4.2 Prestressing contribution

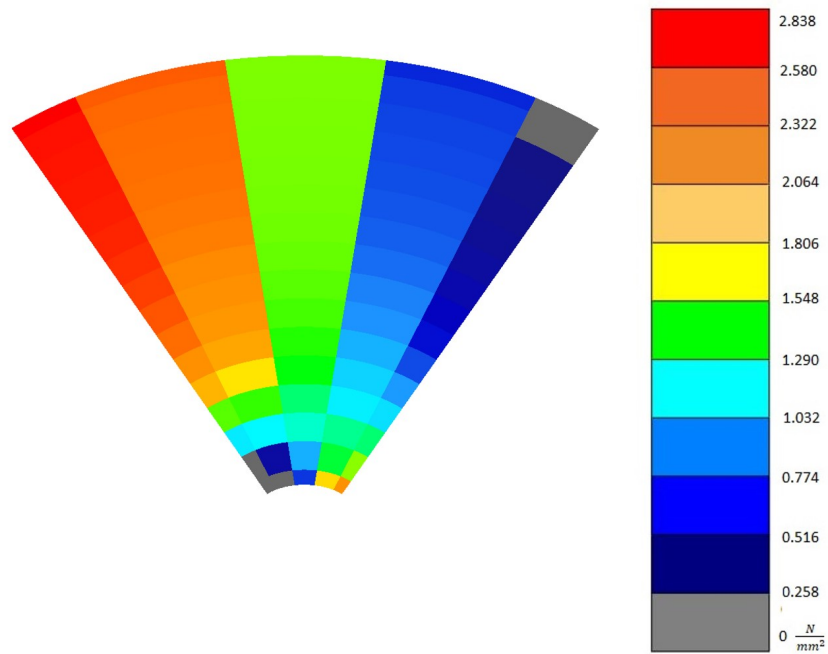
The prestressing contribution result is divided into two type analysis. The first part consist on the normal stress distribution along the lines produced by the compression force induced through the Compression test machine. In this way can be seen how is the influence of the prestressing scattered through the failure surface.

The second analysis is performed by means of the Mohr Coulomb contribution. The magnitude of the prestressing stresses that furnish through the tensile force are shown in several contour plots.

The results for the model 1 are shown in the Figure **64**



(a) Normal stress distribution in local coordinates



(b) Shear stress distribution Mohr Coulomb criterion

Figure 64: Model 1 - stresses distribution due to prestressing in Y direction

Analyzing the effect of σ_n , the distribution reflects the influence of the line position with respect to the surface of the load application. Being located on the

plane perpendicular to the loading surface (YZ) the line one is directly affected by the stresses in the Y plane. For that reason the contribution is higher, because the stresses interacts directly with the mesh. The maximum values either for negative or positive stresses are reported on this line.

On the other hand, while the lines rotate to the right the influence of the prestressing is lower. This is because the planes on which they are located have a relative inclination with respect to the global axis. Following the aforesaid premise only a portion of the total action is resented by the mesh. In addition, the line 5 presents a completely opposite stress spreading. The aforesaid phenomena means that the behavior of the section is changing and the deformation at one side is different with respect to the other one.

Continuing with the chart analysis there is a particular situation at a specific relative position where the behavior of the stresses is almost uniform and for that an apparently intersection point is achieved. To explain the peculiarity the deformation mesh is required.

In the Figure **65** is shown the deformation mesh for the model 1. As can be noticed the deformed shape of the failure cone is obtained in concordance to the stresses above mentioned. At the left of the section there is a little diminution of the cross section while at the right part of the cone there is a little change on the base of the screw. This corresponds to the expected behavior due to the compression state induced.

Talking again about the line one, there is a gradual change of stresses starting from negative values at the beginning of the line and finalizing with positive ones at the end of it. This is explained by the fact that there is a rearrangement of the mesh and the surface is compressed. Remembering the sign convention the negative contribution is associated to the compression and the positive to the tension.

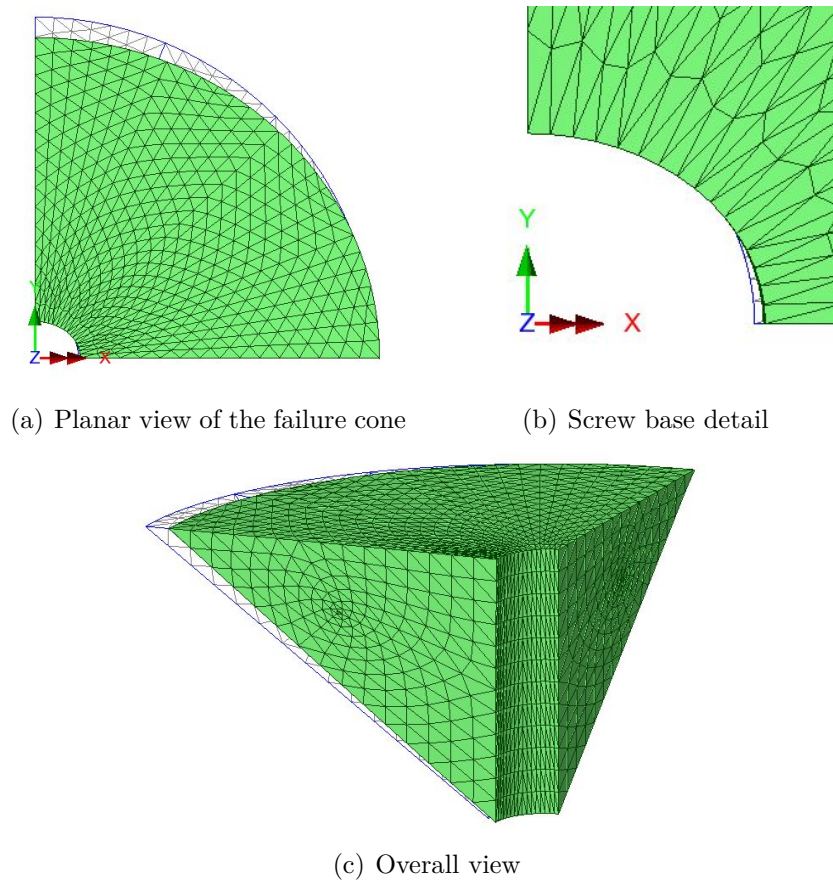


Figure 65: Model 1 deformed mesh

Nevertheless, the point for which all the stresses are the same is not already explained. Lets consider the Figure **66**. In the original mesh can be appreciated the initial geometry determined by the diameters of the involved circles on the problem. There is a point along all the lines where due to the modification of the circles into an ellipsoid shape an almost perfect circumference is created. This is explained by the fact that there is a compensation between the compressed and tensed mesh.

The circumference shape brings the uniform distribution of the stresses along the perimeter. This is the justification of the intersection of the lines at some point in height.

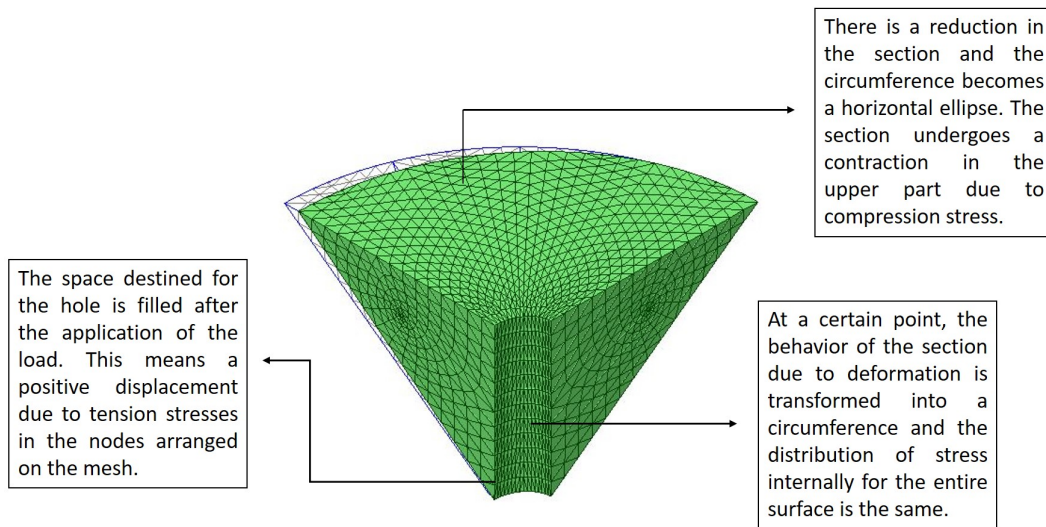
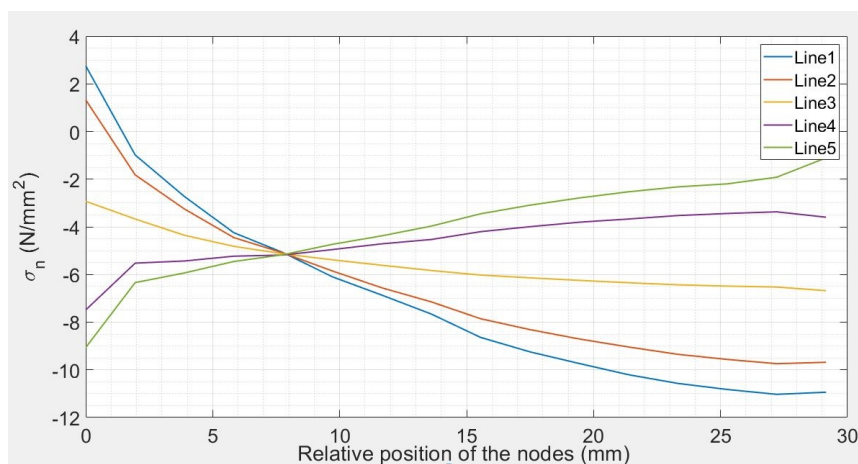


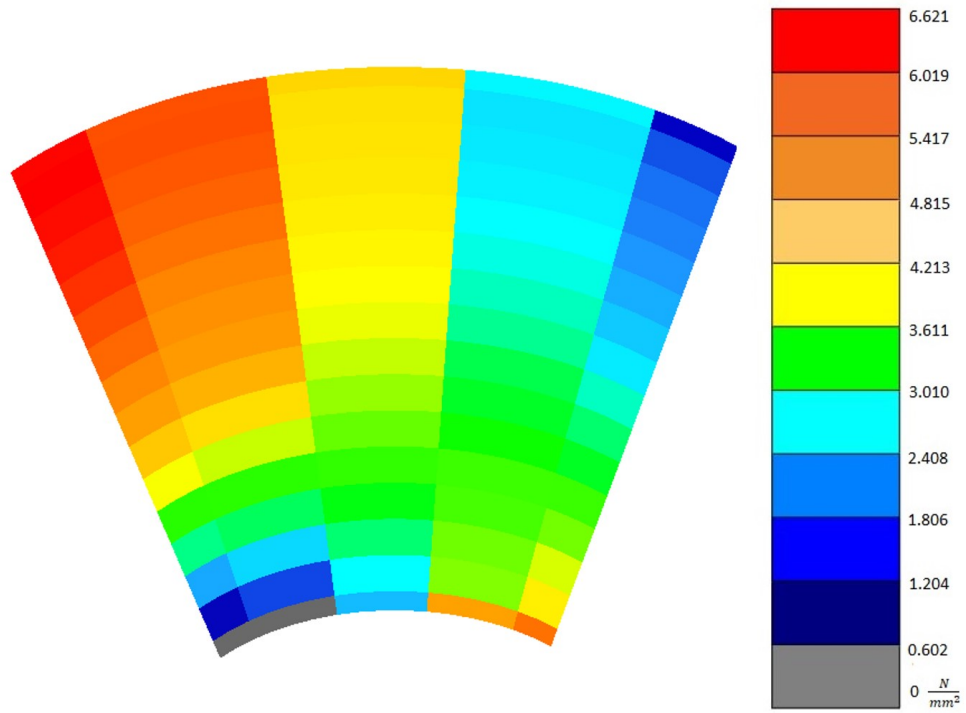
Figure 66: Mesh deformation implications on the stress distribution

The Figure 64 also illustrate the results obtained by the Mohr Coulomb analysis. The contour plot represents the distribution of the stresses that contributes on the extraction force. Where there is a gray color printed, a zero stress is associated. This does not means that on that node there is not stress influence. The explanation of the null value is the positive sign convention, because this value will not influence the result.

In the following figures are shown the results for the other geometries in terms of prestressing and Mohr coulomb approach.

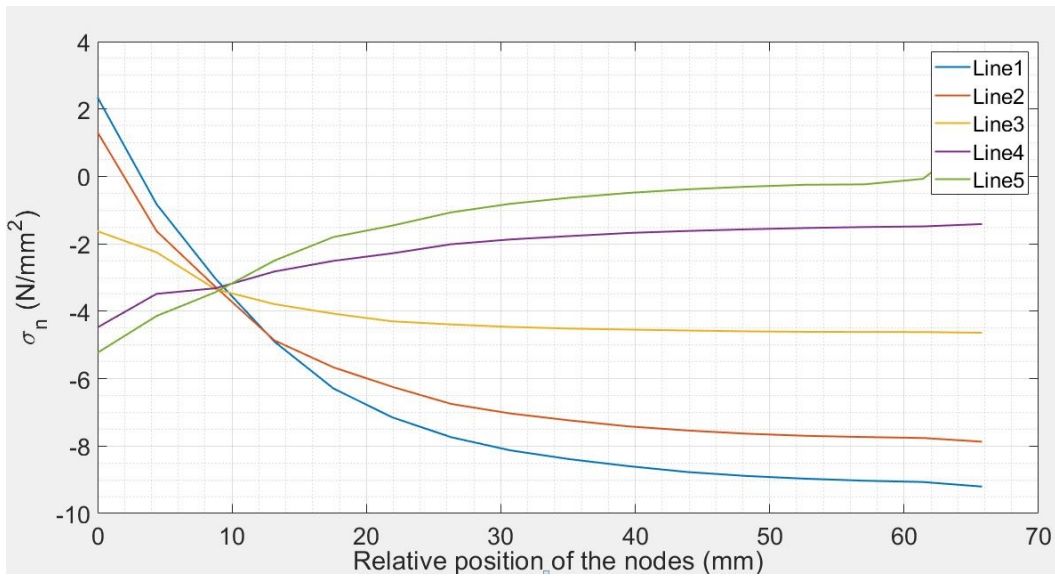


(a) Normal stress distribution in local coordinates

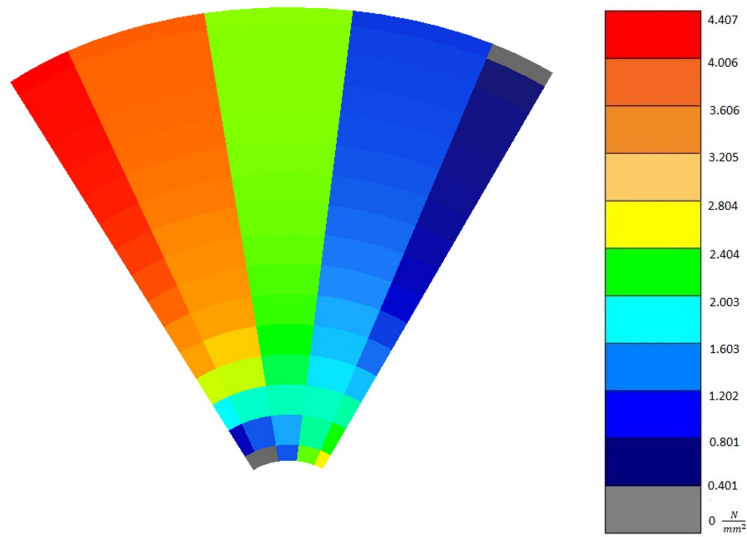


(b) Shear stress distribution Mohr Coulomb criterion

Figure 67: Model 2 - stresses distribution due to prestressing in Y direction

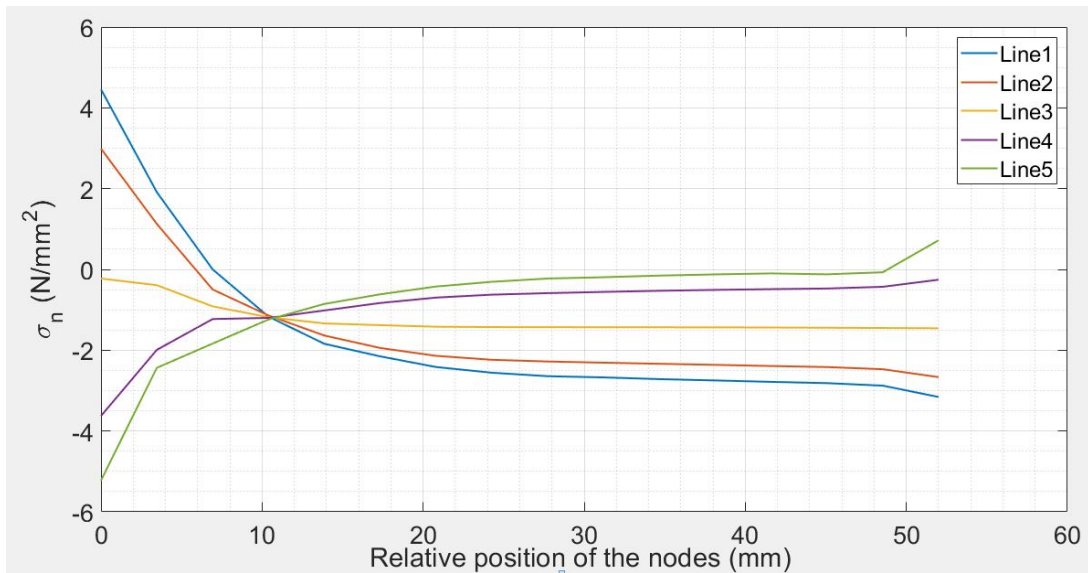


(a) Normal stress distribution in local coordinates

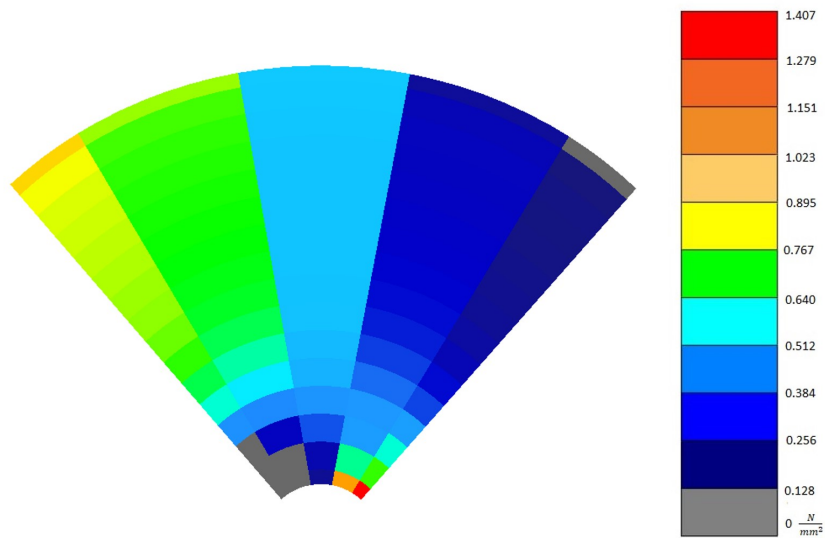


(b) Shear stress distribution Mohr Coulomb criterion

Figure 68: Model 3 - stresses distribution due to prestressing in Y direction

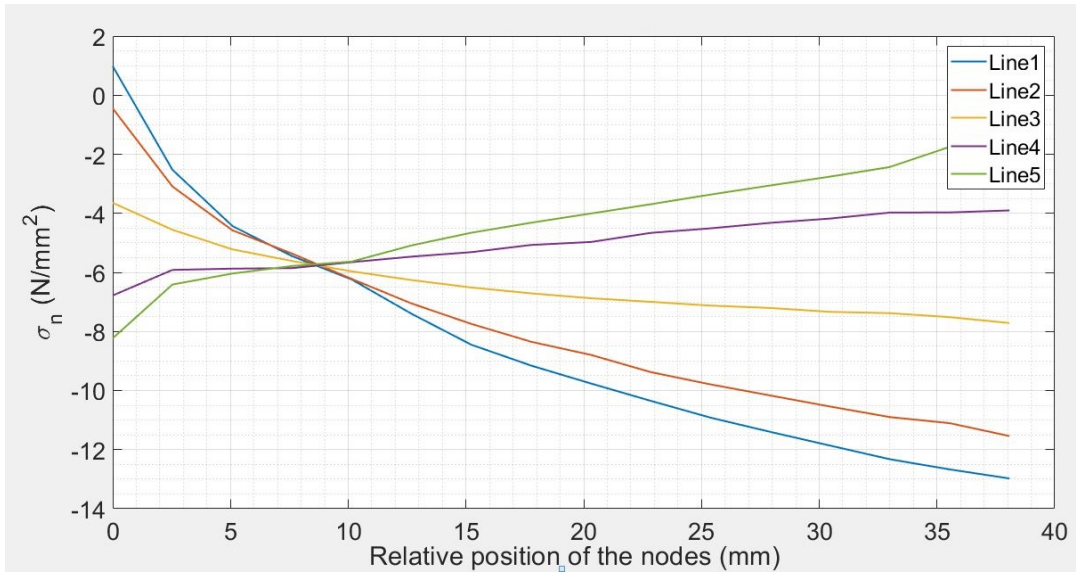


(a) Normal stress distribution in local coordinates

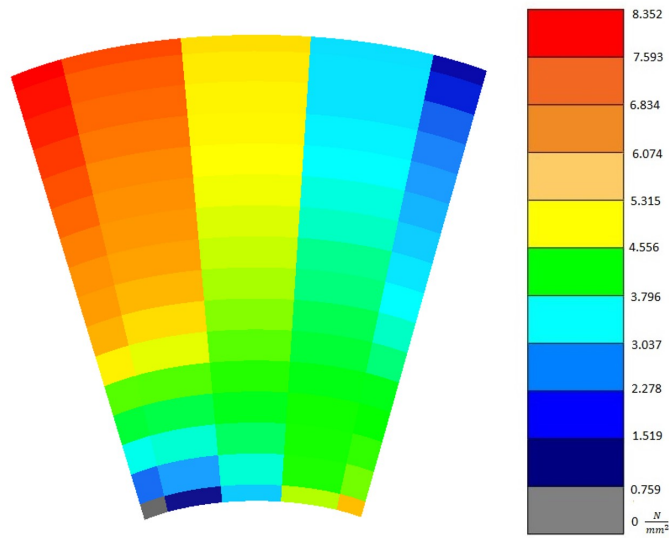


(b) Shear stress distribution Mohr Coulomb criterion

Figure 69: Model 4 - stresses distribution due to prestressing in Y direction

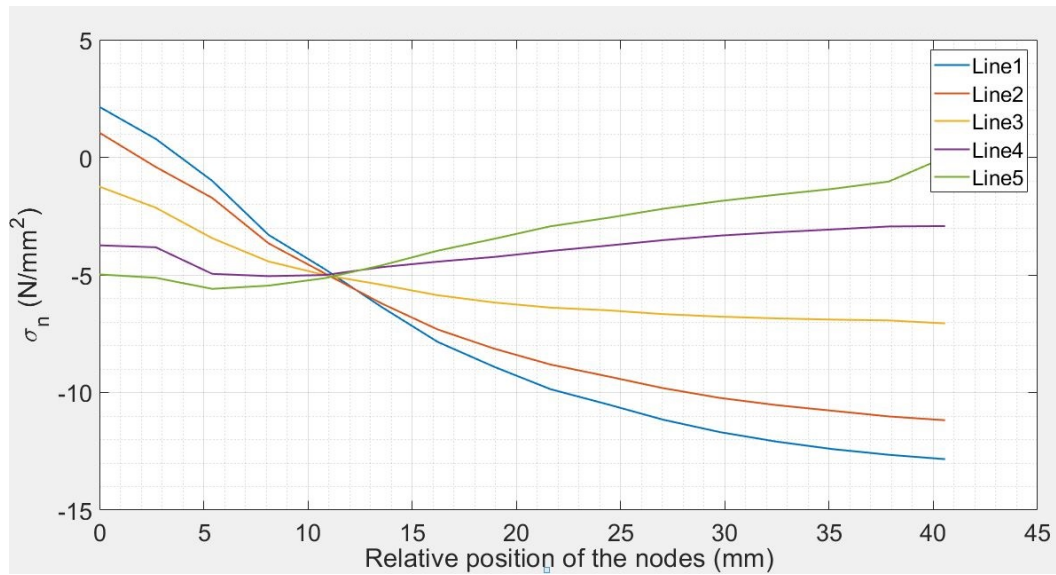


(a) Normal stress distribution in local coordinates

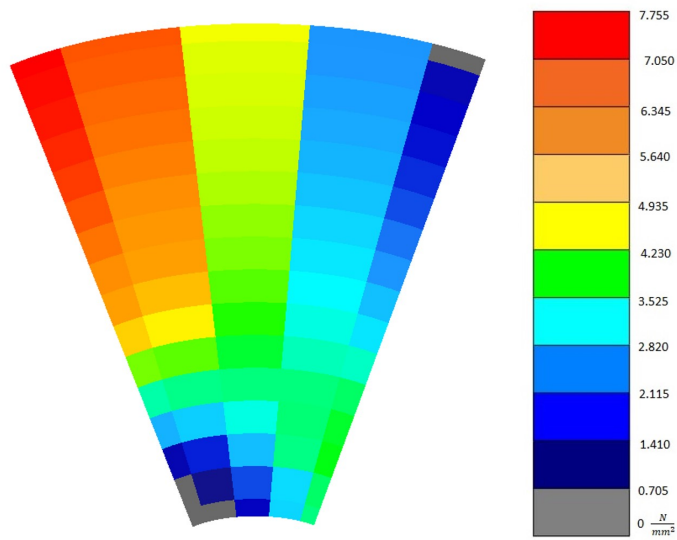


(b) Shear stress distribution Mohr Coulomb criterion

Figure 70: Model 5 - stresses distribution due to prestressing in Y direction

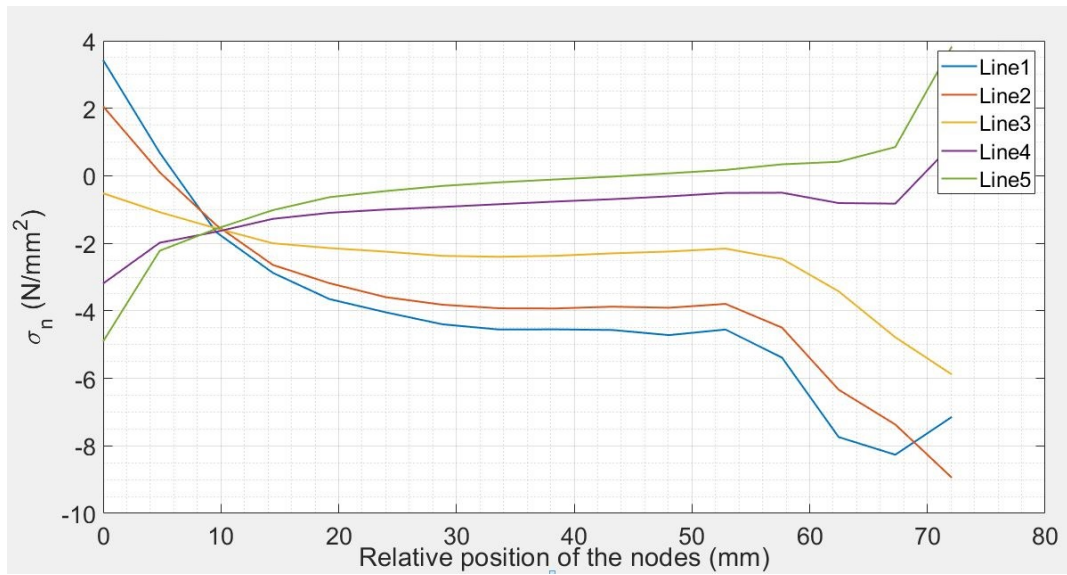


(a) Normal stress distribution in local coordinates

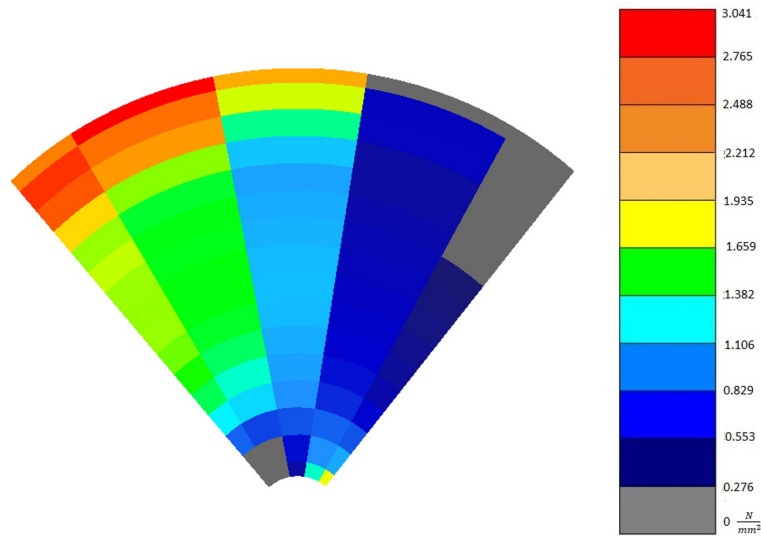


(b) Shear stress distribution Mohr Coulomb criterion

Figure 71: Model 6 - stresses distribution due to prestressing in Y direction

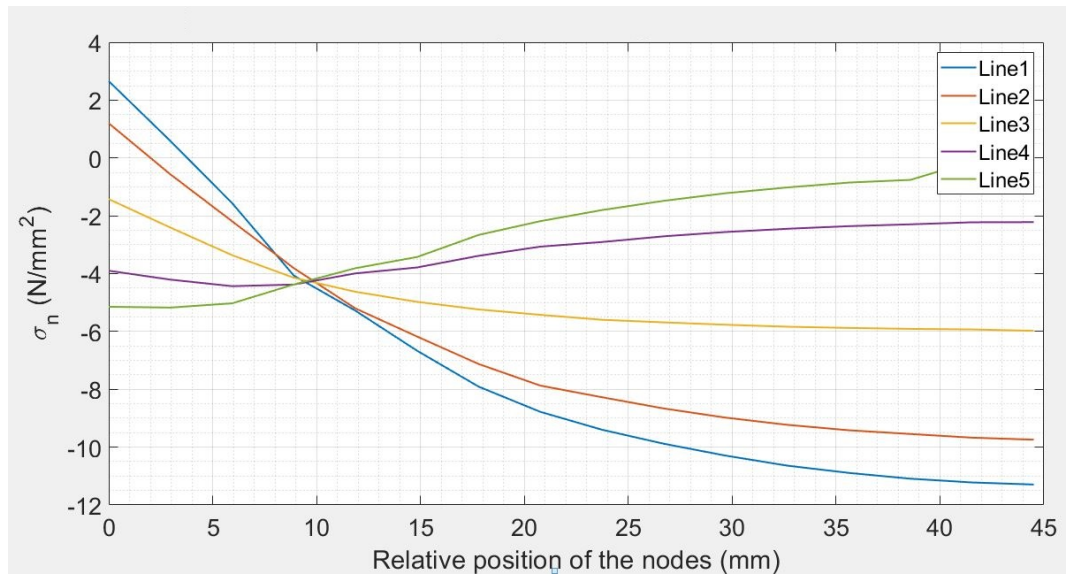


(a) Normal stress distribution in local coordinates

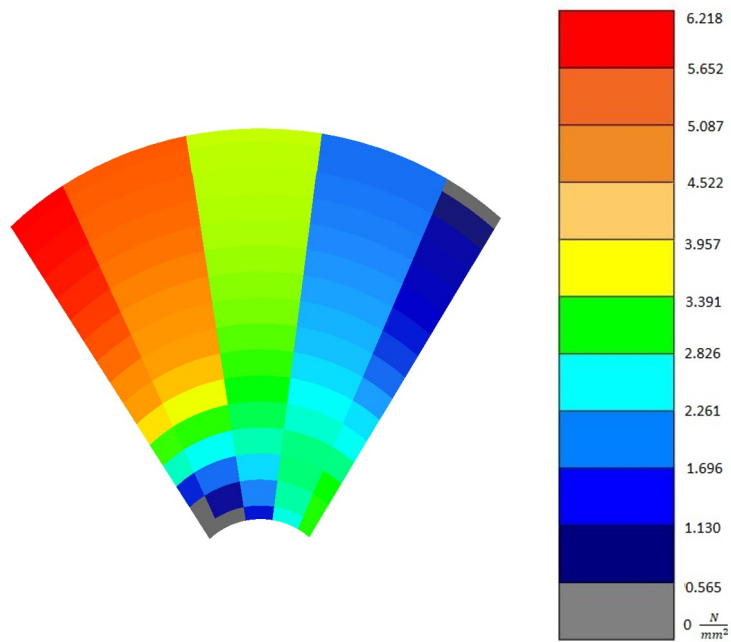


(b) Shear stress distribution Mohr Coulomb criterion

Figure 72: Model 7 - stresses distribution due to prestressing in Y direction

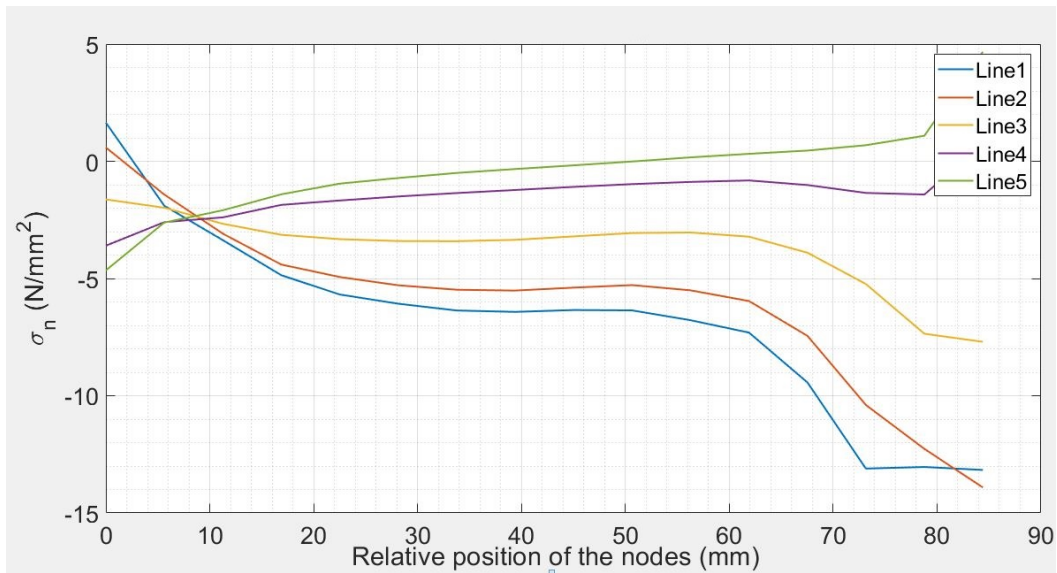


(a) Normal stress distribution in local coordinates

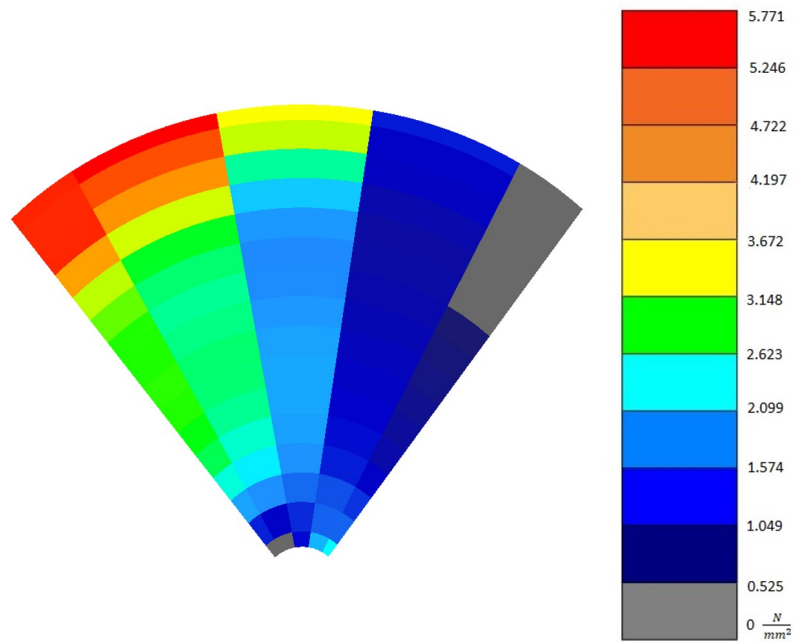


(b) Shear stress distribution Mohr Coulomb criterion

Figure 73: Model 8 - stresses distribution due to prestressing in Y direction

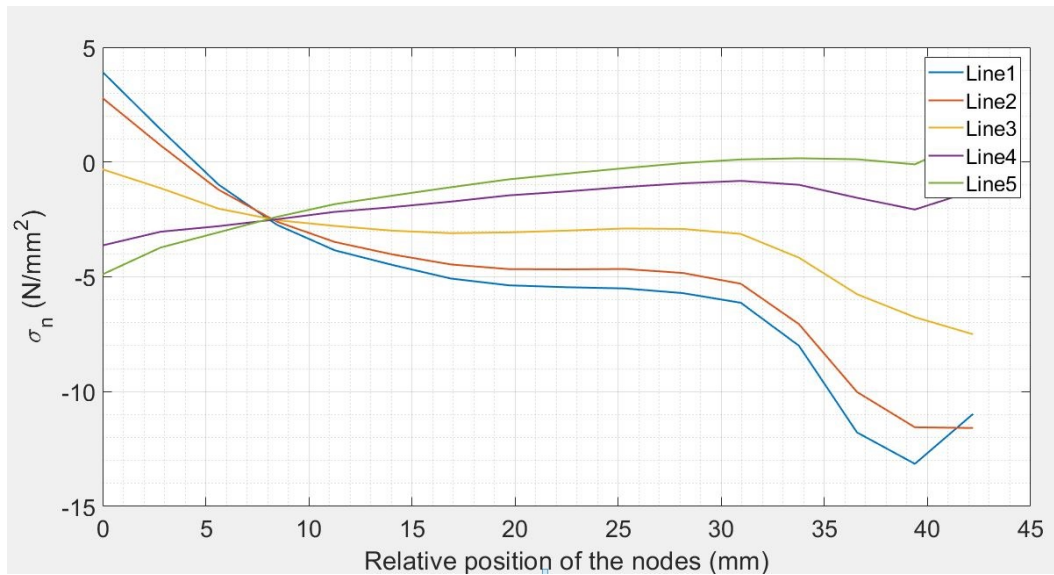


(a) Normal stress distribution in local coordinates

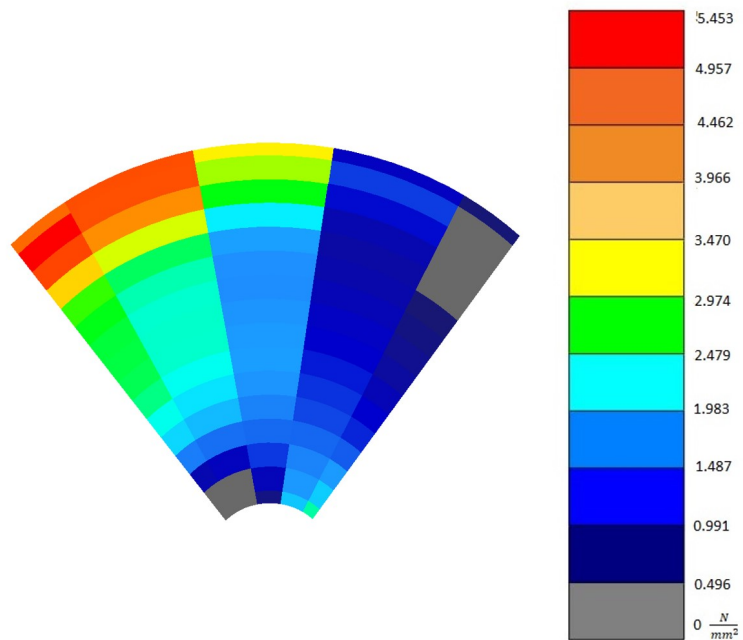


(b) Shear stress distribution Mohr Coulomb criterion

Figure 74: Model 9 - stresses distribution due to prestressing in Y direction

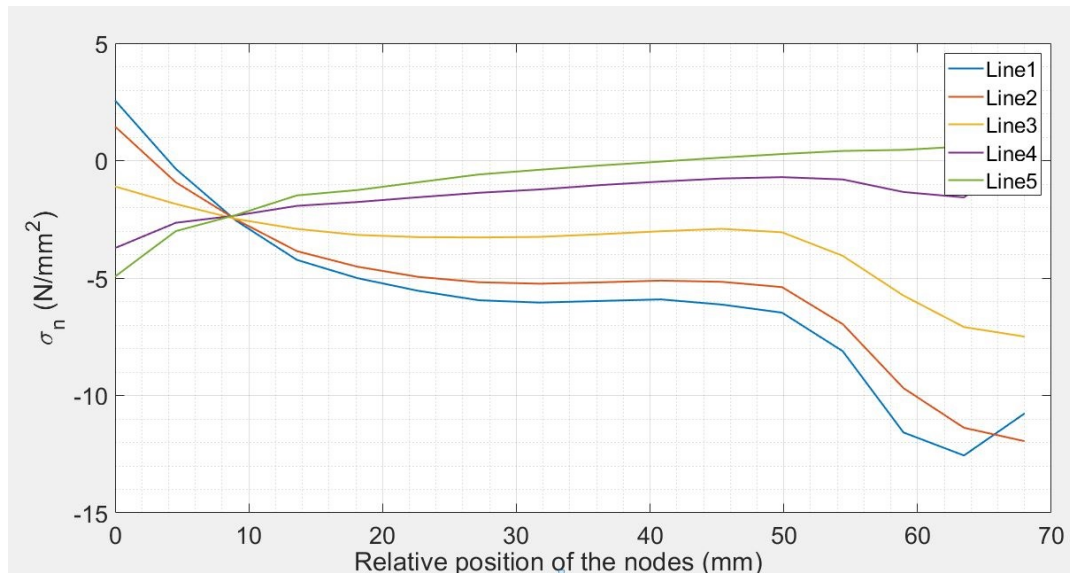


(a) Normal stress distribution in local coordinates

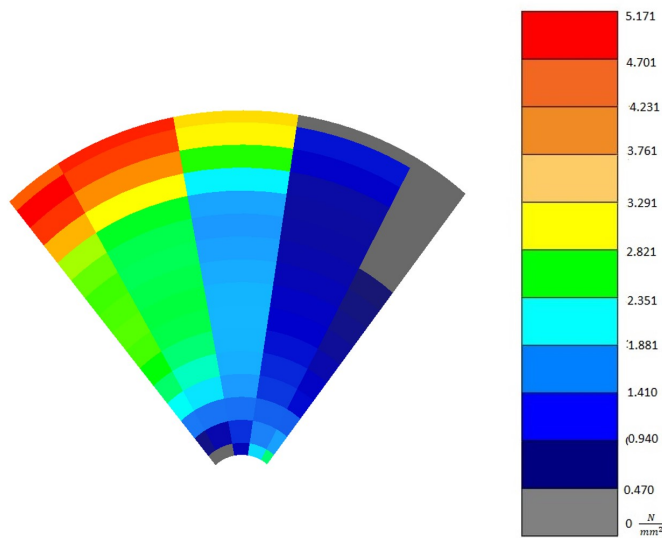


(b) Shear stress distribution Mohr Coulomb criterion

Figure 75: Model 10 - stresses distribution due to prestressing in Y direction



(a) Normal stress distribution in local coordinates

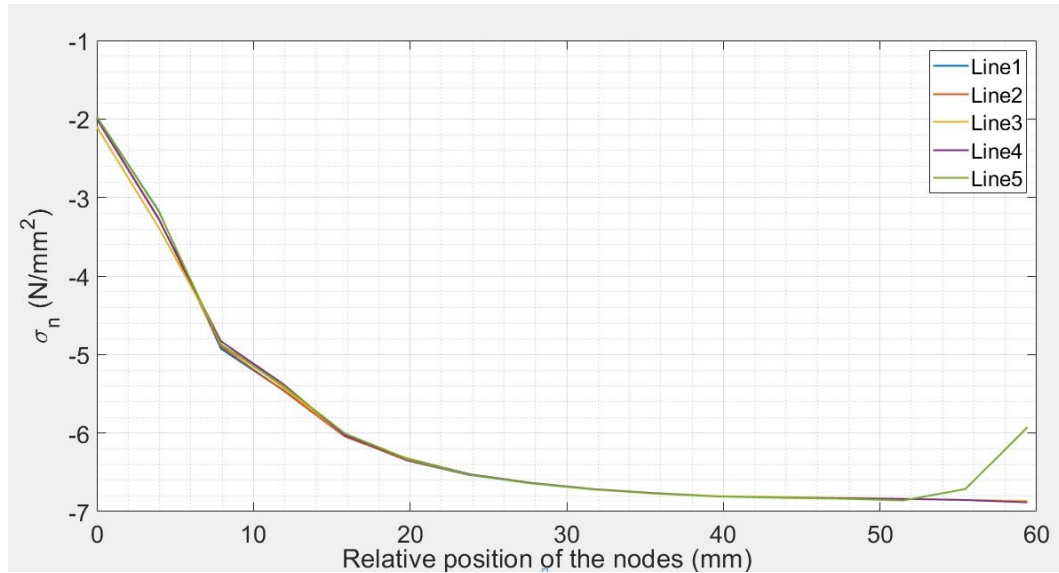


(b) Shear stress distribution Mohr Coulomb criterion

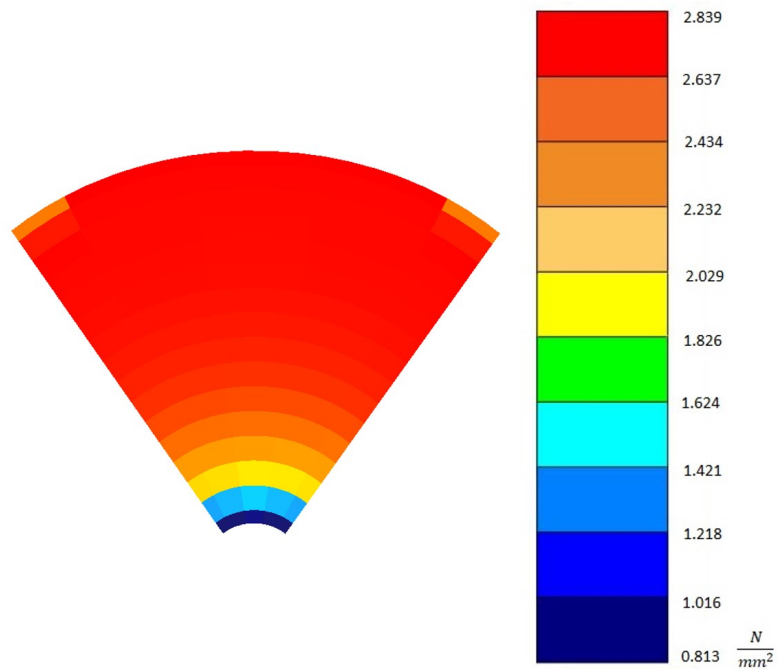
Figure 76: Model 11 - stresses distribution due to prestressing in Y direction

As was explained on the Numerical modeling section, there is another analysis related to the compression force. The prestressing contribution is confronted also with the behavior of the cube under two directions of compression induced. According to that, there is another result related to the X and Y direction loading

case. In the Figure 77 are shown the stress distribution obtained for the model 1 either for the prestressing case or the Mohr Coulomb criterion.



(a) Normal stress distribution in local coordinates



(b) Shear stress distribution Mohr Coulomb criterion

Figure 77: Model 1 - stresses distribution due to prestressing in X and Y directions

As can be noticed the behavior for the prestressing in both directions is different with respect to the one direction case. The distribution of the stresses is the same for any line along the surface. There is only a minimum variation at the end of the line 5. The behavior is linked to the deformed shape that the solid adapts after the loading.

The deformed shape of the cone is displayed on the Figure 80. There is a reduction on the shape due to the compressive effect in both directions. The variation on the geometry can be considered uniform due to the symmetry involved. The equivalence is either on the geometry or on the magnitude of the load. The prestressing induced has the same amount in both directions.

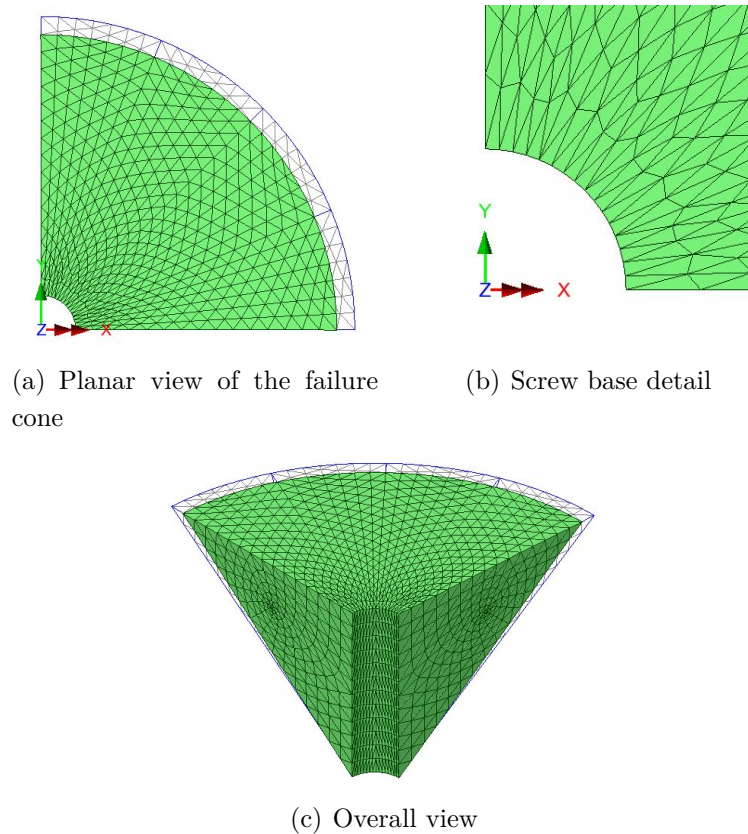
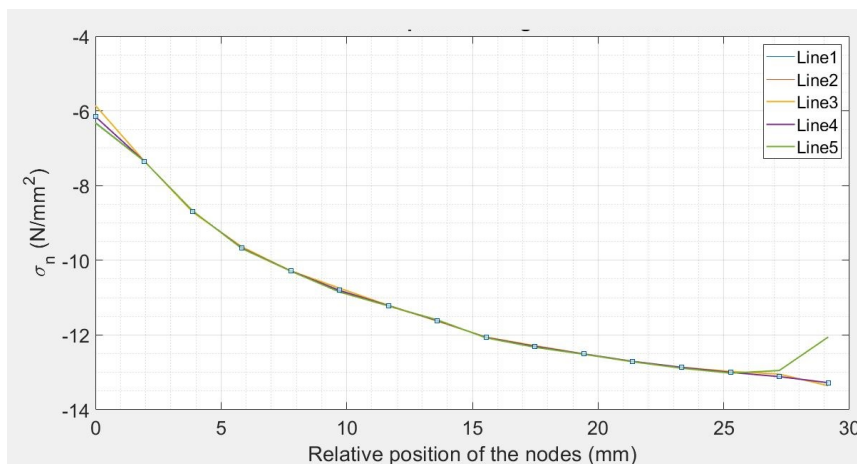


Figure 78: Model 1 deformed mesh after X and Y prestressing

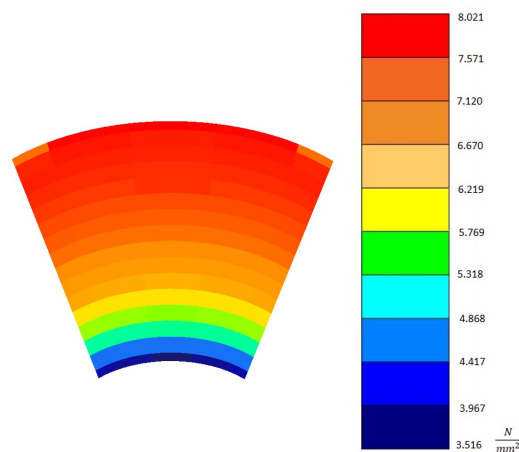
Finally, the compression stress is distributed along the surface and there is not a tensile influence as was induced on the first case (prestressing Y direction). At

the same time, the Mohr Coulomb contribution increase with respect to the first case. There are not present null values in any node and the range increase to higher values.

Going into the second model to interpret the behavior due to the combined action of prestressing, the Figure 79 illustrates the resultant stresses.



(a) Normal stress distribution in local coordinates



(b) Shear stress distribution Mohr Coulomb criterion

Figure 79: Model 2 - stresses distribution due to prestressing in X and Y directions

The trend line of the stresses only change in magnitude. Besides the change on the screw geometry due to the influence of the combined actions in X and Y directions, the comportment of the solid is completely the same. There is a uniform distribution of the stresses along the failure surface and the deformation is equivalent along the section.

In the following figure is shown the deformed mesh. The shape reaffirms the numerical results.

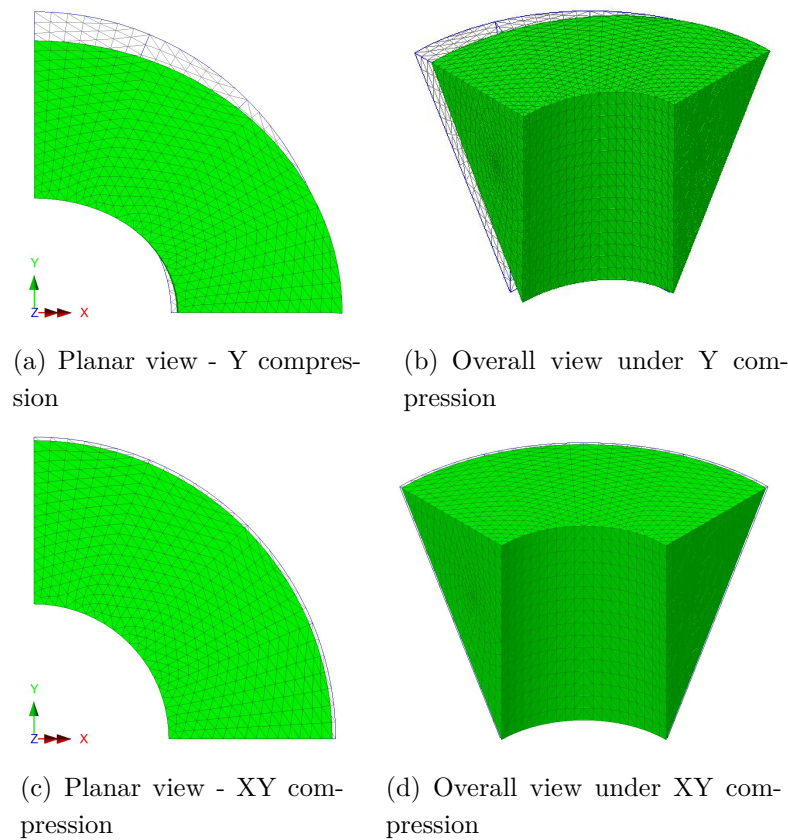


Figure 80: Model 2 deformed mesh after X and Y prestressing

Talking about the Mohr Coulomb contribution, there is also an increment of the quantities in almost twice the original value under the Y direction compression. The legend of the figure is determined by the minimum and maximum value present in the distribution of stresses. Comparing with the one direction display the stresses range start and finish in a greater magnitude.

The situation allow us to conclude that if a combination of loads is applied in all directions, even if the geometry of the bolt involved is different, the failure cone will be subjected to the same distribution of stresses with different amounts.

According to the last premise, the results regarding the prestressing analysis are summarized in the table 8. The results are expressed in terms of Forces and they are relative to one quarter of the solid.

Model number	CP in Y direction [N]	CP in XY direction [N]
1	3891.8	7744.8
2	2789.2	5865.6
3	6751.9	13442.0
4	954.1	1872.2
5	4728.5	9454.5
6	4029.0	8039.9
7	3405.3	7945.1
8	4287.5	8551.8
9	9627.9	18592.0
10	2551.7	5061.7
11	6034.0	11879.0

Table 8: Compression force results related to the prestressing contribution

From the table can be remarked that the influence of the prestressing in the extraction force is almost twice the influence when a one direction stress state is induced. This conclusion applies for any kind of geometry employed.

5.5 Geometry influence

The final step of the results consist on the comparison of the setups tested. There are several ways to segregate the discussion. The arrangements of geometries is the selected option. The evaluation is divided into four cases, as follows.

- Geometry 1 - Same α_1

Being α_1 the inclination angle of the reference model 1. The table 9 recapitulates the obtained results and the features involved on the modeling.

Same α_1 [°]	54				
Model number	CP Y [N]	CP XY [N]	D [mm]	h [mm]	d [mm]
1	3891.8	7744.8	110	35	14
9	9627.9	18592.0	150	50	14
10	2551.7	5061.7	82	25	14
11	6034.0	11879.0	124	40	14

Table 9: Same α_1 results

According to the information, the angle α constant cause a variation on the height and also the bearing ring diameter to compensate the geometric composition. Considering the four models as higher the aforesaid features higher the influence on the magnitude of prestressing detected by the screw during the test.

The model 9, with 150 mm of diameter and 50 mm of depth reaches 9627 N of prestressing while the model 10 with 82 mm and 25 mm of the same characteristics reaches 2552 N. This value is lower than half of the model 9.

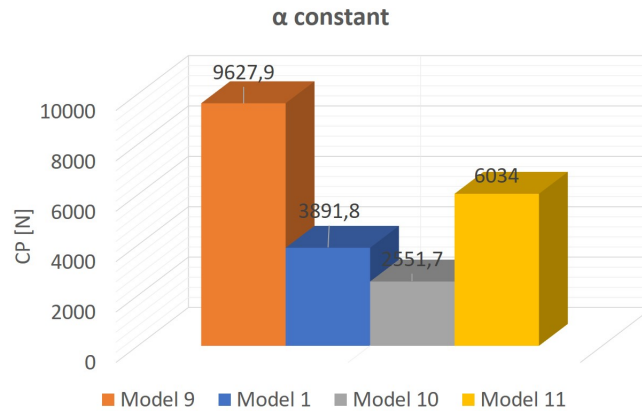


Figure 81: Values of prestressing contribution with alpha constant

- Geometry 1 - Same h_1

Being h_1 the height of the failure cone using as reference the model 1. The table 10 summarize the results and the features involved.

Same h_1 [mm]	35				
Model number	CP Y [N]	CP XY [N]	α [°]	D [mm]	d [mm]
1	3891.8	7744.8	54	110	14
6	4029.0	8039.9	30	55	14
7	3405.3	7945.1	61	140	14
8	4287.5	8551.8	38	69	14

Table 10: Same failure cone height results

The constant height of the cone is compared with the variation of the diameter of the bearing ring and the inclination angle α . Following the same analysis performed on the first approach, the information shows an almost constant behavior of the force. The fluctuation range of the values round the ± 500 N approximately. This means that the height is possibly one of the most important parameters in the prestressing state contribution and its variation influences more than the other two parameters.

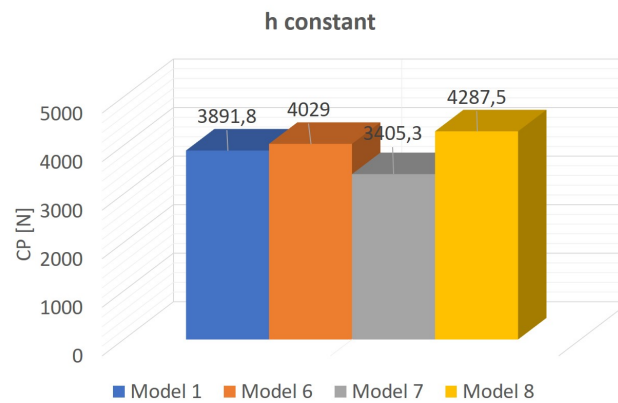


Figure 82: Values of prestressing contribution with height of failure cone constant

- Geometry 1 - Same D_1

Being D_1 the diameter of the bearing ring using as reference the model 1. The table **11** recapitulates the obtained results and the features involved.

Same D_1 [mm]	110				
Model number	CP Y [N]	CP XY [N]	α [°]	h [mm]	d [mm]
1	3891.8	7744.8	54	35	14
3	6751.9	13442.0	47	45	14
4	954.1	1872.2	67	20	14

Table 11: Same bearing ring diameter results

Similarly to the last case, once the bearing ring diameter is fixed, the other features must be changed. For that, a higher and a lower value of α and height are considered.

Looking into the results it is appreciated that again the height has a greater influence on the force behavior and it is related to the smaller inclination angle. In this case the model 3 reaches almost twice the compression force with respect to the model 1. The model 4 is defined by means of the smallest height in the whole arrangements group.

Due to the fact that the length is 20 mm in a depth of 100 mm, the outcome allows to conclude that the effect of the prestressing state compared with the overall forces is almost negligible. The force achieved was lower than 1 kN. This geometry does not represent significantly the induced compression force.

To represent the final results the Figure **83** is employed.

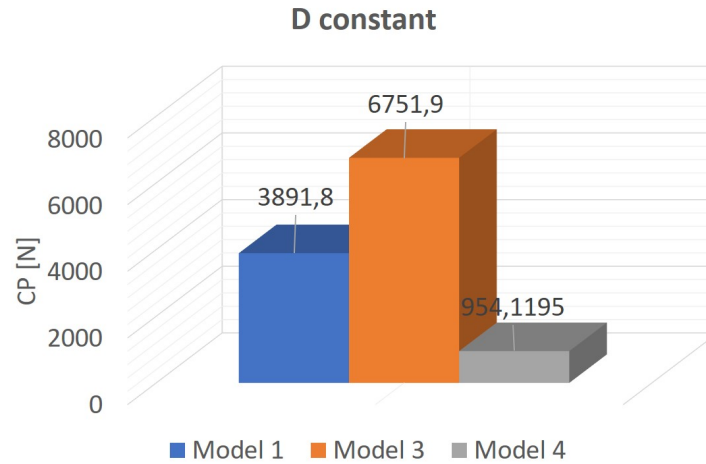


Figure 83: Values of prestressing contribution with bearing ring diameter constant

- Geometry 2 - Same D_2

Being D_2 the diameter of the bearing ring using as reference the model 2. The table 12 synthesizes the obtained results and the features involved.

Same D_2 [mm]	55				
Model number	CP Y [N]	CP XY [N]	α [°]	h [mm]	d [mm]
2	2789.2	5865.6	31	25	18
5	4728.5	9454.5	23	35	18

Table 12: Same bearing ring diameter results for Model 2

The model 2 and the features configuration exhibit the same trend compartment of the resent forces. Nevertheless the obtained value of the compression force even for the model 2 is lower with respect to the geometry 1. The model one achieve a compression force equal to 4 kN while the model 2 reach to detect 2.8 kN. Both for one quarter of the cube.

Making a final analysis of the results considering the theory explained on [12], as higher the inclination angle lower is the effect of the compression. This because

the tensile zones are going to withstand the extraction force by means of the MM straps. This is making reference to the Figure 4.

In conformity with the theoretical approach, if alpha is higher than 45 degree the failure is reached by only tension and the extracting force is supported by the hypothesized straps.

The theory was verified and it can be shown in the Figure 84

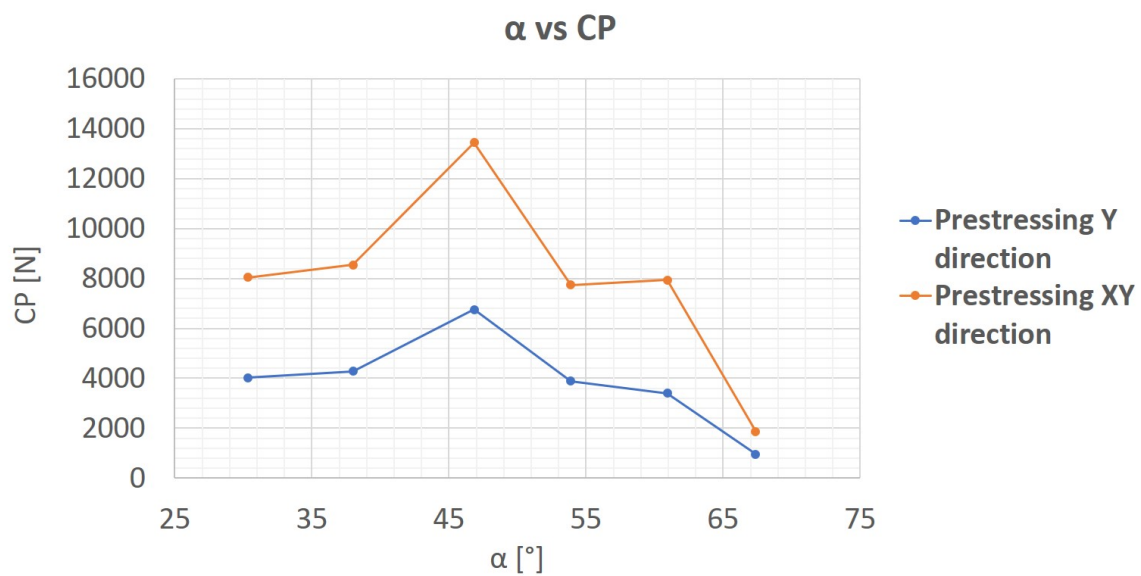


Figure 84: α versus the Compression force

The results are shown for the compression load acting on Y and XY directions. Analyzing the chart the results discussion previously performed applies for both cases.

6 Conclusions

The conclusions of the thesis are related either to the experimental procedure or the numerical modeling carried out.

Regarding to the pull-out method is possible to conclude that it is a methodology with the advantage of the easily performance in existent structures. Without damaging the sections the test involves a little removal of the surface that can be eliminated without difficult. This is performed by means of the addition of determinate materials such as mortar reconstructing the surface.

On the other hand the numerical modeling performed through several geometrical arrangements allow to conclude the importance of the elements employed when satisfactory results of the in situ mechanical properties of the steel cables is required. According to the obtained results, the depth of the screw introduced in the concrete structure can be considered as the most important attribute. This is reflected into a better performance referring to the detection of the influence of the surrounding prestressing state. Furthermore, as higher the depth reached by the screw inside the concrete greater susceptibility of the screw for the detection of the internal state of the structure.

Additionally, the lateral inclination of the truncated cone represented by the α angle and the diameter of the bearing ring employed, contribute to the level of detail obtained through the test execution.

Moreover, it is demonstrated that there is a strictly relationship between the three factors involved on the pull-out. It is not possible to determine a height of a screw without considering the diameter of the bearing ring and the influence of both on the inclination angle.

The maximum value obtained is related to the maximum height and diameter, but the tilt angle lies inside a intermediate range. In turn, the minimum value achieved corresponds to the greater diameter but the lower bolt height. The detection capacity of the precompression is reduced almost entirely.

To carry out the pull-out test the best setup is defined through the implementation of a screw height higher than 40 mm, accompanied by a bearing ring diameter

higher than 100 mm and a tilt angle of the failure cone inside an intermediate range. Otherwise, if a bolt depth is less than or equal to 35 mm, the diameter must be reduced to compensate the variation on the geometry and maintain the inclination closer to the initial value.

The second modeled geometry shows exactly the same than the before mentioned one. Nevertheless, this geometry turns out to be less efficient because the obtained outcome for both arrangements is much higher employing the bolt number 1.

Finally it is found that the geometry is the determinant factor to confirm the initial hypothesis of the prestressing state influence. To determine the impact of the prestressing state on the extraction force an specific configuration must be employed on field. This because not all the arrangements give a significant result.

The structural monitoring to verify the deterioration of the structure due to aggressive environmental effects on the steel cables can be carried out by means of the pull-out test. To perform that it is necessary to take into account either the mechanical properties of the material tested or the elements employed to develop it.

7 Bibliography

- [1] ACI Committee 318. (2014). Building Code Requirements for Structural Concrete (ACI 318-14): An ACI Standard: Commentary on Building Code Requirements for Structural Concrete (ACI 318R-14): an ACI Report. American Concrete Institute.
- [2] Alexandridis, A., & Gardner, N. J. (1981). Mechanical behaviour of fresh concrete. *Cement and Concrete Research*, 11(3), 323-339.
- [3] "Angle of internal friction", Encyclopedia.com, 2019. [Online]. Available: <https://www.encyclopedia.com/science/dictionaries-thesauruses-pictures-and-press-releases/angle-internal-friction>. [Accessed: 03- Dec- 2019].
- [4] ASTM, C. (2015). 900-15,“. Standard test method for pullout strength of hardened concrete.
- [5] BSI. (2009). BS EN 12390-3: 2009: Testing hardened concrete. Compressive strength of test specimens.
- [6] Craeye, B., Van Itterbeeck, P., Desnerck, P., Boel, V., & De Schutter, G. (2014). Modulus of elasticity and tensile strength of self-compacting concrete: Survey of experimental data and structural design codes. *Cement and Concrete Composites*, 54, 53-61.
- [7] Hernández-Montes, E., & Gil-Martín, L. M. (2007). Hormigón armado y pretensado. *Concreto reforzado y preesforzado*.
- [8] Marusak, J. & Ames, A, (2018). Speedway bridge collapse was “a horrible night”. [Online] The Charlotte Observer. Available: <https://www.charlotteobserver.com/sports/nascar-auto-racing/thatsracin/article205419384.html> [Accessed: 03-Dec- 2019].
- [9] Nawy, E. G. (1996). Prestressed concrete. A fundamental approach (No. Second Edition).
- [10] Nepomuceno, M., & Lopes, S. M. R. (2002). Non-destructive Tests on Concrete. *Concrete Technology Today Incorporating Structural Steel*, 14-20.
- [11] Peterson, R. E., & Plunkett, R. (1975). Stress concentration factors. *Journal of Applied Mechanics*, 42, 248.

- [12] P. Bocca (1979). Indagine teorico - sperimentale sulla determinazione della resistenza del calcestruzzo mediante prova di estrazione. *Revista L'Industria Italiana del Cemento*, 1-8.
- [13] P. Masciari (2017). ANCORA UN CROLLO DI UN VIADOTTO, L'ITALIA CADE A PEZZI PER ANNI DI INCURIA E DI MENEFREGHISMO!. Blog degli Amici di Pino Masciari. [Online]. Available: <http://www.pinomasciari.it/?p=37227>. [Accessed: 03- Dec- 2019].
- [14] Rodríguez, J. P. (2017). El hundimiento del puente de la carretera M-527 sobre el río Guadarrama. *Revista de Obras Públicas: Organo profesional de los ingenieros de caminos, canales y puertos*, (3583), 74-95.
- [15] Szabó, B. (2011). *Introduction to finite element analysis: formulation, verification and validation* (Vol. 35). John Wiley & Sons.
- [16] Woodward, R. J. (1989). Collapse of a segmental post-tensioned concrete bridge. *Transportation research record*, (1211).